Spread of Langat virus in the central nervous system in mice

Dissertation

zur Erlangung des akademischen Grades

doctor rerum naturalium (Dr. rer. nat.)

genehmigt durch die Fakultät für Naturwissenschaften der Otto-von-Guericke-Universität Magdeburg

von: **M.Sc. David Fritzsch**

geb. am: 17. Januar 1990 in: Stollberg

Gutachterinnen: Prof. Dr. Andrea Kröger

Prof. Dr. Stefanie Christine Becker

eingereicht am: 16.12.2022 verteidigt am: 16.05.2023

Zusammenfassung

Das durch Zecken übertragene TBEV (engl.: tick-borne encephalitis virus = TBEV) ist ein neurotropes Flavivirus. Dieses sich ausbreitende Virus zeigt über die letzten Jahrzehnte einen Anstieg der Morbidität in Europa und eine Ausweitung der Risikogebiete [1–4]. Zwar gibt es wirksame Impfstoffe zur Prävention, aber beim Auftreten der Erkrankung ist nur eine symptomatische Therapie möglich. Ausprägungen wie Meningitis und Enzephalitis bis hin zu neurologischen Folgeerscheinungen oder sogar tödliche Verläufe sind charakteristisch für diese schwere Erkrankung des zentralen Nervensystems [4, 3]. Allerdings ist bisher nicht bekannt, auf welchem Weg das Virus in das Gehirn eindringt. In dieser Arbeit wurde das Langat Virus (LGTV) als Modell verwendet, um die Neuroinvasion und Neurovirulenz in Abhängigkeit der Typ I Interferon (IFN) Antwort in asymptomatischen Wildtyp C57BL/6 (WT) und hoch suszeptiblen Interferon-α Rezeptor defizienten ($Ifnar^{-/-}$) Mäusen zu untersuchen. Die Ausbreitung des Virus während des Infektionsverlaufs wurde in verschiedenen Hirnregionen untersucht und infizierte Zelltypen wurden identifiziert. Die Blut-Hirn-Schranke (BHS) und die Blut-Liquor-Schranke (BLS) wurden als mögliche Eintrittswege für LGTV ins Gehirn untersucht. Schließlich wurde der Einfluss der viralen Infektion auf die Expression der tight junction (engl. für „enge Verbindung“) Proteine analysiert. Der Bulbus olfactorius (engl.: olfactory bulb = OB) war die Gehirnregion, unabhängig von der Typ I IFN Antwort, in der LGTV am frühesten repliziert. Das macht den OB zum wahrscheinlichsten Kandidaten für den Eintrittsort von LGTV in das zentrale Nervensystem. Eine beeinträchtigte IFN Signalübertragung führte zu einer Verschiebung der Ausbreitung des Virus in Richtung einer heftigen Infektion des Plexus choroideus (engl.: choroid plexus = CP), in dem zuvor keine virale RNA bei WT Mäusen nachgewiesen werden konnte. Dies weist auf eine wichtige Rolle der Typ I IFN Antwort im CP hin, um die LGTV Infektion im Gehirn zu kontrollieren. Außerdem war eine starke Infektion von $Iba\text{-}1^{+}$ Zellen in OB, CP und den Hirnhäuten von $Ifnar^{-/-}$ Mäusen zu beobachten, was darauf hinweist, dass die Typ I IFN Signalübertragung in diesen Zellen eine essentielle Rolle bei der Abwehr gegen LGTV im Gehirn spielt. Eine direkte Infektion der BHS, BLS und der Hirnhäute konnte während den späteren Zeitpunkten der Infektion nachgewiesen werden. Während der frühen Zeitpunkte, wenn sich LGTV bereits im OB befindet, war das Niveau der RNA Expression von den tight Junction Proteinen Claudin-5 und Zonula occludens-1 Protein in WT Mäusen relativ stabil. In $Ifnar^{-/-}$ Mäusen hingegen waren diese sowohl in nicht infizierten als auch infizierten Tieren negativ beeinflusst. Das weist darauf hin, dass LGTV keine gestörte Funktion der Barrieren benötigt um in das Gehirn zu gelangen, auch wenn die beeinträchtigte Expression der tight junction Proteine in $Ifnar^{-/-}$ Mäusen vermutlich zur verstärkten und veränderten Neurovirulenz von LGTV beiträgt.

Abstract

Tick-borne encephalitis virus (TBEV) is a neurotropic arthropod borne flavivirus that is transmitted by ticks. TBEV is an emerging virus and the risk areas expanded over the past decades together with an increase in morbidity in Europe [1–4]. Although several protective vaccines provide an effective prevention, there is only symptomatic therapy available in the case of an onset of TBE. Manifestations from meningitis via encephalitis through to neurological long-term sequelae or death are characteristic for this severe disease of the central nervous system (CNS) [3, 4]. However, it is not known how the virus infiltrates the brain.

In this work, the Langat virus (LGTV) has been used as a surrogate model to study the neuroinvasion and neurovirulence depending on the type I interferon (IFN) response in asymptomatic wild-type C57BL/6 (WT) and highly susceptible Interferon-α receptor deficient ($Ifnar^{-/-}$) mice. The viral distribution across several brain regions was examined during the course of infection and infected cell types were identified. The blood-brain-barrier (BBB) and the blood-cerebrospinal fluid-barrier (BCSFB) together with the cerebrospinal fluid (CSF) and the meninges were examined as possible entry routes for LGTV. Finally, the influence of the viral infection on the tight junction protein expression was analyzed.

The olfactory bulb was confirmed as the brain region with the earliest onset of LGTV replication independent of the type I IFN response, identifying it as the most probable entry site for LGTV into the CNS. An impaired IFN signaling caused a shift in the viral distribution pattern towards a heavy infection of the choroid plexus (CP) in which viral RNA was not detectable for WT mice. As a conclusion, this hints at a critical role for the type I IFN response in the CP for controlling LGTV infection in the CNS. Additionally, Iba-1^{+} cells were strongly infected in OB, CP and meninges of $Ifnar^{-/-}$ mice, indicating that the regular type I IFN signaling in those cells is crucial to control the LGTV infection in the brain. A direct infection of the BBB, BCSFB and the meninges could be detected at the later stages of the infection. During the early time points, when LGTV RNA was already detectable in the OB, the RNA expression levels of the tight junction proteins claudin-5 (CLDN-5) and zonula occludens-1 protein (ZO-1) were mostly stable in the WT mice. In $Ifnar^{-/-}$ mice however, the RNA expression levels were significantly negatively influenced in the steady state as well as during the infection with LGTV. This indicates that LGTV does not need a disturbed barrier function to enter the brain, although impaired tight junction protein expression in $Ifnar^{-/-}$ mice can promote the neurovirulence of LGTV.

Table of contents

1. Introduction 1

1.1 Viral neuroinvasion, neurotropism and neurovirulence 1

1.2 Viral strategies for neuroinvasion 1

1.3 Tick-borne flavivirus LGTV as infection model for neuroinvasion 2

1.3.1 Flaviviruses: structure, entry & life cycle 2

1.3.2 TBEV and LGTV 3

1.3.3 Transmission, symptoms and pathogenesis 4

1.3.4 Interaction with the innate immune system and type I IFN 5

1.3.5 TBEV & LGTV neuroinvasion 8

1.4 Barriers protecting the brain against viral neuroinvasion 9

1.4.1 The blood-brain-barrier 9

1.4.2 The blood-cerebrospinal fluid-barrier 10

1.4.3 The meninges 10

1.4.4 The role of tight junctions in the BBB and the BCSFB 11

2. Aim of this Work 13

3. Results 14

3.1 Viral distribution 14

3.1.1 Viral RNA of LGTV detected earliest in the olfactory bulb 14

3.1.2 Late infection of meninges and brain microvessels 17

3.1.3 CSF stays clear of replicable LGTV during early CNS infection 18

3.2 Cellular tropism of LGTV in the CNS 20

3.2.1 LGTV is detectable mainly in the OB and the CP by immunohistology 20

3.2.2 Abundant LGTV infection of Iba-1^{+} cells 22

3.2.3 No LGTV infection in epithelial or endothelial cells of the BCSFB and BBB 26

3.2.4 LGTV infection of Iba-1^{+} cells in the meninges in the absence of Ifnar 29

3.3 Effects of LGTV on BBB and BCSFB 31

3.3.1 Tight junction proteins are regulated differently in different brain regions 31

4. Discussion 39

4.1 OB as brain region with earliest LGTV replication in WT and Ifnar$^{-/-}$ mice 39

4.2 CP is significantly affected by LGTV infection in the absence of Ifnar 41

4.3 LGTV infects barrier associated macrophages and pericytes in the CP of Ifnar$^{-/-}$ mice 42

4.4 Type I IFN response in Iba-1^{+} cells as possible key factor for protection against LGTV neurovirulence 43
4.5 BBB and BCSFB during LGTV infection 44
4.5.1 CLDN-5 expression does not correlate with early LGTV infection 45
4.5.2 ZO-1 expression reduced by LGTV in infection site independent manner 46
5. Material and methods 48
5.1 Materials 48
5.1.1 Consumables 48
5.1.2 Chemicals and reagents 49
5.1.3 Virus 51
5.1.4 Laboratory Equipment 51
5.1.5 Computer software 52
5.1.6 Statistical analyses 52
5.2 Methods 53
5.2.1 Animal experiments 53
5.2.2 Cerebrospinal fluid and serum collection 54
5.2.3 Brain isolation 55
5.2.4. Meninges isolation 55
5.2.5 Choroid plexus isolation 56
5.2.6 Brain microvessel isolation 56
5.2.7 Histology and Immunofluorescence labeling 57
5.2.8 RNA isolation and qRT-PCR 60
5.2.9 Focus forming unit assay 61
6. References 63
7. Attachment 87

1. Introduction

1.1 Viral neuroinvasion, neurotropism and neurovirulence

The central nervous system (CNS) is a target for a variety of viruses [5]. While some respiratory viruses like multiple influenza strains or the respiratory syncytial virus seem to act more opportunistic [6, 7], other viruses like rabies virus [8], herpes virus [9] or flaviviruses [10] act more specific towards a CNS infection with concerted strategies to evade the immune system while entering or persisting in the CNS. Cellular and humoral components of the immune system together with the meninges, the blood-brain-barrier (BBB) and the blood-cerebrospinal fluid-barrier (BCSFB) represent a strong combination of measures to prevent such attempts. However, viruses are able to make well-orchestrated moves to bypass, overcome or impair those hindrances by different manners, to reach the CNS. This is called neuroinvasion [5]. Only reaching the brain does not necessarily mean a virus is capable of much interaction. If a virus is aiming and able to infect neurons or glial cells, including also agents in the periphery, it is called neurotropism [5]. The interplay of a virus inherent tropism, the way of neuroinvasion and the basic nature of the infection (acute or abortive/persistent) determine the clinical manifestation, which is called neurovirulence [5]. For neurotropism or neurovirulence to come into effect, the preliminary neuroinvasion is the obstacle to overcome first.

1.2 Viral strategies for neuroinvasion

Usually beginning in the peripheral tissues, virus infections can spread and invade other tissues including the peripheral nervous system (PNS) and less often the CNS. Although several physical and immunological barriers successfully prevent that from happening in many cases, viruses are still capable to outmaneuver those security measurements [11] and even benefit from the unique immunological environment in the CNS [12].

One option for the viral entrance to the CNS is the infection of different types of neurons in the PNS. The rabies virus is able to enter the axons of motor neurons at the neuromuscular junctions via receptor mediated transport and is retrogradely transported in endosomal transport vehicles and moves trans-synaptically until it reaches the CNS [12–14]. Alpha herpesviruses like herpes simples virus type-1 can infect sensory neurons by receptor-mediated transport and are transmitted by retrograde or anterograde transport to the CNS. They are capable of establishing acute or latent infections [11, 15].

Another option to enter the CNS is the olfactory route. This is used for example by the vesicular stomatitis virus (VSV) [16], borna virus [17] or rabies virus [18, 19]. Usually it starts with the infection of receptor neurons in the nasal olfactory epithelium followed by anterograde axonal transport along the olfactory nerve and thereby reaching the olfactory bulb [20, 11]. Further routes for the viral CNS entry are associated with the blood flow. Some viruses are able to infect leucocytes in the periphery. Inside them, the virus reaches the brain microvascular endothelial cells (BMECs) and traverse the BBB into the CNS (Trojan horse mechanism) [21–23]. Another blood stream associated way is the transport of virus particles to the BMECs followed by their infection and a possible impairment of their barrier function [24–26]. Further studies show evidence and suggest the assumption that several viruses rely on extracellular vesicles to infect BMECs and enter the CNS on that way [27].

1.3 Tick-borne flavivirus LGTV as infection model for neuroinvasion

Various types of arthropod borne diseases are distributed all around the globe. Elicitors can be parasites, bacteria or viruses [28]. Among the latter, the genus *Flavivirus* contains over 50 members [29] with many of them known to harm humans. This makes them one of the major origins for arthropod borne diseases [30]. These include well-known representatives like the West Nile virus (WNV), the yellow fever virus (YFV), the Japanese encephalitis virus (JEV), the dengue virus (DENV) and the tick-borne encephalitis virus (TBEV) [31–34].

1.3.1 Flaviviruses: structure, entry & life cycle

Flaviviruses are spherical, enveloped, positive sense single stranded ribonucleic acid (+ssRNA) viruses with a genome of around 11 kilo bases and a virion size of ca 50nm in diameter [35–38]. Their genome has a single open reading frame. It is flanked by 5’ – and 3’ – noncoding regions and the translation generates a single polyprotein [39]. The cleavage by cellular and viral proteases results into three structural proteins (capsid (C), precursor-membrane / membrane (prM/M), envelope (E)) and seven nonstructural proteins (NS) (NS1, NS2A, NS2B, NS3, NS4A, NS4B, NS5) [39–41]. At a mature flavivirus virion, the E protein organizes in homodimers associated with the M protein, which is anchored in a lipid bilayer. Together they form the viral envelope [42, 37, 43, 40]. Beneath that, the icosahedral RNA-containing capsid is located, consisting of multiple copies of the C protein [41, 44].

To replicate, the virus needs to attach to and enter a host cell. For arthropod transmitted flaviviruses, multiple proteins have been suggested to play a role for the attachment and internalization (reviewed in [44]). Further, some indistinct polypeptides were identified as possible entry receptors [45, 46]. However, until now it applies the assumption that there is not a solely candidate for an entry receptor [44, 47]. Instead, most studies came to the finding that attachment and entry of arthropod transmitted flaviviruses is mediated by more than one protein and differs further across different viruses, strains and different host species because of their ability to infect multiple hosts among mammals and arthropods [44–46, 48, 49]. After a flavivirus virion entered a cell by clathrin-mediated endocytosis, it needs to interact with an endosome to proceed [44]. The low pH within the endosome leads to several processes, one of which is the realignment of the E protein from a dimer into a trimer. This exposes more of the lipid bi-layer and facilitates the fusion of the viral membrane with the endosomal membrane [38, 50, 40]. This ultimately leads to the release of the viral genome into the cytoplasm of the host cell. Once the host cell has recognized the viral RNA as a messenger RNA, it is translated into a single polyprotein [40, 39]. Cotranslationally as well as posttranslationally this protein is cleaved by proteases of viral and host origin into the three structural and seven non-structural proteins [51]. This processing of the viral protein takes place on the endoplasmic reticulum (ER) in proximity to the site of RNA replication. While the C, M and E proteins are important for the structure of the virus, the seven NS proteins serve different purposes in the viral replication and maturation process and for interactions with the host. All NS proteins and the viral RNA are colocalized in vesicles in the ER. Together they form the viral replication complex [52]. The replicated, positive-sense RNA associates with the structural C protein and forms the nucleocapsid, which in turn is then encased by the prM and the E protein [52]. The resulting immature virus particles are budded into the ER lumen and are further passing the Golgi network while maturing in succession to the acidic pH and a concomitant cleavage of prM by the cellular serine protease furin [53]. The mature viral particles leave the cell via exocytosis [51].

1.3.2 TBEV and LGTV

Concerning flaviviruses, the neurotropic tick-borne encephalitis Virus (TBEV) is considered one of the most important viral disease agents within the European region [54].

Different vaccines exist as effective prevention but after infection and with an onset of the disease, only supportive and symptomatic therapy is available. Potential, specific antivirals and immunoglobulins against TBEV are under investigation but not available jet [2]. A better understanding of the infection process and the CNS infiltration is crucial to develop new therapeutic strategies. The Langat virus (LGTV) is a tick-borne flavivirus of the TBEV serogroup. It shares over 80% of serological identity with TBEV [55]. Cross-neutralization between TBEV and LGTV [56] and even more distantly related flaviviruses like powassan virus [57] has been described. No cases of naturally caused LGTV associated diseases in humans have been reported. Only following vaccination with live attenuated LGTV-based vaccines, few cases of LGTV caused encephalitis were described and this kind of vaccination has been stopped [58]. In mouse models with immunocompetent mice, LGTV infections showed rather asymptomatic courses. However, even without showing signs of disease, anxiety reduction and impaired memory formation were found in the mice subsequent to a LGTV infection [59]. Additionally, mice with knockouts referring to the type I interferon (IFN) system like interferon-α receptor deficient ($Ifnar^{-/-}$) or mitochondrial antiviral-signaling protein deficient ($MAVS^{-/-}$) mice, showed comparable courses of disease like known for the more virulent subtypes of TBEV with the inflammation of the CNS and with a fatal outcome [60, 61]. Referring to these data, LGTV is a suitable model virus in mice to investigate the neuroinvasive strategy of tick-borne flaviviruses of the TBEV serogroup concerning the influence of the type I IFN system.

1.3.3 Transmission, symptoms and pathogenesis

TBEV and LGTV are both arthropod-borne viruses that usually are cycling between arthropod vectors and vertebrate hosts. The major vectors for TBEV are the ticks *Ixodes ricinius* for the European subtype and *Ixodes persulcatus* for the Far Eastern and the Siberian subtype [62]. The discovery of LGTV (TP21 stain) was also in a tick of the Ixodes family, *Ixodes granulatus* in Malaysia [63] and LGTV was found in South-east Asia and Siberia [31]. Infecting a host is possible via the contagious saliva of the tick, via an alimentary route (dairy products from infected hosts) [64] or vertical from the mother to the fetus or new-born (shown for small rodents [65]). A tick to tick transmission is described transovarial, via sexual contact or during co-feeding [66, 67]. Another way of transmission is the feeding of ticks on a viremic host. The virus is also capable of outlasting the different developmental stages of the tick [68].

Small mammals have been identified as the main transmission hosts for TBEV [62]. Humans are also susceptible to the virus however; they do not serve as so-called reservoir hosts [2]. If an infection occurs in humans, about one-third of the infected individuals are estimated to develop clinical symptoms [69–73]. According to the subtype of the virus and to further less defined factors, the course of the disease can vary [74]. TBEV is often referred to as a biphasic disease. The first febrile illness phase can be accompanied by fever, muscle pain, headache and rashes while lasting for 2-7 days [71]. Characteristic for the second phase is the involvement of the CNS with manifestations like meningitis, encephalitis, meningoencephalitis and even chronic infections as well as neurological sequelae like paresis or ataxia [71]. It is often stated that around one-third of the patients which suffered from symptoms of the first phase, also pass on to the second phase [75, 76, 58]. However, it is still under discussion to which extent the first phase passes into the second phase and how often the two phases occur independently [77, 74]. During a tick bite, TBEV is transmitted via the saliva of the infected tick into the skin of the host. There, first the dermal cells and subsequently Langerhans cells, macrophages and neutrophils are infected [78]. When TBEV is transmitted via the alimentary route, the gut epithelial cells are suggested to be the site of the first replication while later proceeding to dendritic cells [79, 80]. Via the activated immune cells, TBEV reaches local lymph nodes and during the ongoing infection, a viremia occurs by which the virus also infects other organs like liver, spleen and thymus.

1.3.4 Interaction with the innate immune system and type I IFN

The body provides multiple lines of defense against pathogens. Considered as the first obstacles to overcome for a pathogen are the physical and chemical barriers like skin, mucus or the acidic pH of the gastric acid [81]. Along with that, the innate immune system provides a diverse, complex and early set of measures against infiltrating pathogenic agents. So-called pattern recognition receptors (PRRs) are highly expressed in immune cells and to a certain extend also in other cells of the body [82, 83]. They are located transmembrane or cytosolic, have the ability to detect various pathogen associated molecular patterns (PAMPs) and can trigger multiple distinct signaling pathways to counteract an infection [83]. For the (+)ssRNA flaviviruses like TBEV and LGTV, which produce intermediate double stranded (ds) RNA during the replication process, the relevant PRRs are the toll-like receptor (TLR)3, TLR7 and TLR8 as well as the retinoic acid-inducible gene I (RIG-I), and melanoma differentiation-associated protein-5

(MDA-5) [84, 85]. The three listed TLRs sense PAMPs in cellular compartments, whereas TLR3 recognizes dsRNA [86] and TLR7 and TLR8 recognize ssRNA [87–91]. RIG-I recognizes short and MDA5 long dsRNA in the cytosol [92–94]. The recognition of the respective PAMPs leads to the recruitment of distinct adaptor proteins at the PRRs.

TLR3 interacts with TIR-domain-containing adapter-inducing interferon-β (TRIF) [95] while TLR7 and TLR8 use the myeloid differentiation primary response 88 (Myd88) as an adaptor [96]. Different to the TLRs, RIG-I and MDA-5 recruit the mitochondrial antiviral-signaling protein (MAVS)(also known as VISA, IPS-1 or Cardif [97–100]). The infection with TBEV revealed that among brain resident cells, astrocytes are important IFN-β producers. This was dependent on MAVS at the early stages and on MyD88 and TRIF at the later stages [101]. Further downstream of those recruitments, the pathways lead to the activation of the transcription factor nuclear factor - κB (NF-κB) or the interferon regulatory factor (IRF)3 and IRF7, that translocate into the nucleus and induce the expression of different pro-inflammatory cytokines [102]. Among them, the type I IFNs are commonly known to be crucial for the defense mechanisms against viral infections. The expressed type I IFNs are released by the cell and are recognized in an autocrine and paracrine manner by the interferon-α receptor (Ifnar) 1 and Ifnar2 chains on the cell surface [103]. This in turn leads to the activation of Janus kinase (JAK)1 and the non-receptor tyrosine-protein kinase (TYK)2. They facilitate the phosphorylation of the signal transducer and activator of transcription (STAT) – molecules STAT1 and STAT2. Together with IRF9, the two STAT molecules from a trimeric complex. This complex enters the nucleus and enhances the transcription of a plethora of interferon stimulated genes (ISGs) by binding to an IFN-stimulated response element (ISRE) in the promoter of the ISGs [104–106]. One of those ISGs is IRF7, which is able to establish a positive feedback loop of type I IFN induction (Figure 1). This enhanced type I IFN production together with hundreds of ISGs promotes the often-referred antiviral state. This includes numerous modulations of cell survival, proliferation, physiology, differentiation, protein translation, and metabolism [82]. Furthermore, it is assumed that IFNs and ISGs interfere with almost every stage of the viral lifecycle [82, 107]. For several ISGs and interferon-induced proteins, an interaction with TBEV or LGTV was shown. Interferon-induced transmembrane proteins (IFITMs) (especially IFITM3) have been shown to have protective functions during TBEV infection in cell culture, however the virus showed partial escape by using cell-to-cell spread [108].

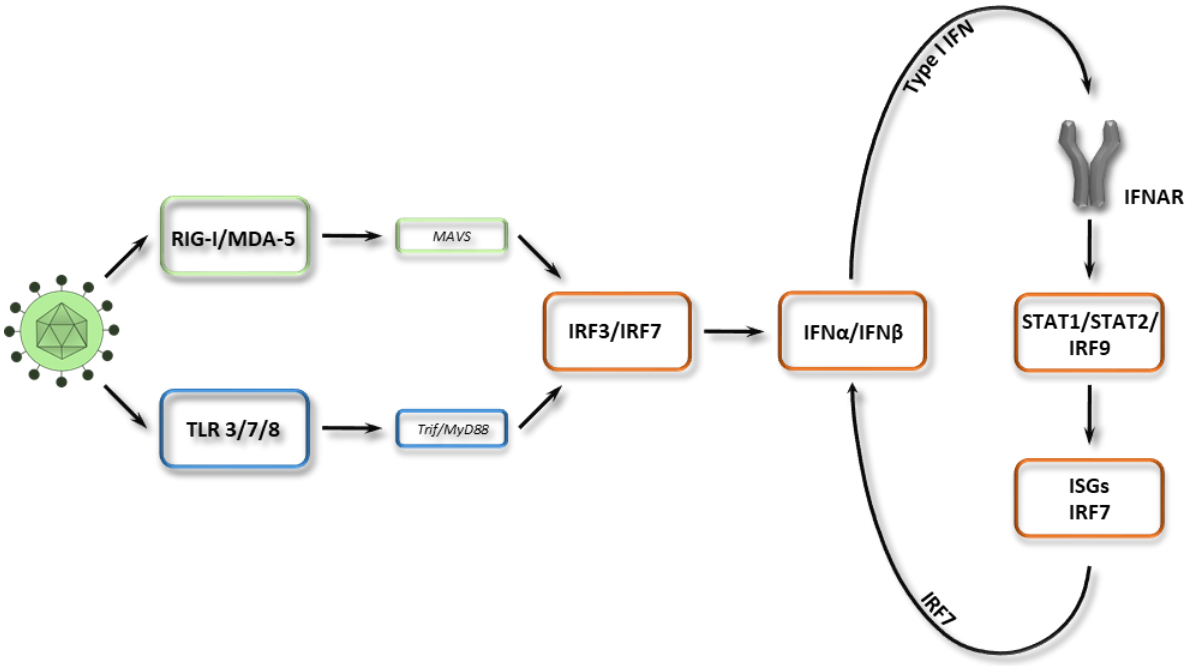

Figure 1: Simplified depiction of the type I interferon signaling pathways
Retinoic acid-inducible gene-I (RIG-I), melanoma differentiation-associated protein 5 (MDA-5), mitochondrial antiviral-signaling protein (MAVS), toll-like receptor (TLR) 7/9, toll-interleukin-1 receptor (TIR) homology domain-containing adapter-inducing interferon-β (Trif), myeloid differentiation primary response 88 (MyD88), interferon regulatory factor (IRF) 3/7/9, interferon (IFN) α/β, interferon-α/β receptor (Ifnar), signal transducer and activator of transcription (STAT) 1/2, interferon stimulated genes (ISGs)

Viperin is an ISG and has a protective function in flavivirus infection in a region specific manner [109] and targets NS3 for proteasomal degradation [110]. The tripartite motif (TRIM) protein, TRIM79α, is another ISG that showed protective qualities against TBEV by mediating lysosome-dependent degradation of the flavivirus RNA polymerase NS5 [111]. Additionally, certain polymorphisms of the interferon-induced antiviral protein family members of 2'-5'-oligoadenylate synthethase are associated with the predisposition to TBEV induced disease in humans [112], indicating the importance of those proteins during an active TBEV infection. However, TBEV, LGTV and flaviviruses in general are able to interfere with the orchestrated immune response in different ways. While it could be shown that IFNβ induction is mediated by the PRR RIG-I and not MDA-5, it was found that IFN induction is delayed following a TBEV infection [113]. This delay could be ascribed to the ability of flaviviruses to form replication vesicles in the endoplasmic reticulum.

Those structures allow the virus to hide the emerging dsRNA from the cytoplasmic PRR and therewith delays the immunological response against the cellular infection [113–115]. Moreover, flaviviruses can antagonize IRF-1 signaling to inhibit distinct functions of dendritic cells [116]. Additionally, for TBEV the inhibition of the host rRNA synthesis and protein production in human cells of neural origin was described [117]. Further, the flaviviruses NS proteins have been investigated extensively and were found to play a prominent role for impairments of the immune system. While intracellular NS1 rather contributes to the viral replication [118], extracellular NS1 binds C1s and C4 in a complex and thereby promotes efficient degradation of C4 to C4b leading to a functional impairment of the complement system [119]. However, NS1 is also a suitable antigen for TLR activation, in dengue virus namely TLR2 and TLR6, which contributes to the induction of a protective, anti-viral immune response [120, 121]. Interestingly, the NS1 of TBEV activates the expression of protective immunoproteasome subunits [122]. NS2A has not been assigned an independent role [41] but together with NS2B and the small hydrophobic NS4A and NS4B it serves as a scaffold for the viral replication complex [52] and they have an inhibiting effect on the type I IFN signaling [123–126]. NS2B is further known as an important co-factor for the protease activity of NS3. With its enzymatic function, NS3 serves as a serine protease, helicase and RNA nucleoside triphosphatase during viral replication and polyprotein processing [41]. Besides NS3, NS5 is the only other NS protein with an enzymatic function. Mainly it functioned as a viral RNA dependent RNA polymerase however; NS5 is an interferon antagonist and inhibits IFN stimulated JAK-STAT signaling [127, 128]. Further, it binds to prolidase and therwith inhibits the suface expression of Ifnar1 [129]. In Addition, it has been shown that TBEV NS5 interacts with the scribble protein which possibly leads to the subversion of the apico-basal cell polarity [130]. For Dengue virus and west Nile virus this could be shown in addition to the interaction with zonula occludens-1 protein (ZO-1) [131].

1.3.5 TBEV & LGTV neuroinvasion

Different approaches have been made to elucidate, how TBEV or LGTV reach the brain, however a clear answer has not been found so far. A possible and already discussed option is the infiltration via the BBB. It has been shown that TBEV is able to infect brain microvascular endothelial cells *in vitro* [132].

However, although the infection with TBEV and LGTV ultimately leads to the breakdown of the BBB in susceptible mice, this was not necessary for the virus to reach the brain in the first place [133, 60]. For Exosomes containing LGTV, transwell-migration assays showed the potential of those extracellular vesicles, enriched with viral RNA and protein, to infect microvascular endothelial cells of the BBB and a further infection of neuronal cells after crossing the barrier [134]. Taken together, this indicates that the disruption of the BBB is not mandatory for TBEV and LGTV to infiltrate the CNS however, the BBB cannot be excluded as a pathway. Further, possibly LGTV and TBEV use more than one route, as it has been shown for other neurotropic viruses like rabies virus [14] and zika virus [135]. Some studies showed an early [136] or strong [61, 60] infection with LGTV of the olfactory bulb in susceptible mice. This, and the possibility to intranasally infect mice with LGTV [136] indicates that an CNS entry could take place via the olfactory route. However the intranasal infection led to a delay in the onset of the disease and to a reduced mortality [136], which reduces the probability that the olfactory route is the initial pathway. Another interesting finding was the early and strong LGTV infection of the deep cervical lymph nodes that drain the cerebrospinal fluid (CSF) [136]. This is hinting at an early involvement of the BCSFB in the entry strategy of LGTV into the brain, which makes it an interesting target for further investigation. For a better understanding of the inherent processes, it is important to understand the barriers a virus has to face.

1.4 Barriers protecting the brain against viral neuroinvasion

1.4.1 The blood-brain-barrier

Made up of cerebral microvascular endothelial cells, specialized in structure and function, the BBB is in charge for protecting the brain and its neuronal network from blood-borne substances and maintaining proper homeostasis and nutrition [137]. Those endothelial cells are supported by neurons, interneurons, astrocytes, basal lamina covered with smooth muscular cells, pericytes and extracellular matrix [138]. Those components are intertwined with each other and make up a structural and highly functional whole, forming what is called the concept of the neurovascular unit [138–141]. The endothelial cells of the BBB are connected paracellularly by tight and adherens junctions. Those connections strictly confine passive diffusion of blood-borne substances and the paracellular migration of cells [142]. Tight junctions are oriented towards the luminal or apical side of the cell [143].

Beside the transport restrictions caused by the tight and adherens junctions, the BBB provides a strictly regulated transport system. While oxygen, carbon dioxide and small lipophilic substances can pass without hindrance, hydrophilic molecules like glucose [144], amino acids [145] and others get blocked [141]. Nutrients can pass the barrier to the CNS by carrier-mediated transport and proteins are transported via receptor-mediated transport [141, 146, 147]. To transport molecules from the CNS to the blood, special active efflux transporters are needed, most of them belonging to the ATP-binding cassette transporter superfamily [137]. An alternative for the paracellular way is the transcellular transport. Via different kinds of endocytosis, molecules can pass the BBB [142].

1.4.2 The blood-cerebrospinal fluid-barrier

Formed by the arachnoid membrane and the choroid plexus (CP) epithelial cells, the blood-cerebrospinal fluid-barrier (BCSFB) barrier protects the CSF and further, analog to the BBB, the brain from blood-borne substances and potentially detrimental influences[148]. Contrary to the BBB, the tight junctions of the ependymal epithelial cells form the BCSFB of the CP. As the endothelium of the CP is fenestrated and lacking tight junctions, it does not block the movement of small molecules [149]. Though the tight junctions of the CP are quantitatively leakier, the BCSFB of the CP is hosting many of the same transporters like the BBB [149, 148]. Primarily performed by the CP, the CSF secretion is driven by active ion transport via Na^+ and Cl^-. In general, the composition of the CSF has a lot in common with the plasma, but concentrations are different, partly 200 fold lower (e.g. as for total protein) or equal or even slightly higher as for some electrolytes and metabolites [148, 150]. For compounds like Ca^{2+} and various hormones the CP is the mayor site of entry whereas the BBB dominates in the transport of glucose, CO_2, O_2 and amino acids [148].

1.4.3 The meninges

The meninges are a membranous structure and can be divided into three different layers [151]. Starting from the brain, the pia mater is the innermost layer of the meninges. It is attached to the brain parenchyma and allows the influx of CSF into the parenchyma, driven by arterial pulsation [152]. The second layer is the arachnoid mater, which is connected in a web-like structure to the pia mater.

Together they are called the leptomeninges and they build and provide a cavity, called the subarachnoid space, traversed by branches of the arachnoid mater (trabeculae) and filled with CSF [153, 154]. Further, a layer of cells in the arachnoid mater is equipped with tight junctions and thus is able to effectively protect the CSF from unwanted agents. As a result, the arachnoid mater in particular and the meninges as a whole are also referred to as a part of the BCSFB or blood-meningeal barrier [151, 154]. The outermost layer and also connected to the arachnoid mater is the dura mater. While tight junctions are present in the arachnoid mater, the dura mater does not feature them. Instead, the dura mater is strongly vascularized with fenestrated endothelium and provides an eminent interface for exchange of matter and immunological interactions [155, 151].

1.4.4 The role of tight junctions in the BBB and the BCSFB

The tight and adherens junctions are essential for the barrier properties of the BBB and the BCSFB. The integral membrane proteins of the claudin (CLDN) family, junction adhesion molecules (JAMs) and occludin form dimers in the extracellular space and establish a paracellular barrier between adjacent cells [156, 157]. The tight junctions restrict paracellular diffusion and passage of cells, they inhibit intramembrane diffusion of membrane lipids and proteins between the basolateral and apical side of the cell [158, 157, 159, 160] and they are discussed to be maintaining the polarity of the cells [160, 158, 161]. In fact, the tight junction proteins are differentially expressed in several tissues or regions respectively and perform very distinctive and diverse functions, which are not all fully uncovered to date. While CLDN-1, -2, -3, -6, -9, -19 and -22 show a relevant selectivity for the epithelial cells of the CP, CLDN-4, -5 and -16 are considerably more enriched in the microvessels of the brain [162]. Further it has been found, that CLDN-2, -4, -10a, -10b, -15, -17 and -21 can form selective ion channels or even grant permeability to water, as it goes for CLDN-2 and -15 [163]. Therefore, they are able to change a tight junction into a rather leaky one under certain circumstances [164, 165]. Beside the claudins, JAMs are also differentially expressed and provide different functions by different interactions. While they interact homophilic, their adhesive potential links neighboring cells [166] and influences the permeability of the tight junctions [167, 168]. Heterophilic interactions have been found for different JAMs as well as JAMs interacting with other adhesion molecules. By forming such heterodimers, JAMs influence the transendothelial migration of immune cells [168].

The expression of JAMs has further been reported to be proportional to the number of tight junctions and appear very early during the formation of cell-cell contacts [169]. This indicates that they play an important role for the initial formation of tight junctions and further to the assignation of the cell polarity [170, 168]. Occludin is without a family of molecules but is considered a versatile component of the tight junctions. Although a certain redundancy of its function is discussed [171], it has been reported that occludin is involved in establishing cell-cell contact [172], supporting the assembly of tight junctions and the regulation of the actin cytoskeleton [173, 171]. To develop this multiplicity of functions, the transmembrane tight junction proteins are associated with cytoplasmic scaffolding and adaptor proteins like zonula occludens (ZO), cingulin, afadin (AF-6) and 7H6 [157]. The ZO proteins (ZO-1, ZO-1 and ZO-3) themselves can bind to the actin cytoskeleton which provides further regulation of paracellular permeability by relaxation (e.g. via cyclic-AMP) or contraction (e.g. via vascular endothelial growth factor VEGF) of actin stress fibers [137]. Adherens junctions are oriented towards the basal side of the cell [143]. They consist of the membrane protein cadherin, either VE-Cadherin in endothelial cells or E-Cadherin in epithelial cells. By homophilic interactions, they form adhesive contacts between neighboring cells. Via intermediary proteins, the catenins, they interact with the cytoskeleton and via ZO-1 they are interacting and influencing the tight junctions [137].

2. Aim of this Work

TBEV is a neurotropic flavivirus, which can lead to an infection with a severe course of disease including meningitis and meningoencephalitis with the possibility of a fatal outcome or the appearance of serious temporary and long-lasting neurological sequelae. A central but unanswered question is, on which route the virus initially enters the brain and how the type I IFN system is involved in this process. In humans, a TBEV infection is often asymptomatic and only a small fraction of the infected individuals develops severe neurological symptoms. Since this is not reflected in laboratory animal models, LGTV should be used as a surrogate model. LGTV and TBEV share over 80% of their serological identity and with LGTV asymptomatic infections can be investigated in mice. Further, while TBEV has to be handled under biosafety level 3 conditions, LGTV can be handled under biosafety level 2 conditions. The type I IFN system is crucial for the effective defense against infections. To elucidate the influence of the type I IFN system on several aspects of the LGTV invasion in the brain, two different genotypes of mice were used for all experiments. Highly susceptible Ifnar$^{-/-}$ mice were compared to asymptomatic WT mice. To approach the question of the viral brain entry, the kinetic of the viral replication in several brain regions should be determined. Moreover, viruses can use different ways to reach the brain and spread further inside. Often, the blood or the CSF are the expedient means for that. By determining the viral load in the serum and the CSF, their role in infection and spreading of the virus in the brain should be analyzed. Additionally, viruses can show all kinds of different cellular tropisms and those in turn can often give information about the course of infection and cell type specific functions. To examine if the type I IFN system takes over a cell-specific function after LGTV infection, the cells in the brains of the two different genotypes should be examined concerning their susceptibility towards an LGTV infection. Furthermore, several barriers protect the brain, namely the BBB, the BCSFB and the meninges, which limit and regulate the entry of molecules and cells. Therefore, the time point for the infection of those barriers should be determined. Finally, overcoming the protective brain barriers can be realized by different mechanisms and is often associated with an affected barrier integrity. To examine to which extend a LGTV infection influences the brain barriers, the expression of several tight junction genes should be analyzed during the course of infection.

3. Results

3.1 Viral distribution

Infection with TBEV can lead to infection of the brain and produce severe disease states. Although there is several information in the literature about TBEV and LGTV and their ability to cause a disease in the CNS, it is unknown how they initially infiltrate the brain and infect the brain parenchyma. With no specific treatment against TBE available, it is important to understand the mechanisms, which TBEV relies on to reach the brain. With those in hand, it could be possible to develop strategies that prevent or reduce the transition of TBEV from the periphery into the CNS. As a recent study shows [74], there could be a usable therapeutic window between the systemic expansion, often associated with febrile illness like symptoms, and the neurological manifestation of TBE. To address this issue, we use LGTV as a surrogate model for TBEV, to examine the distribution of the virus in connection to infected cells and the influence on the barriers of the CNS.

3.1.1 Viral RNA of LGTV detected earliest in the olfactory bulb

For LGTV it has been shown *in vivo* that viral RNA is detectable in the brain of Ifnar$^{-/-}$ mice two days before the breakdown of the BBB verified by Evans blue [60]. This indicates that the virus can enter the brain without an opening of the BBB. Recently, another study showed an early infection of the olfactory bulb (OB) and the deep cervical lymph nodes with LGTV, hinting at an early involvement of the BCSFB in the entry strategy of LGTV into the brain [136]. The CP with its structure and function is the essential part of the BCSFB [146]. To investigate the role of the BSCSF in the virus entry to the brain and the spread in different brain parts, the viral replication in different brain regions and the CP was determined during the course of infection. At first, different regions of the brain were compared to the CP to examine the regions at the time point of LGTV replication and the role of type I IFNs. For that purpose wild-type C57BL/6 (WT) mice and Interferon-α receptor deficient (Ifnar$^{-/-}$) mice were infected with 10^2 focus forming units (FFUs) subcutaneous (SC) in the right hind leg. WT mice survive the infection and show no signs of disease. Ifnar$^{-/-}$ mice succumb to the infection after four to six days and show distinct signs of disease [136, 60]. The time points 0 (uninfected), 24, 48 and 72 hours post infection (hpi) were chosen for analysis.

At those time points, the brains of the mice were isolated. It has been shown that the OB is the brain region where LGTV RNA was detected first [136] and to the highest amount [60] during the course of infection. To discern if the virus is spreading from the OB to an adjacent or far off region, also the frontal cortex (FC), which lies in direct vicinity to the OB, and the cerebellum (Cbel), which lies on the opposite side of the brain, were isolated. Further, the CP from the lateral ventricles and the fourth ventricle was isolated and pooled. RNA of LGTV (RNA coding for LGTV NS3 protein) was measured by quantitative real-time, reverse transcriptase polymerase chain reaction (qRT-PCR) (Figure 2A). In WT mice, no LGTV RNA was measurable during the first analyzed time point post infection (24 hpi) in any of the examined brain regions. After 48 hpi, the first and only brain region which showed viral RNA in WT mice was the OB (Figure 2B). At the last analyzed time point of 72 hpi, the OB showed an equal amount of virus as during the previous time point (Figure 2B) and the FC started to show viral RNA to a similar extend as the OB (Figure 2C+F). The Cbel and the CP stayed free of measurable amounts of LGTV RNA during all measured time points in the WT mice (Figure 2D+E). In Ifnar$^{-/-}$ mice the earliest time point at which LGTV was measurable was 24 hpi in the OB (Figure 2B). At this time point the amount of virus in Ifnar$^{-/-}$ mice was comparable to the 48 hpi time point in WT mice (Figure 2B). While 48 hpi the amount of LGTV RNA in the OB of Ifnar$^{-/-}$ mice did not increase significantly compared to the earlier time point and was comparable to the WT mice at the same time point (Figure 2B), the FC and the CP started showing viral RNA. This was not the case for the WT mice at this time point (Figure 2C+E). At 72 hpi, the amount of LGTV RNA in Ifnar$^{-/-}$ mice significantly increased over the values at 48 hpi in the OB, Cbel and CP while it kept steady in the FC. For the Cbel, 72 hpi was the only time point at which virus could be detected. Across all analyzed brain regions, the amount of viral RNA was significantly higher in Ifnar$^{-/-}$ mice compared to the WT mice at 72 hpi. Although the earliest detection of viral RNA was in the OB of Ifnar$^{-/-}$ mice 24 hpi, the direct comparison of the latest time point in the experiment, 72 hpi, showed the significantly highest proportion of viral RNA in the CP of Ifnar$^{-/-}$ mice at that point (Figure 2F). These results show that the type I IFN system has a varying impact on the amount of viral RNA in distinct brain regions. Type I IFN protects the Cbel and the CP completely during the early stages of LGTV infection in WT mice. However, in the OB and the FC only the onset of viral replication is delayed and the amount of viral RNA stays at lower levels in WT mice compared to Ifnar$^{-/-}$ mice.

In addition, although the OB lies in direct vicinity to the FC, in the latter the onset of infection is later and never reaches these high amounts of viral RNA than what can be seen in the OB. This indicates that the brain region plays a role for the entry of LGTV into the brain.

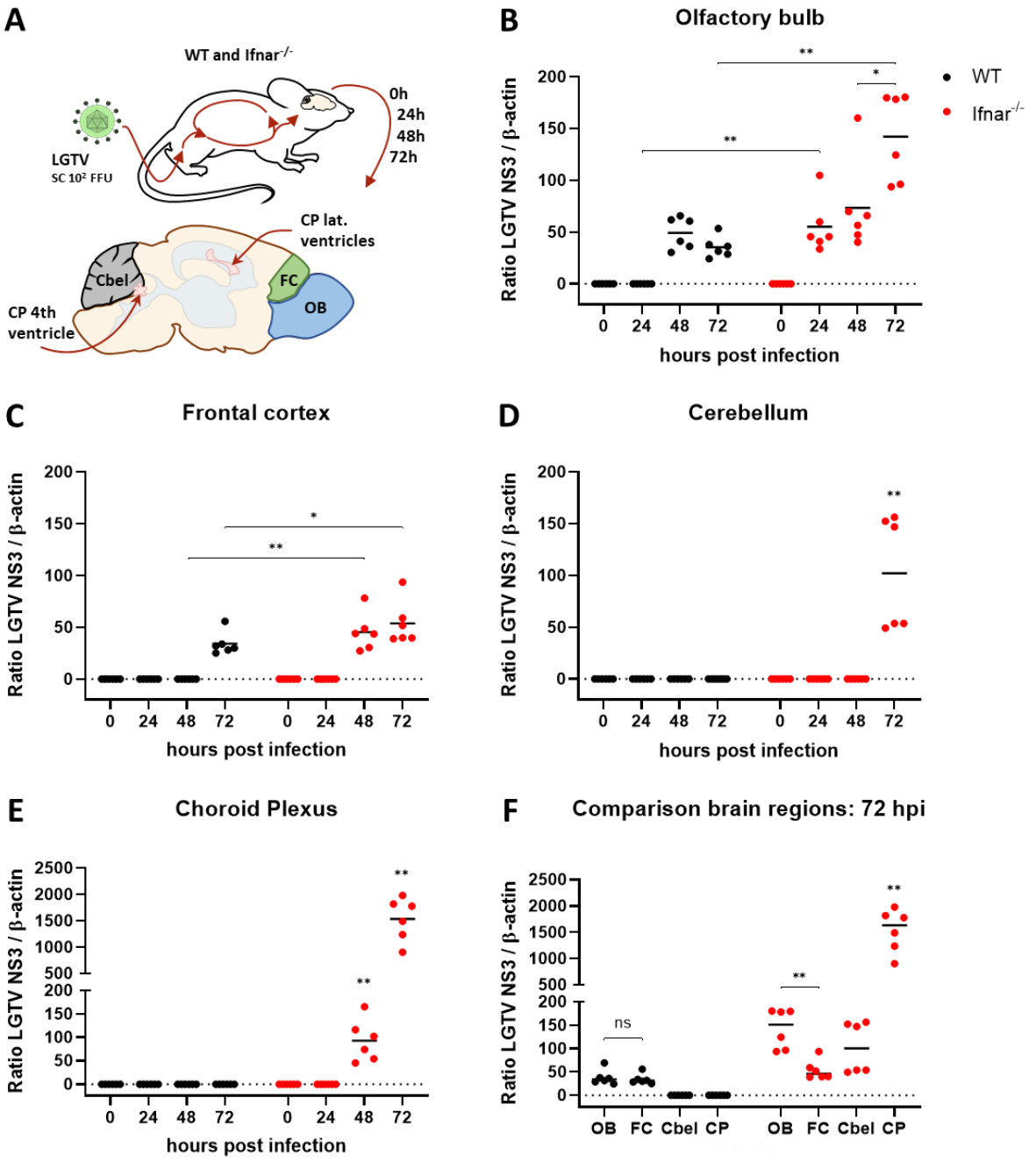

Figure 2: Detection of LGTV in different brain regions via qRT-PCR
A. Schematic depiction of the experimental procedure. WT and Ifnar$^{-/-}$ mice were infected via SC injection at the left hind leg with 10^2 FFUs LGTV. The RNA levels for LGTV at the indicated time points were analyzed by qRT-PCR for **B.** the OB, **C.** the FC **D.** the Cbel and **E.** the CP. The time point 0 represents the uninfected controls. **F.** Direct comparison of the results from figures B-E between the different brain regions at the time point 72 hpi. The results are representative for two independent experiments (n = 6). Error bars represent the mean. For statistical analysis pairwise, two-tailed Mann-Whitney test was used (ns, not significant; *, $P < 0.05$; **, $P < 0.01$).

3.1.2 Late infection of meninges and brain microvessels

Beside the CP as producer of the CSF, also the meninges share a great contact surface with the CSF and are crossed by meningeal lymphatic vessels [174]. Like the CSF, those lymphatic vessels are drained by the deep cervical lymph nodes. In part, the meninges have been identified as infected during a LGTV infection [60]. As a result, they represent a possible target for the entry strategy of LGTV into the brain. Alongside the meninges, the microvessels of the brain parenchyma as part of the BBB are a further interesting target. In *in vitro* studies, it has been shown that TBEV is able to infect brain microvascular endothelial cells without an impairment of the functionality of the BBB [132]. However, it is not clear if the infection takes place *in vivo* and already in early stages of the LGTV infection. To address these questions and compare them to the obtained data from the OB, FC, Cbel and CP, WT mice and Ifnar$^{-/-}$ mice were infected with 10^2 FFUs SC in the right hind leg. At the time points 0 (uninfected), 24, 48 and 72 hpi the skull of the mice was opened in a transversal plane without damaging the brain or the skullcap. The brains were isolated from the skull base and the obtainable meninges (dura mater and partly the arachnoid mater) from the skullcap (Figure 3A). After removing the remaining parts of the meninges from the brain (pia mater and partly the arachnoid mater), the whole brain was minced thoroughly and processed by multiple density gradient centrifugation steps (Figure 3B). For the isolated meninges and brain microvessels (BMVs), the RNA of LGTV was analyzed by qRT-PCR (Figure 3C+D). In WT mice, no LGTV RNA was detectable at all, neither in the meninges nor in the BMVs. While in the CP the RNA of LGTV was already detectable 48 hpi in Ifnar$^{-/-}$ mice, the meninges were firstly infected 72 hpi (Figure 3C). The BMVs shared the same finding, but with a much higher variability and proportion among the RNA amounts (Figure 3D). The late infection of the BMVs and the meninges compared to other regions in the brain indicates a less relevant contribution to the initial brain entry of LGTV.

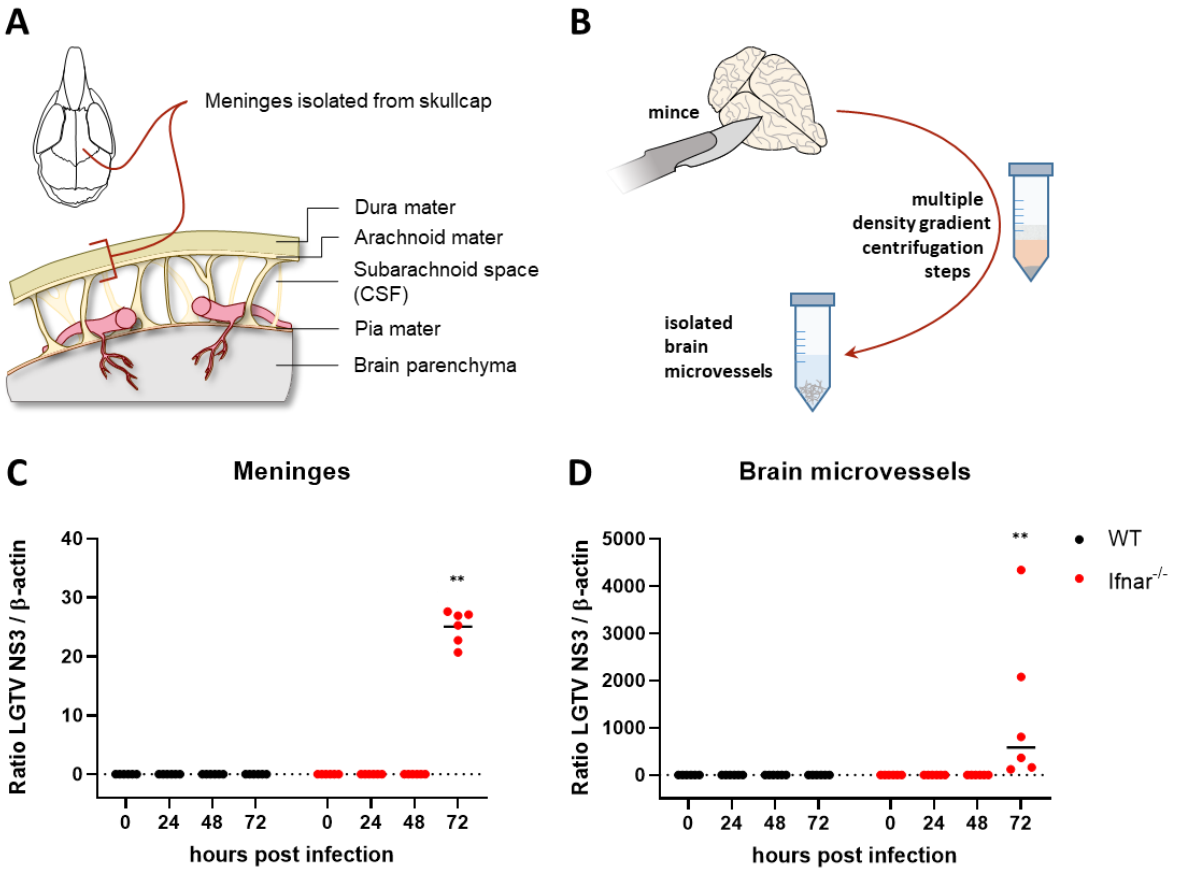

Figure 3: Detection of LGTV in relevant tissue for the BBB and the BCSFB
Schematic depiction of the experimental procedure for **A.** the isolation of the meninges and **B.** the BMV isolation. WT and Ifnar$^{-/-}$ mice were infected via SC injection at the left hind leg with 10^2 FFUs LGTV. The RNA levels for LGTV at the indicated time points were analyzed by qRT-PCR for **C.** the meninges and **D.** the BMVs. The time point 0 represents the uninfected controls. The results are representative for two independent experiments (n = 6). Error bars represent the mean. For statistical analysis pairwise, two-tailed Mann-Whitney test was used (ns, not significant; *, P < 0.05; **, P < 0.01).

3.1.3 CSF stays clear of replicable LGTV during early CNS infection

Several studies of human TBEV infection showed [175–177], that viral RNA is rarely detectable in the CSF during the earlier stages of the disease. Therefore, it is considered an unreliable marker for diagnosis. As the infection with TBEV is often going unnoticed [71] the timeframe of patient examination and possibly small amounts of viral RNA in the samples might be underlying for some inconsistencies in the analysis of the CSF regarding TBEV patients. To assess if the CSF could still play a relevant role for the entry or distribution of LGTV into the brain, it needs to be determined if and at which time point replicable LGTV is present in the CSF and to which amount. For this purpose WT and Ifnar$^{-/-}$ mice were infected with 10^2 FFUs, SC in the right hind leg.

At the time points 0 (uninfected), 24, 48 and 72 hpi the mice were killed with an overdose of CO_2 and directly afterwards all fur, skin and tissue was removed from the back part of the head to expose the cisterna magna. CSF was collected with a very thin glass capillary by cisterna magna puncture. Hearth blood was collected to isolate serum as a positive control. Replication competent virus was determined by a FFU assay.

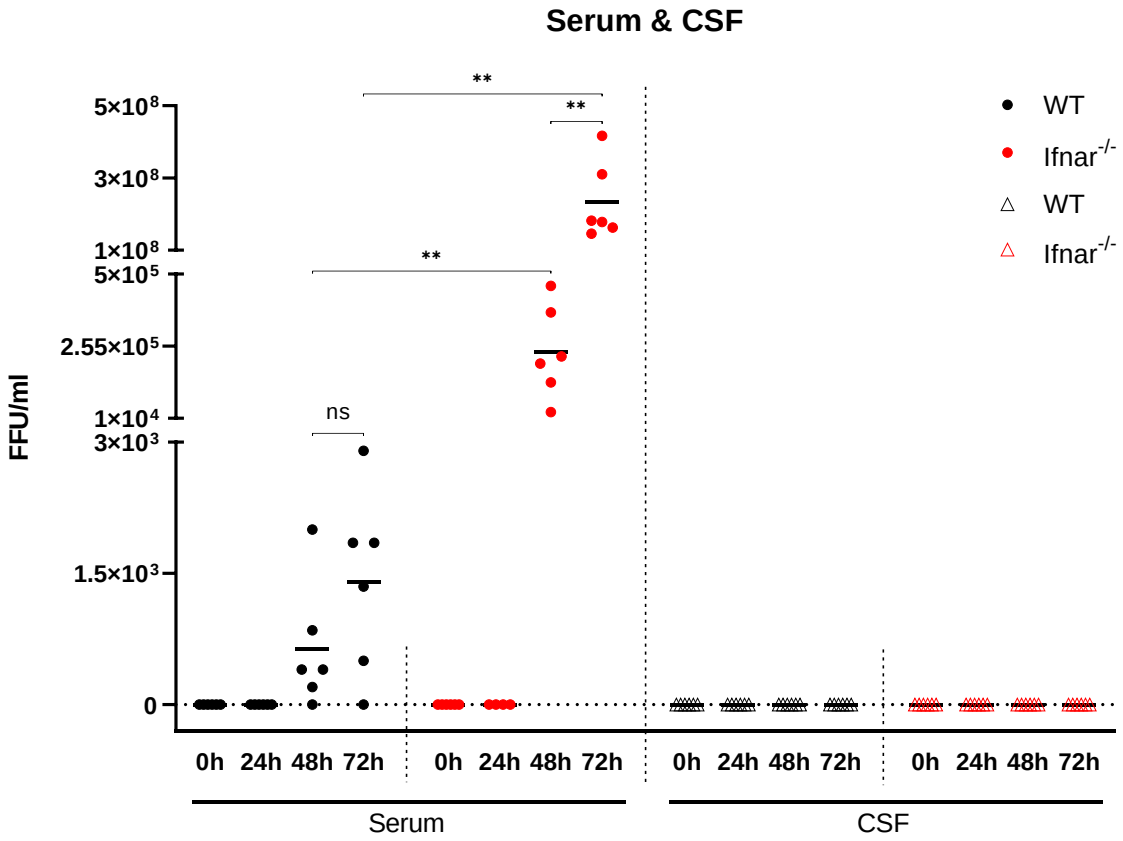

Figure 4: The CSF shows no LGTV RNA after peripheral infection with LGTV
WT and Ifnar$^{-/-}$ mice were infected via SC injection at the left hind leg with 10^2 FFUs LGTV. The cisterna magna was punctured and the CSF was isolated. Subsequently hearth blood was obtained to isolate the serum. The FFUs for LGTV at the indicated time points were determined with a FFU assay performed on Vero cells. Biological duplicates were made for each sample. The results are representative for two independent experiments (n = 6). Error bars represent the mean. For statistical analysis pairwise, two-tailed Mann-Whitney test was used (ns, not significant; *, $P < 0.05$; **, $P < 0.01$).

In the serum, LGTV foci were detected earliest 48 hpi for WT and Ifnar$^{-/-}$ mice (Figure 4). However, the detected concentration of viral particles was significantly higher in Ifnar$^{-/-}$ mice. Towards 72 hpi, the number of FFUs increased slightly in WT mice and significantly in the Ifnar$^{-/-}$ mice. Furthermore the virus concentration in the serum of Ifnar$^{-/-}$ mice is significantly higher 72 hpi compared to the WT mice at the same time point. For the CSF, no FFUs could be verified at any examined time point in WT and Ifnar$^{-/-}$ mice.

This indicates that the entry strategy for LGTV to reach the brain might not primarily rely on the CSF, although the low amount of CSF that could be extracted and the sensitivity of the assay have to be taken into account.

3.2 Cellular tropism of LGTV in the CNS

Neurons have been described as a main target of LGTV and TBEV [178, 61, 60], but also Iba-1^{+} microglia and GFAP^{+} astrocytes showed some level of infection [179, 61].
Still, *in vivo* there are LGTV infected cells that remained unidentified and it has not been made clear, which cells are infected at the early time points when LGTV initially gains entry to the CNS. As this could provide information about the entry strategy or the possible entry site of LGTV, the brains of LGTV infected mice were immunohistologically examined to gather more data about the viral kinetics inside the brain.

3.2.1 LGTV is detectable mainly in the OB and the CP by immunohistology

To identify the sites of LGTV infection in the brain, immunohistological analyses were performed. WT and Ifnar$^{-/-}$ mice were infected with 10^2 FFUs LGTV, SC in the right hind leg. At the time points 0 (uninfected), 24, 48, 72 and 96 hpi the brains were harvested and prepared for immunofluorescence analyses. 30 µm tissue slices were labeled with an antibody against the LGTV non-structural protein 3 (NS3) to locate the virus in the brain. As a result, LGTV was not detectable by immunohistology at any analyzed time point in WT mice (data not shown). The earliest time point at which LGTV was detectable in the brain of Ifnar$^{-/-}$ mice was 72 hpi in the CP (shown in detail under 3.2.2). At 96 hpi, LGTV could be shown in the OB, the CP and at the meninges that were still attached to the brain (Figure 5). The bigger black or empty areas in the microscopic pictures of Figure 5 were identified as air bubbles or folds and were not the result of the LGTV infection. A comparison of immunofluorescence and qRT-PCR results showed, that immunofluorescence was less sensitive and detection of low amounts of viral protein at early stages of the infection or in general in the brain of WT mice was impossible. Nonetheless, immunofluorescence microscopy was still essential to identify infected cells and to gain insights about their distribution in the brain. By qRT-PCR, LGTV was detectable first in the OB and with a 24h delay in the FC and CP of Ifnar$^{-/-}$ mice.

By immunofluorescence microscopy, the virus was detectable earliest in the CP 72 hpi. This corresponds with the qRT-PCR data that showed the highest viral load for the CP compared to the other analyzed brain regions at that time point.

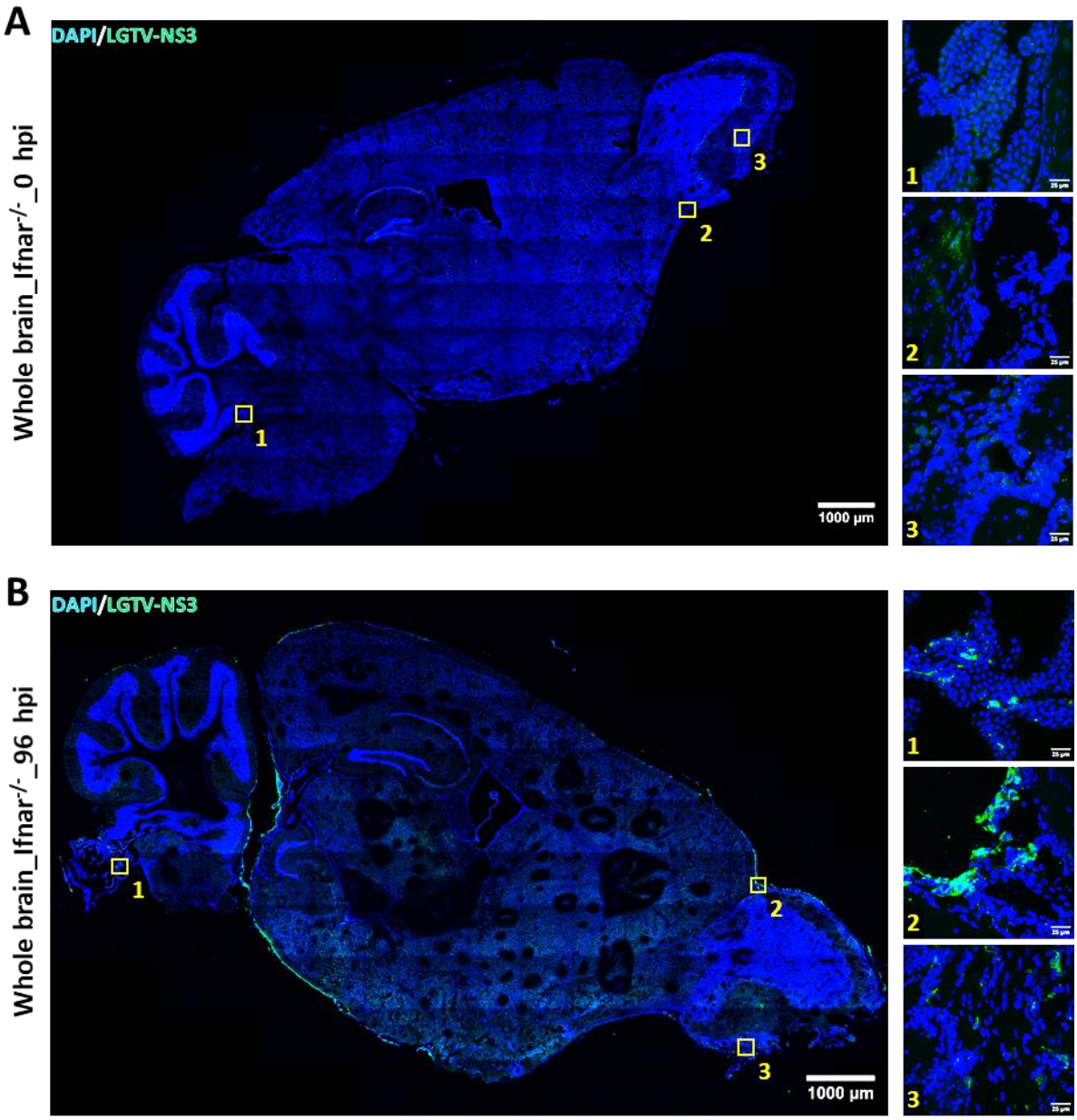

Figure 5: Immunohistological detection of LGTV in OB, CP and meninges of Ifnar$^{-/-}$ mice 96 hpi. Brains of SC infected Ifnar$^{-/-}$ mice were isolated after the indicated time points. Thereof gained 30 µm sections were labeled with an antibody against LGTV NS3. A Secondary antibody labeled with a fluorophore was used for detection with immunofluorescence microscopy in the indicated color. DAPI was used to stain AT rich DNA (nuclei). The generated microscopy images were stitched together for a full view image of the whole brain section. Yellow square 1 indicates area of the CP depicted zoomed in. Yellow square 2 indicates area of the meningeal tissue depicted zoomed in. Yellow square 3 indicates area of the OB depicted zoomed in. The images are representative for two independent experiments (n=6).

Assuming that the viral load in the other infected brain regions increases further over time in the Ifnar$^{-/-}$ mice, the visualization of the infection at 96 hpi in the OB, CP and the meninges is a coherent finding. The qRT-PCR data and the immunofluorescence observations show that locally distant brain regions are infected in short temporal succession in Ifnar$^{-/-}$ mice. This data could indicate that either LGTV uses the CSF for spreading from the entry site to regions that are more distant or that the virus has multiple entry sites into the brain.

3.2.2 Abundant LGTV infection of Iba-1^{+} cells

As previously shown in this work, an infection could not be detected by immunofluorescence microscopy for the time points 0 (uninfected), 24 and 48 hpi in Ifnar$^{-/-}$ mice and for all time points in WT mice. For that reason, in the following figures the focus is on the 0, 72 or 96 hpi time points of Ifnar$^{-/-}$ mice in order to be able to compare these time points in more detail. As it has been published that LGTV targets neurons in the brain, 30 µm tissue slices were labeled with antibodies against neuronal nuclei (NeuN) and LGTV. NeuN is a protein that is mainly located in the cell nuclei and to lesser extend in the perinuclear cytoplasm of differentiated postmitotic neurons [180]. Interestingly, in the infected regions of the brain, no NeuN^{+} cells were infected with LGTV (Figure 6A+B). In addition, the infected cells showed evidently high similarities in morphology with microglia or macrophages (Figure 6B). Hence, brain sections were labeled with antibodies against the ionized calcium-binding adapter molecule 1 (Iba-1), the transmembrane protein 119 (TMEM119) and LGTV. Iba-1 is a marker for microglia activation in the brain and allows valuable insight into the morphological changes of those cells in different physiological conditions [181–183]. Peripheral macrophages can infiltrate the brain [184–187], share morphological traits of microglia in the brain and they share Iba-1 as a marker [188]. TMEM119 was identified as microglia specific marker [189, 190] and is used in combination with Iba-1 to allow a more reliable differentiation between infiltrating macrophages and resident microglia [191]. The Iba-1 staining showed the expected ramified phenotype of microglia cells in a healthy brain (Figure 6C). Characteristic are the many fine processes that expand around the cell body and the rather homogenous distribution pattern across the tissue [183, 181, 182]. The TMEM119 staining is mostly matching the Iba-1 staining, especially at the processes of the microglia (Figure 6C).

At 96 hpi, when the LGTV infection was clearly traceable by immunofluorescence microscopy, the phenotype of the Iba-1^{+} cells clearly changed to a lesser ramified, more amoeboid shape with fewer processes and a more patchy distribution pattern (Figure 6D).

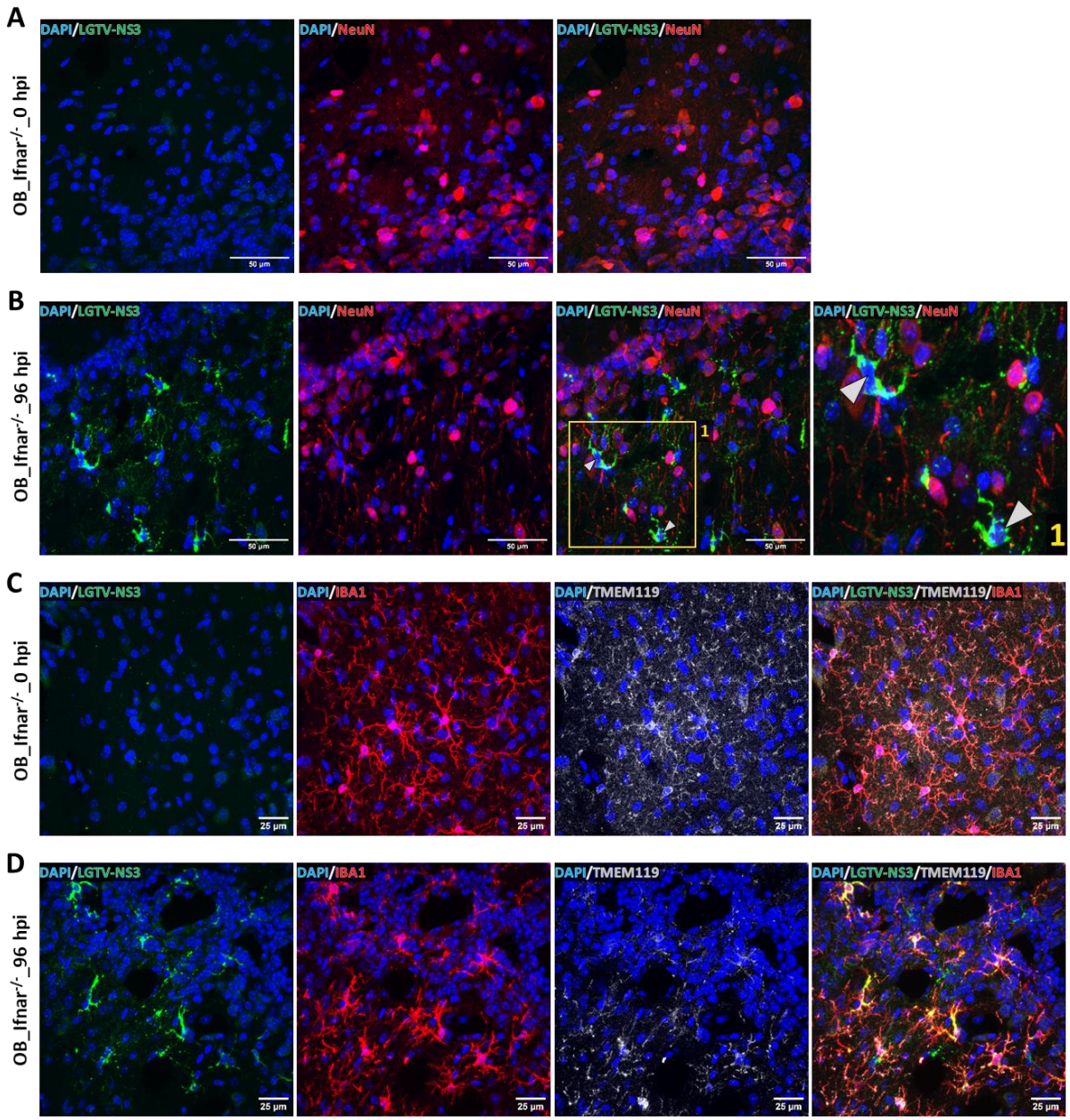

Figure 6: LGTV infects Iba-1^{+} cells in the OB of Ifnar$^{-/-}$ mice 96 hpi.
Brains of SC infected Ifnar$^{-/-}$ mice were isolated after the indicated time points. Thereof gained 30 µm sections were labeled with antibodies against Iba-1 (microglia/macrophages), TMEM119 (microglia) NeuN (neurons) and LGTV NS3. Secondary antibodies labeled with fluorophores were used for detection with immunofluorescence microscopy in the indicated colors. DAPI was used to stain AT rich DNA (nuclei). **A-D.** The depicted regions belong to the outer plexiform and the glomerular layer of the OB. **B.** Yellow square 1 indicates the region of interest depicted zoomed in at the right. White arrows indicate LGTV infected cells. The images are representative for two independent experiments (n=6).

The fluorescence for TMEM119 was decreased but resembled the changed morphological state the microglia were in. It could clearly be shown, that the signal for LGTV was overlapping with the Iba-1 fluorescence, indicating an abundant infection of Iba-1^{+} cells (Figure 6D). Caused by the reduced fluorescence intensity of the TMEM119, the overlap with the Iba-1 signals was harder to determine as in the uninfected animals. This led to the observation that not all LGTV infected cells could be identified as TMEM119^{+} or TMEM119^{-}.

Shifting the attention from the OB to the CP, in the next step the cellular tropism of LGTV in the CP was examined. Therefore, 30 µm tissue sections were used. Sections were labeled with antibodies against LGTV, Iba-1 and CD45 (infiltrating leukocytes). CD45 is expressed, although in different patterns, on all cells of the hematopoietic lineage [192]. While T-, B- and NK-Cells show stronger expression patterns, erythrocytes, activated neutrophils and macrophages show a weaker expression of CD45 [192]. In addition, most brain resident cells usually show no CD45 expression. In the case of the distinction between brain resident microglia and infiltrating macrophages, the specification of CD45 – intermediate or CD45 - low (CD45^{med}/ CD45^{low}) has often been assigned to resident microglia and macrophages while CD45 - high (CD45^{high}) is assigned to the infiltrating macrophages [193–196]. Microscopic analyses of the immunolabeling in the CP showed Iba-1^{+} and CD45^{+} cells in Ifnar$^{-/-}$ mice to similar amounts in uninfected animals and 72 hpi (Figure 7A+B). Addressing LGTV, the images show Iba-1^{+}, CD45^{low} infected cells (Figure 7B+C) as well as Iba-1^{low}, CD45^{low} /CD45^{-} infected cells (Figure 7B+D). CD45^{high} cells were not infected. The fluorescence for CD45 was not always precisely identifiable as low or negative. This Data indicates that a resident phenotype of macrophages is infected in the CP. The infiltrating, CD45^{high} cell population was not infected with LGTV. Hence, these cells might not play a role for the migration of the virus into the CP.

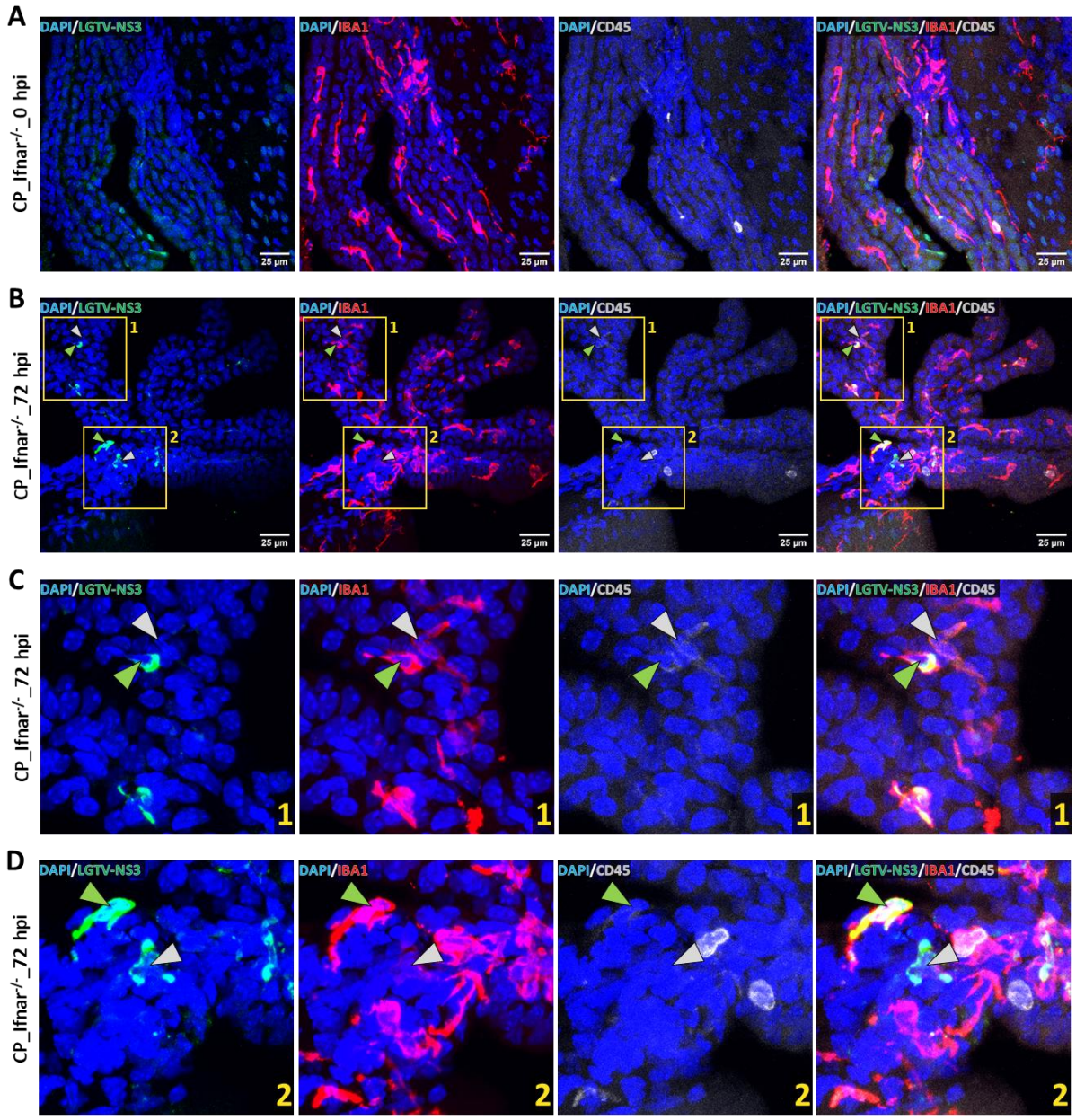

Figure 7: LGTV infects CD45^{low} Iba-1^{+} cells in the CP of Ifnar$^{-/-}$ mice 72 hpi.
Brains of SC infected Ifnar$^{-/-}$ mice were isolated after the indicated time points. Thereof gained 30 µm sections were labeled with antibodies against Iba-1 (microglia/macrophages), CD45 (infiltrating leucocytes) and LGTV NS3. Secondary antibodies labeled with fluorophores were used for detection with immunofluorescence microscopy in the indicated colors. DAPI was used to stain AT rich DNA (nuclei). **A-B.** Sections of the CP are depicted. Yellow square 1 indicates region of interest depicted zoomed in for **C**. Yellow square 2 indicates region of interest depicted zoomed in for **D**. Green arrows indicate Iba-1^{+}, CD45^{low} LGTV infected cells. White arrows indicate Iba-1^{low}, CD45^{-} LGTV infected cells. The images are representative for two independent experiments (n=6).

3.2.3 No LGTV infection in epithelial or endothelial cells of the BCSFB and BBB

As the qRT-PCR results showed an infection of the BMVs in Ifnar$^{-/-}$ mice, immunofluorescence microscopy was used to identify infected cells of the barrier facilitating microvessels in the BBB. Additionally, the leaky microvessels and the adjacent border forming epithelial cells of the BCSFB in the CP and their environment were analyzed. Starting with the BBB, histological sections of the brain were labeled with an antibody against LGTV, CD45 (infiltrating leukocytes) and with *solanum tuberosum* lectin (STL) (binds N-acetylglucosamine of blood vessels and macrophages/microglia [197, 198]). The staining showed no differences between the blood vessels of uninfected and infected Ifnar$^{-/-}$ mice 96 hpi (Figure 8A+B). The blood vessels were always without any double positive staining for LGTV. Interestingly, the infected cells in Ifnar$^{-/-}$ mice were often located near the blood vessels as well as the CD45^{+} cells, but a co-staining with LGTV was not observed (Figure 8B). Further, the staining with STL indicated that the infected cells near the blood vessels were microglia (Figure 8C).

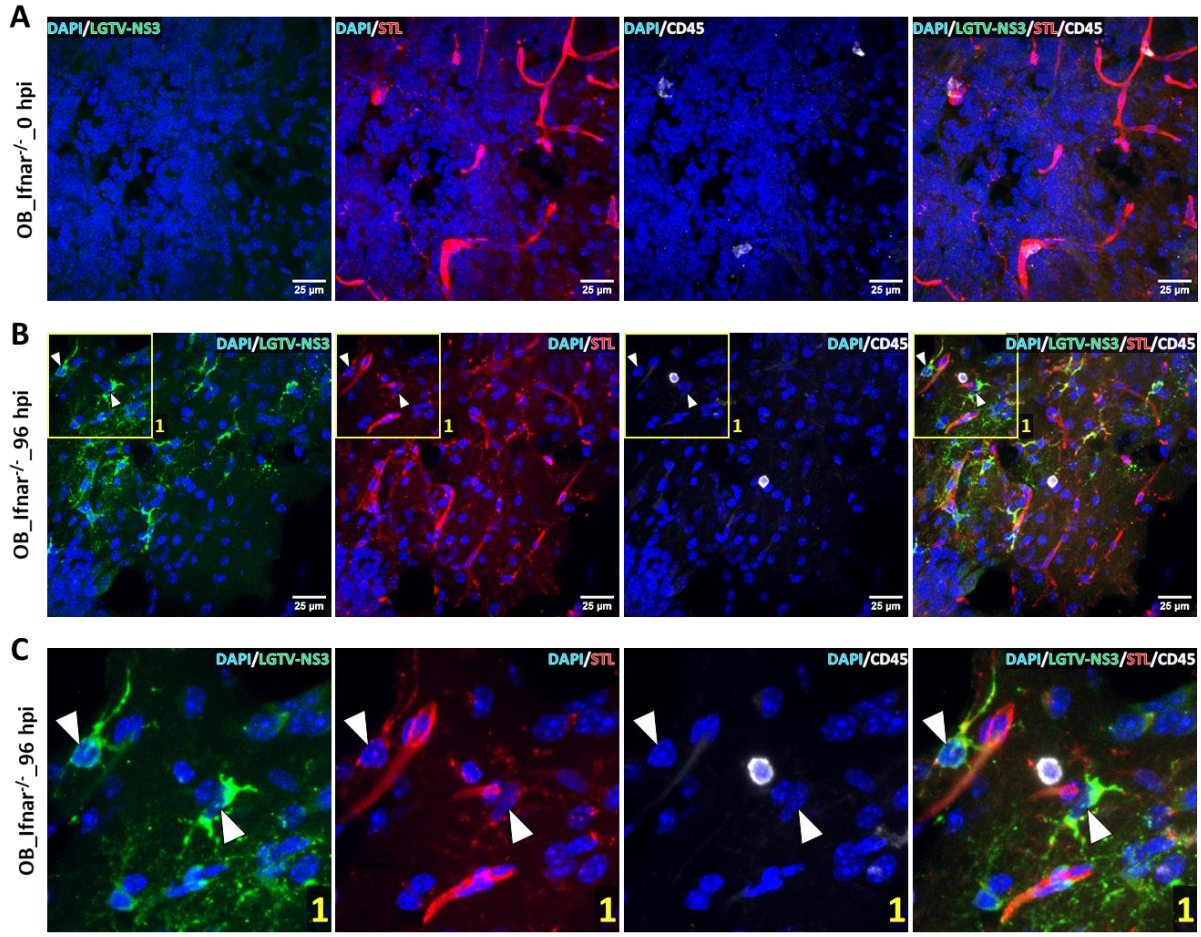

Figure 8: LGTV infected cells are located near blood vessels in the OB of Ifnar$^{-/-}$ mice 96 hpi.
Brains of SC infected Ifnar$^{-/-}$ mice were isolated after the indicated time points. Thereof gained 30 µm sections were labeled with primary antibodies against CD45 (infiltrating leukocytes) and LGTV NS3. Biotinylated STL was used to bind N-acetylglucosamine (blood vessels). Secondary antibodies labeled with fluorophores were used for detection with immunofluorescence microscopy in the indicated colors. AlexaFluor488 labeled streptavidin was used to detect biotin. DAPI was used to stain AT-rich DNA (nuclei). **A-B**. The depicted regions belong to the outer plexiform and the granular layer of the OB. Yellow square 1 indicates the region of interest depicted zoomed in at **C.** White arrows indicate LGTV infected microglia. The pictures are representative for two independent experiments (n=6).

To examine the BCSFB in the CP, 30 µm brain sections were labeled with antibodies against LGTV and E-Cadherin (epithelial cells of the CP), to assess if they are possible targets for LGTV. E-Cadherin is expressed specific in most epithelial cells [199, 200] and has successfully been used to study infections of the CP [201, 202]. The epithelial cells of the CP are of special interest in the context of LGTV infection as they express tight junction proteins and form the BCSFB. The microscopic images show a strong staining for E-Cadherin in the uninfected CP as well as in the CP of Ifnar$^{-/-}$ mice 72 hpi (Figure 9A+B). Further, the honeycomb-like morphology of the epithelial cells could be seen.

The evaluation of the staining in the infected Ifnar$^{-/-}$ mice at 72 hpi revealed, that E-Cadherin showed no co-staining with LGTV and the morphology of the epithelial cells differs largely from the infected cells, them showing a much more amorphic shape with visible outstretching dendrite elements (Figure 9B). This data is indicating that LGTV does not infect CP epithelial cells *in vivo*.

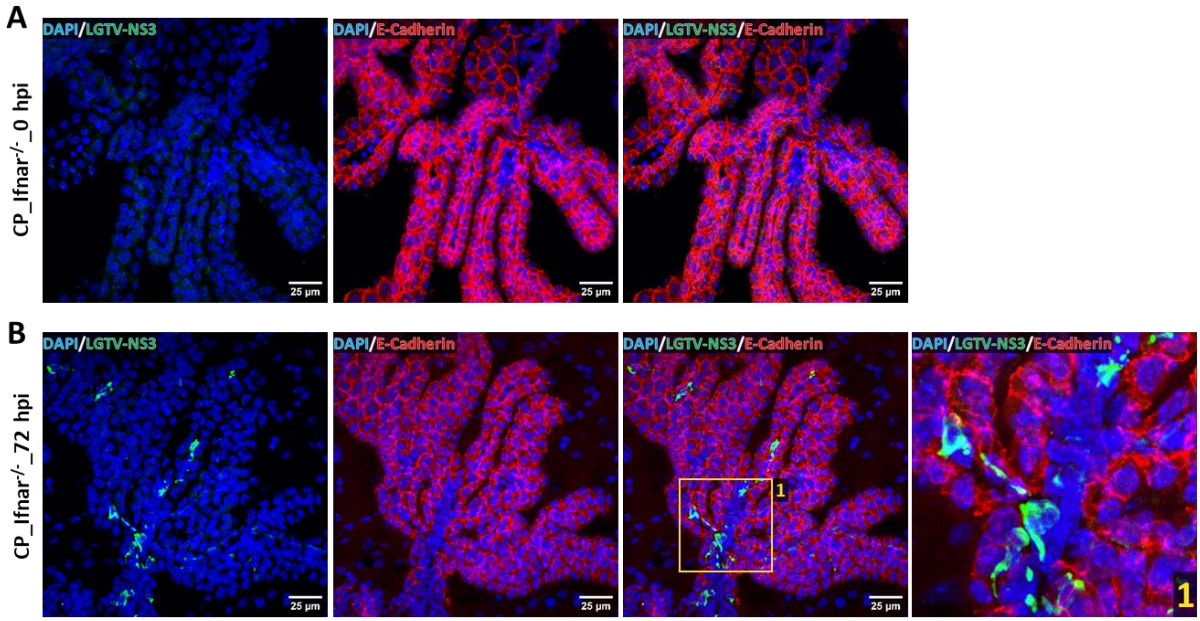

Figure 9: Epithelial cells in the CP are no target of LGTV in Ifnar$^{-/-}$ mice 72 hpi
Brains of SC infected Ifnar-/- mice were isolated after the indicated time points. Thereof gained 30 µm sections were labeled with primary antibodies against LGTV NS3 and E-Cadherin (epithelial cells). DAPI was used to stain AT-rich DNA (nuclei). **A-B.** The section of the CP is depicted. The pictures are representative for two independent experiments (n=6).

For the following experiment, whole-tissue mounts of the CP were labeled with antibodies against LGTV and CD140b (also known as platelet-derived growth factor receptor β (PDGFR-β)) to see if pericytes are infected. PDGFRβ is considered to be downregulated in more mature pericytes [203, 204] but still has been identified as a specific marker for pericytes [205] and used successfully to stain pericytes in a Zika infection model in the CP of mice [206]. Further, STL was used to label the blood vessels in the CP. With the staining it was possible to locate the vessels and pericytes in CP whole tissue mounts of uninfected Ifnar$^{-/-}$ mice and after 72 hpi (Figure 10A+B). The results showed that, like in the OB, the infected cells in the CP were located in proximity to the blood vessels, but the endothelium could not be found infected with LGTV. In addition, the occasional infection of pericytes was found (Figure 10 B+C).

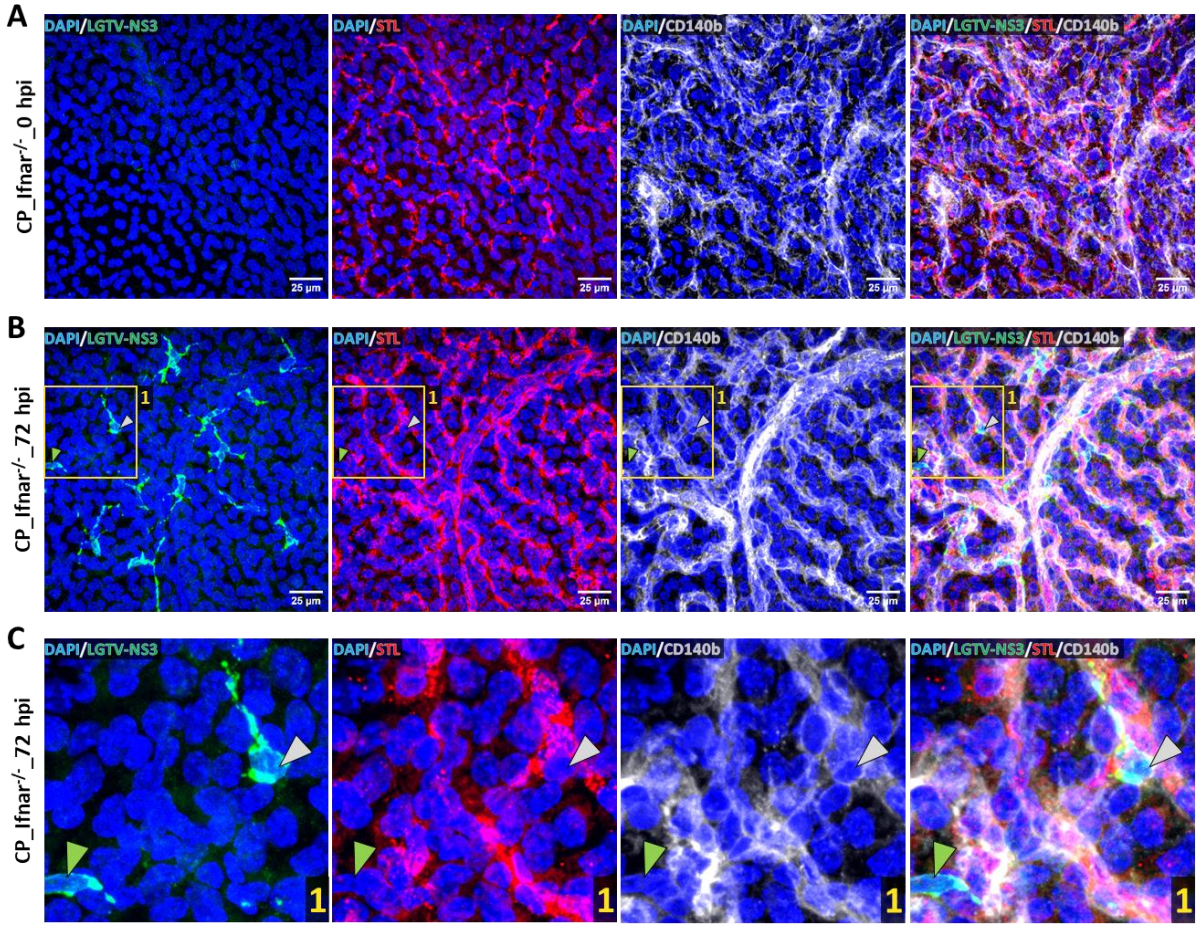

Figure 10: Sparse LGTV infection of pericytes near blood vessels in the CP of Ifnar$^{-/-}$ mice 72 hpi. Brains of SC infected Ifnar$^{-/-}$ mice were isolated after the indicated time points. Thereof gained whole mount samples were labeled with primary and secondary antibodies for immunofluorescence microscopy in the indicated colors. DAPI was used to stain AT-rich DNA (nuclei). **A-B.** The whole-tissue mount of the CP is depicted, labeled with antibodies against LGTV NS3 and CD140b (pericytes). Biotinylated STL was used to bind N-acetylglucosamine (blood vessels) and AlexaFluor488 labeled streptavidin was used to detect biotin. The yellow square 1 indicates the region of interest depicted zoomed in for **C.** The green arrows indicates a CD140b^{-} LGTV infected cell outside of the microvessels. The white arrow indicates a CD140b^{+} LGTV infected cell outside the microvessels. The pictures are representative for two independent experiments (n=6).

3.2.4 LGTV infection of Iba-1^{+} cells in the meninges in the absence of Ifnar

To obtain information on the tropism of LGTV in the meninges, they were isolated from skullcaps as whole-tissue mounts and labeled with antibodies against CD45, Iba-1 and LGTV.

In uninfected Ifnar$^{-/-}$ animals, the staining of the meninges showed CD45^{+} and very few Iba-1^{low} cells (Figure 11A). After 72 hpi, a great number of LGTV infected cells was detected. While the number of CD45^{+} cells remained almost the same after infection, the number of Iba-1^{+} cells increased strongly (Figure 11B).

Further, it could be estimated that there was no big difference between the uninfected animals compared to the infected ones in CD45^{high} cells. However, the pictures allow the assumption that there are more CD45^{low} cells in the infected animals (Figure 11A+B).

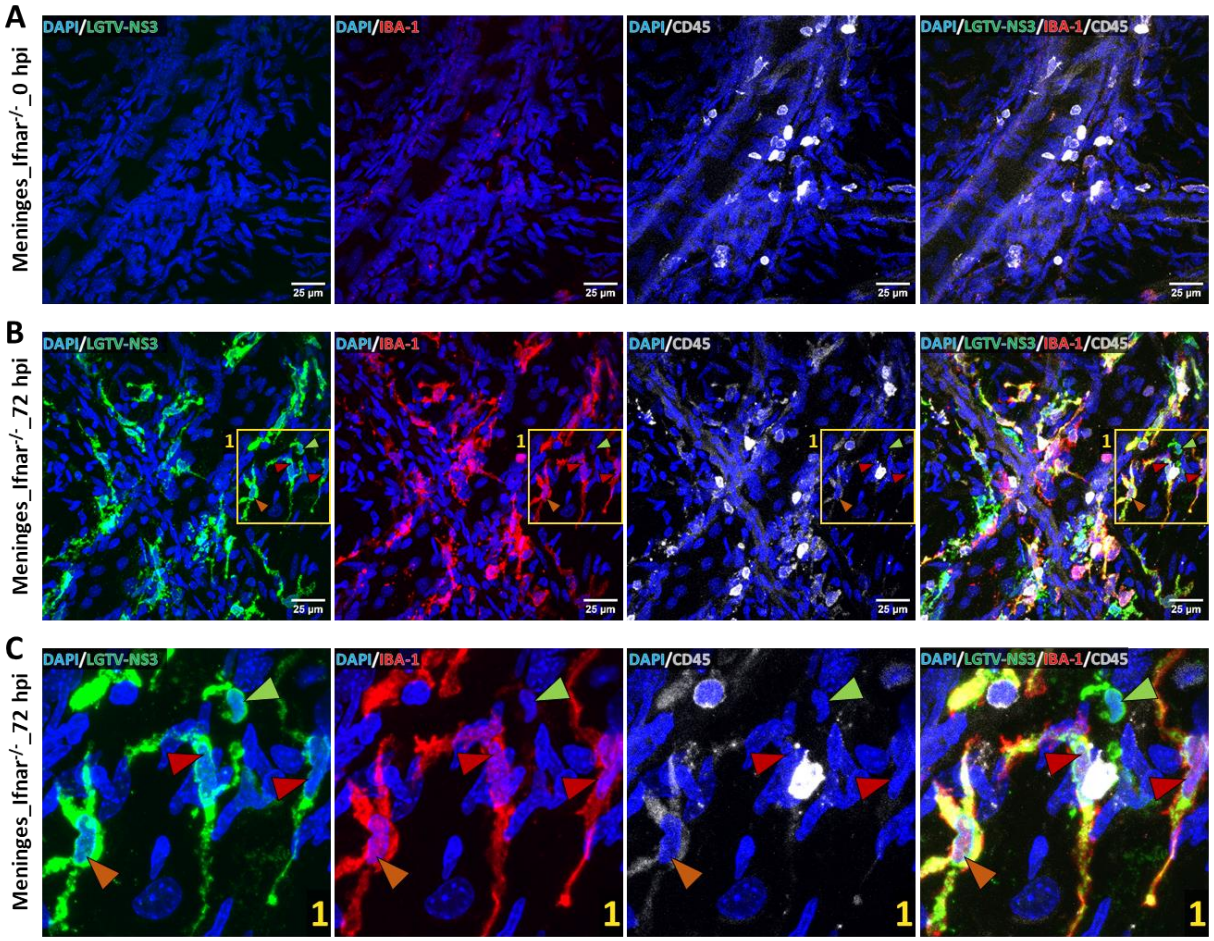

Figure 11: CD45^{+} cells and Iba-1^{+} cells in the meninges are infected by LGTV in Ifnar$^{-/-}$ mice 72 hpi. Skullcaps of SC infected Ifnar$^{-/-}$ mice were isolated after the indicated time points. **A-B.** Thereof gained whole-tissue mounts of the meninges were labeled with antibodies against Iba-1 (macrophages), CD45 (leukocytes) and LGTV NS3. Secondary antibodies labeled with fluorophores were used for detection with immunofluorescence microscopy in the indicated colors. DAPI was used to stain AT rich DNA (nuclei). The yellow square 1 indicates the region of interest depicted zoomed in for **C.** The green arrow indicates a LGTV infected cell, which is Iba-1^{-} and CD45^{-}. Red arrows indicate LGTV infected cells that are Iba-1^{+} and CD45^{-}. Orange arrows indicate a LGTV infected cell, which is Iba-1^{+} and CD45^{low}. The images are representative for two independent experiments (n=6).

As the clear identification of the number of CD45^{low} cells was not possible for every section given to the inconsistent fluorescence concomitant with the low amount of antigen, this could not be proven statistically. Moreover, the LGTV infected cells could be identified as Iba-1^{+} and CD45^{low} or also as Iba-1^{-} and CD45^{-}.

Like in the OB and CP, again Iba-1^{+} and CD45^{low} cells could be identified as targets for LGTV. Like in the CP, this data is indicating that LGTV infects a rather resident phenotype of macrophages than infiltrating ones.

3.3 Effects of LGTV on BBB and BCSFB

Although the BBB and the BCSFB act as highly functional and effective barriers, they are also potential gateways for viruses migrating from the periphery into the CNS. Largely, those barrier functions are formed and regulated by several distinct cell types and proteins that form the tight junctions and adherens junctions. The tight junctions are distributed and regulated differently in the BBB and the BCSFB [207, 157]. Strong or exuberant immunological responses during infections are known to cause structural and functional alterations resulting in a leaky BBB or BCSFB that allows or supports the entry of pathogens into the brain [208]. Apart from severe inflammation, neurotropic viruses show various approaches of interactions with the barriers in order to invade the CNS [209, 11].

3.3.1 Tight junction proteins are regulated differently in different brain regions

To characterize the barriers during LGTV infection, different tight junction proteins were examined for their expression in different regions during the course of the LGTV infection. WT and Ifnar$^{-/-}$ mice were infected with 10^2 FFUs, SC in the right hind leg. BMVs or whole brains, separated into OB, FC, Cbel and CP, were isolated at the time points 0 (uninfected), 24, 48 and 72 hpi. The RNA levels of different tight junction proteins were determined by qRT-PCR. Analysis of the different brain parts revealed that in the OB of WT mice, the CLDN-5 levels increased significantly over time. In contrast, the mRNA level of CLDN-5 in the OB of Ifnar$^{-/-}$ mice stayed constant and was significantly lower at 48 hpi compared to the WT mice (Figure 12A). In the FC of WT mice the expression of CLDN-5 increased significantly during the course of infection. In the FC of Ifnar$^{-/-}$ mice the CLDN-5 expression level in uninfected mice was significantly higher compared to uninfected WT mice. However, the CLDN-5 levels decreased during the course of infection (Figure 12B). In the Cbel of Ifnar$^{-/-}$ mice the CLDN-5 expression was significantly lower in the absence of an infection and did not change due to the infection (Figure 12C).

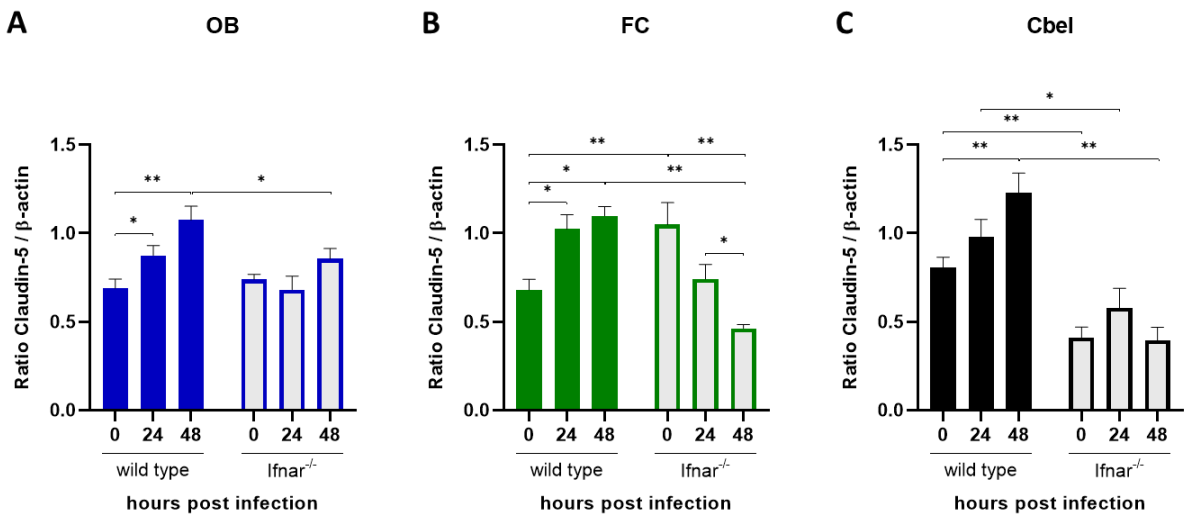

Figure 12: CLDN-5 expression is dependent on type I IFN in different brain regions
WT and Ifnar$^{-/-}$ mice were infected via SC injection at the left hind leg with 10^2 FFUs LGTV. The RNA levels of CLDN-5 in **A.** the OB, **B.** the FC and **C.** the Cbel were analyzed by qRT-PCR for the indicated time points. The time point 0 represents the uninfected controls. The results are representative for two independent experiments (n = 6). Error bars represent the SEM. For statistical analysis pairwise, two-tailed Mann-Whitney test was used (ns, not significant; *, $P < 0.05$; **, $P < 0.01$).

In the Cbel, the CLDN-5 levels were significantly lower in uninfected Ifnar$^{-/-}$ mice compared to uninfected WT mice. In the OB the absence of Ifnar had no influence on the steady state expression of CLDN-5. This indicates that type I IFN is important for the regulation of the tight junction protein CLDN-5 even without an infection, but in a brain region specific manner. So far, the CLDN-5 expression was analyzed per brain region comparing the two genotypes. To answer the question, if the CLDN-5 expression is different within a respective genotype across the three different brain regions, another depiction was chosen. Comparing the three measured infection time points for WT mice showed no significant differences across the different brain regions (Figure 13A). Interestingly the same kind of analyses in Ifnar$^{-/-}$ mice showed some deviations for the CLDN-5 expression across the brain regions. While the LGTV infection led to an increase of CLDN-5 levels in all brain regions for WT mice, this was different for Ifnar$^{-/-}$ mice. There was a significant reduction of the CLDN-5 steady state expression in the Cbel, no induction of CLDN-5 expression in the OB and the Cbel during the infection and even a reduction of CLDN-5 expression in the FC (Figure 13B). This revealed that type I IFN is needed for the induction of CLDN-5 expression during the infection with LGTV in all analyzed brain regions and in the FC in particular, as even a reduction was shown during the infection. Further, type I IFN is significantly influencing the CLDN-5 homeostasis in the FC (increased) and Cbel (reduced) in an opposing manner.

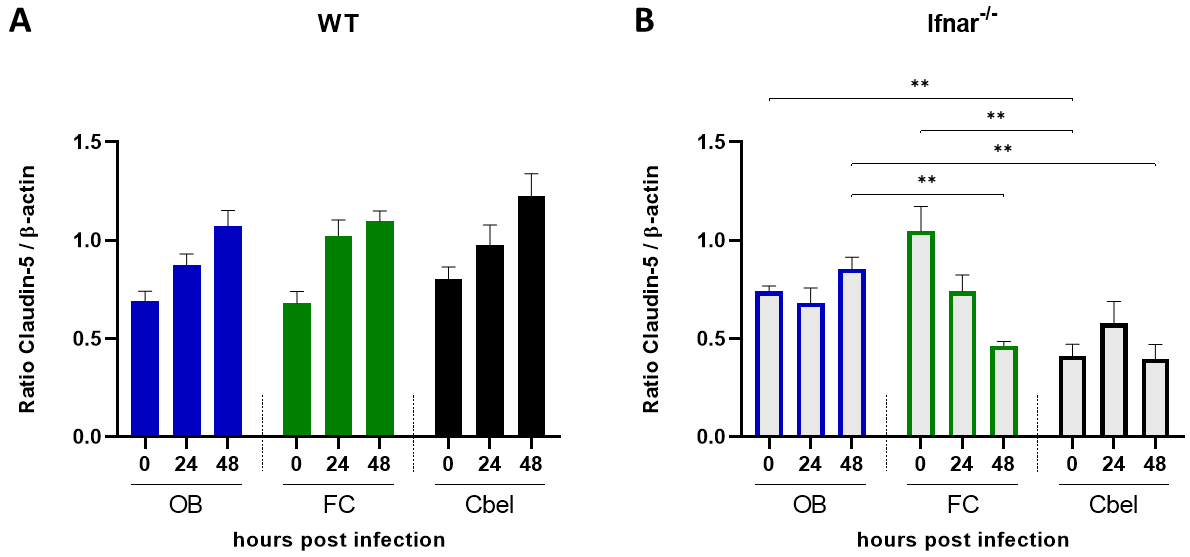

Figure 13: CLDN-5 is differentially regulated across brain regions in Ifnar$^{-/-}$ mice
WT and Ifnar$^{-/-}$ mice were infected via SC injection at the left hind leg with 10^2 FFUs LGTV. The RNA levels of CLDN-5 in the OB, the FC and the Cbel for **A.** WT and **B.** Ifnar$^{-/-}$ mice were analyzed by qRT-PCR for the indicated time points. The time point 0 represents the uninfected controls. The results are representative for two independent experiments (n = 6). Error bars represent the SEM. For statistical analysis pairwise, two-tailed Mann-Whitney test was used (ns, not significant; *, $P < 0.05$; **, $P < 0.01$).

ZO-1 was the next tight junction protein that was analyzed. This cytosolic protein is known as a scaffold protein that can connect a transmembrane tight junction protein like CLDN-5 to the actin cytoskeleton and by this enabling a stable linkage between cells [210–212]. The expression patterns for the tight junction protein ZO-1 were analyzed in the same manner as for CLDN-5. In the OB of WT mice the ZO-1 expression increased significantly from the uninfected time point towards 24 hpi. After 48 hpi, the ZO-1 expression decreased and reached the a level like before the infection. In Ifnar$^{-/-}$ mice the ZO-1 levels significantly decreased from 24 hpi and remained at the lower level during the 48 hpi time point (Figure 14A). Additional to the different regulation of ZO-1, the comparison of WT and Ifnar$^{-/-}$ mice shows that the overall expression of ZO-1 in Ifnar$^{-/-}$ mice is significantly lower during all three measured time points, reaching only about half the levels of the WT mice. In the FC of WT mice the ZO-1 expression was steady at the 0 hpi and 24 hpi time point and was then significantly decreasing towards 48 hpi. In the FC of Ifnar$^{-/-}$ mice the levels of ZO-1 were significantly increasing towards 24 hpi and then slightly decreasing again towards 48 hpi (Figure 14B).

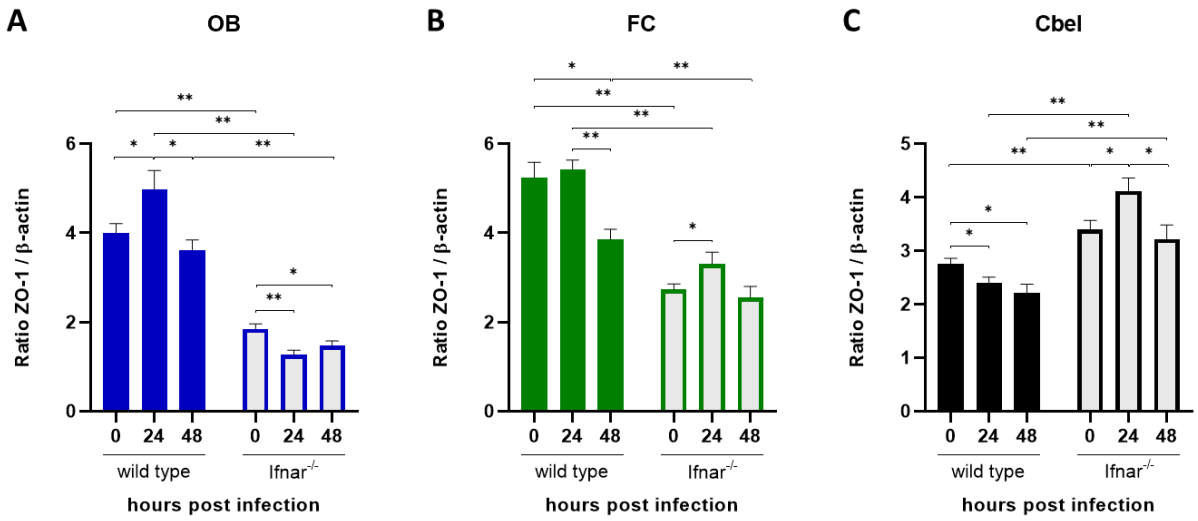

Figure 14: ZO-1 regulation is dependent on type I IFN in different brain regions
WT and Ifnar$^{-/-}$ mice were infected via SC injection at the left hind leg with 10^2 FFUs LGTV. The RNA levels of ZO-1 in **A.** the OB, **B.** the FC and **C.** the Cbel were analyzed by qRT-PCR for the indicated time points. The time point 0 represents the uninfected controls. The results are representative for two independent experiments (n = 6). Error bars represent the SEM. For statistical analysis pairwise, two-tailed Mann-Whitney test was used (ns, not significant; *, $P < 0.05$; **, $P < 0.01$).

Once more, the levels of ZO-1 expression were always lower in the Ifnar$^{-/-}$ mice. In the Cbel of WT mice the ZO-1 expression did decrease significantly after 24 hpi and remained at the lower level also 48 hpi. In Ifnar$^{-/-}$ mice, the ZO-1 levels increased towards 24 hpi and then decreased again towards 48 hpi (Figure 14C). Interestingly the ZO-1 levels in the Cbel were higher in the Ifnar$^{-/-}$ mice at any time point compared to the WT mice in that brain region. The brain regions showed different reactions in the expression patterns of ZO-1. While the ZO-1 levels were always higher for WT mice in the OB and FC, the finding for the Cbel was the other way around. The data for ZO-1 indicates that type I IFN is important for its regulation and that different brain regions show distinct responses to an LGTV infection, depending on the ability to react to type I IFN. Already in the uninfected steady-state condition, the analyzed brain regions show differences between WT and Ifnar$^{-/-}$ mice. Analyzing the three brain regions for only WT, the data shows that the ZO-1 levels in the Cbel are lower at any measured time point compared to the OB and the FC (Figure 15A). Further, the ZO-1 expression in the uninfected FC of WT mice is significantly higher compared to the OB at the same time point. The same analysis for only Ifnar$^{-/-}$ mice shows that the expression levels for ZO-1 are always lower in the OB compared to the FC and the Cbel. Additionally the ZO-1 expression in the Cbel of uninfected Ifnar$^{-/-}$ mice is significantly higher compared to the FC at this time point (Figure 15B).

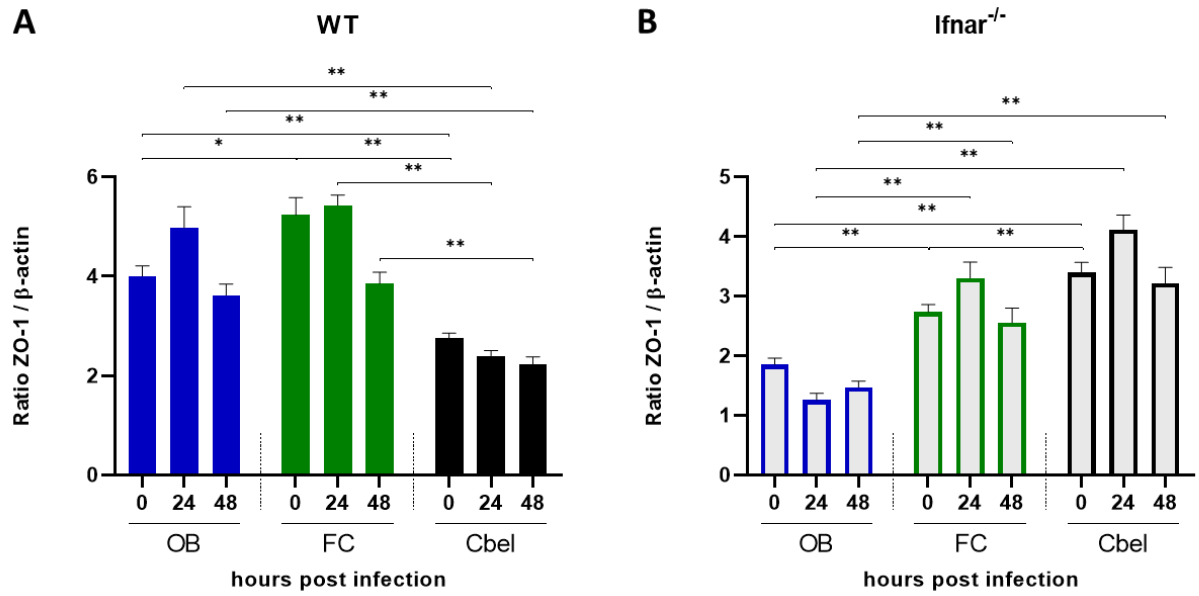

Figure 15: ZO-1 5 is differentially regulated across brain regions in WT and Ifnar$^{-/-}$ mice
WT and Ifnar$^{-/-}$ mice were infected via SC injection at the left hind leg with 10^2 FFUs LGTV. The RNA levels of ZO-1 in the OB, the FC and the Cbel for **A.** WT and **B.** Ifnar$^{-/-}$ mice were analyzed by qRT-PCR for the indicated time points. The time point 0 represents the uninfected controls. The results are representative for two independent experiments (n = 6). Error bars represent the SEM. For statistical analysis pairwise, two-tailed Mann-Whitney test was used (ns, not significant; *, $P < 0.05$; **, $P < 0.01$).

Taken together, these data shows that both, the expression of CLDN-5 and ZO-1, are influenced by type I IFN. The data clearly show that there are differences in the regulation of the tight junction genes between the different brain regions. In addition, the tight junction proteins are regulated individually. While CLDN-5 is equally regulated during the early stages of infection in WT mice across the brain regions, ZO-1 is clearly differentially regulated in the WT mice across the same brain regions. Further the Ifnar knockout led to an overall decrease of CLDN-5 in the Cbel while it led to an overall increase of ZO-1 in the same region compared to the WT. As a further step, it was looked for tight junction gene regulation in the CP as representative for the BCSFB and the BMVs as representative for the BBB of the whole brain. Like for the previous experiment, ZO-1 was analyzed, as it is essential for the tight junctions in the BBB and the BCSFB as well [210–212]. Further, Occludin was added as a target for analysis, as a second tight junction protein, which shares its importance with the BBB and the BCSFB [212, 173]. Additional the tight junction proteins CLDN-2 and CLDN-5 were examined. CLDN-2 is known to be especially important for the BCSFB in the CP while CLDN-5 is considered one of the crucial proteins for the barrier function of the BBB [162].

In the CP of WT mice, the ZO-1 expression levels started highest in the uninfected animals and decreased with every further measured time point. In the CP of Ifnar$^{-/-}$ mice, the ZO-1 expression dynamics were similar but started already at a significantly lower level compared to the WT mice (Figure 16A). The measurements for CLDN-2 in the CP of WT mice suggests a slight upregulation from uninfected to 24 hpi and 48 hpi, while it was then decreasing significantly toward 72 hpi. The same analysis for Ifnar$^{-/-}$ mice showed a comparable pattern but at a lower level of expression (Figure 16D). However, CLDN-2 was by far the tight junction protein with the highest variation among the ratio values, which led to high variances for some time points. Like for ZO-1 and CLDN-2, for occludin also a decrease in the expression levels over the course of infection was measured in WT as well as in Ifnar$^{-/-}$ mice (Figure 16B). However, the Ifnar knockout seemed not to affect the expression levels except for the 72 hpi time point, where the expression of occludin was significantly lower in Ifnar$^{-/-}$ mice compared to WT mice. Changing the focus to the BMVs, the expression values for ZO-1 in WT mice showed some variances but not with a clear direction towards any increase or decrease over time. In the Ifnar$^{-/-}$ mice the deviation of the values within a single time point seemed to be less and expression dynamics showed a significant decrease (Figure 16E), with lower levels of ZO-1 at 48 hpi and 72 hpi compared to the WT mice. CLDN-5 in the BMVs of WT mice increased until the 48 hpi time point and then abruptly decreased significantly towards the 72 hpi time point. In the Ifnar$^{-/-}$ mice the expression was more steady without any significant changes (Figure 16C). For WT mice compared to the Ifnar$^{-/-}$ mice, the CLDN-5 expression levels were significantly lower in the uninfected animals and also at the 72 hpi time point. In the BMVs, occludin showed some bigger variances inside the single measured time points, but no significant changes could be measured across the time points or genotypes (Figure 16F).

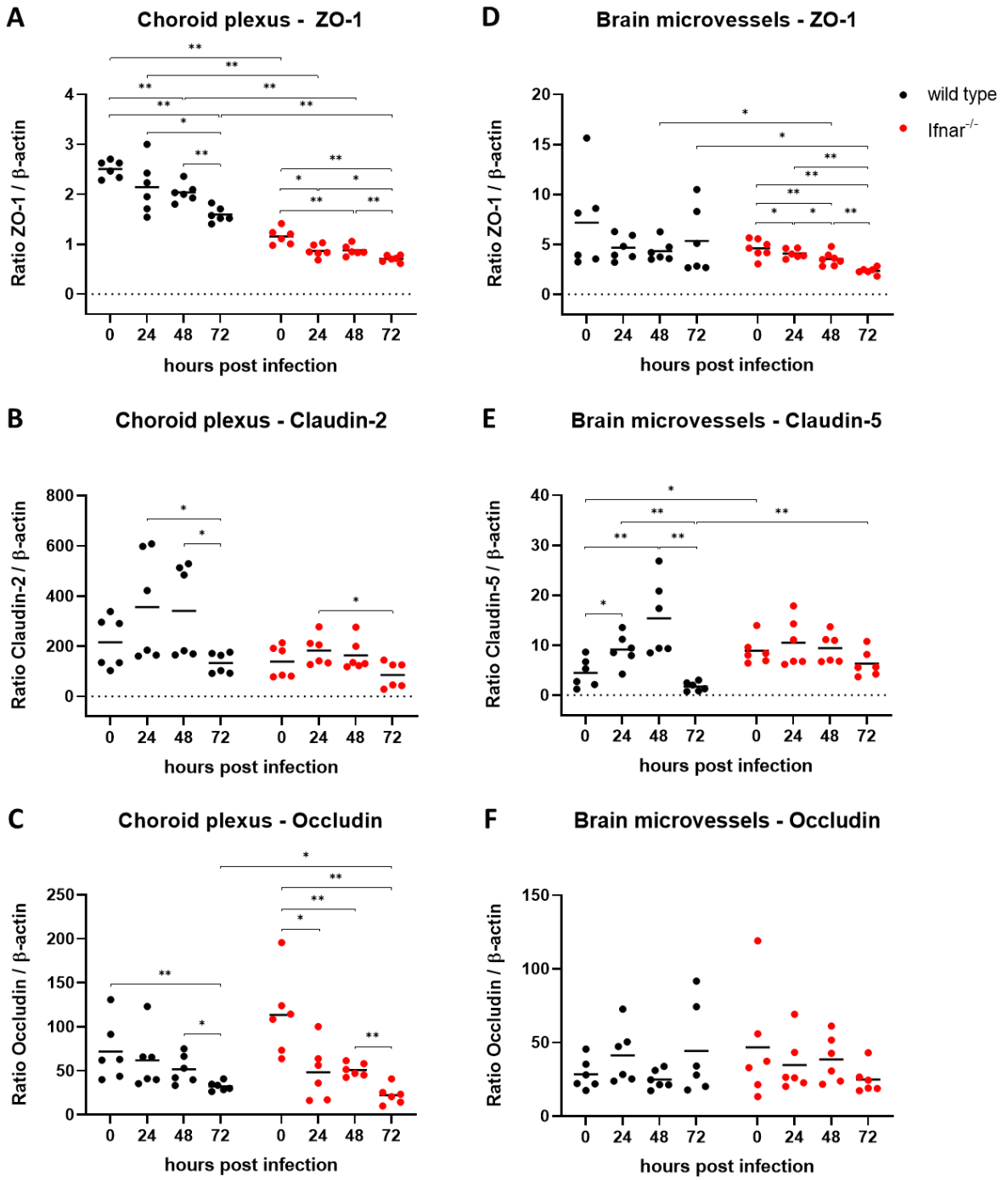

Figure 16: ZO-1 is tightly regulated in the CP during LGTV infection

WT and Ifnar$^{-/-}$ mice were infected via SC injection at the left hind leg with 10^2 FFUs LGTV. The RNA levels of **A.** ZO-1 in the CP, **B.** CLDN-2 in the CP, **C.** occludin in the CP, **D**. ZO-1 in the BMVs, **E.** CLDN-5 in the BMVs and **F.** occludin in the BMVs were analyzed by qRT-PCR for the indicated time points. The time point 0 represents the uninfected controls. The results are representative for two independent experiments (n = 6). Error bars represent the SEM. For statistical analysis pairwise, two-tailed Mann-Whitney test was used (ns, not significant; *, P < 0.05; **, P < 0.01).

Table 1 shows a summary of the up- and downregulations of CLDN-5 and ZO-1 in the different brain regions including CP and BMVs. These data indicates that type I IFN is essential for the regulation of the in this work analyzed tight junction proteins. However, the analyses made also clear, that this regulation is influenced differently in distinct regions and therefore might have direct effects on the infection dynamics of LGTV in those brain regions. Together with the results of the qRT-PCRs and the immunofluorescence microscopy, the data indicates that type I IFN is influencing the infection of the CP and the Cbel with LGTV at later time points. Further, type I IFN influences the amount of viral load to be found in all analyzed brain regions.

Table 1: Summary of significant up- and downregulations for CLDN-5 and ZO-1
The table shows a summary of all significant up- and downregulations found for the experiment depicted in Figure 12. Green arrows indicate a significant upregulation of a marker at least between two different time points during the course of infection. Red arrows indicate a significant downregulation of a marker at least between two different time points during the course of infection. The fourth column indicates significant differences between the genotypes in distinct brain regions.

CLDN-5	**WT**	**Ifnar**	**WT vs. Ifnar**
OB	↑	-	WT higher at 48h
FC	↑	↓	WT lower at 0h WT higher at 48h
Cbel	↑	-	WT higher anytime
BMVs	↑ + ↓	-	WT lower at 0h WT lower at 72h

ZO-1	**WT**	**Ifnar**	**WT vs. Ifnar**
OB	↑ + ↓	↓	WT higher anytime
FC	↓	↑	WT higher anytime
Cbel	↓	↑ + ↓	WT lower anytime
BMVs	-	↓	WT higher at 48h WT higher at 72h
CP	↓	↓	WT higher anytime

4. Discussion

The neuroinvasion of viruses is often associated with critical disease processes and limited treatment options. Further, the exact pathways and mechanisms of neuroinvasion can vary from virus to virus and are not completely understood in many cases. For the tick-borne flaviviruses TBEV and LGTV several pieces of information about the neurotropism are known. However, the route for the CNS infiltration has not been identified and further steps in this direction will pave the way for a better understanding of the disease and can ultimately lead to new approaches for possible treatment options.

4.1 OB as brain region with earliest LGTV replication in WT and Ifnar$^{-/-}$ mice

It has been shown that the OB is the site of early and major LGTV replication in WT mice [61, 136]. It is well known that the type I IFN system is a crucial part of the innate immune system in terms of protection against viral infections. Corresponding to that, it has been shown that LGTV replication and spread is controlled by type I IFN in the periphery and directly in the brain [60]. As part of those findings, the CP has been identified as another site of heavy LGTV infection together with the OB [60]. In several studies it was already discovered that cells from different brain regions have different innate immune profiles and hence are affected variously by viral infection [213–215]. As an example for the region specific immune response for LGTV in the OB, it has been shown that the OB is the only brain region analyzed so far, that is depending significantly on MAVS signaling for the upregulation of type I IFN [61]. Such characteristics paired with the different viral abilities to interfere with the immune response, lead to the circumstance that viruses cannot spread equally well in every brain regions. The brain region in which virus replication is highest depends on the virus in question. In this and other works, it was shown that the RNA of LGTV was detectable in the OB already 48 hpi in WT and 24 hpi in Ifnar$^{-/-}$ mice (Figure 2B). There are different possible ways how the virus could enter the OB. It is known for other viruses like the Rift Valley fever virus (RVFV) [216], vesicular stomatitis virus (VSV) [16] or severe acute respiratory syndrome coronavirus-2 (SARS-CoV-2) [217] that they infiltrate the brain via infection of olfactory receptor neurons in the olfactory epithelium that pass through the cribriform plate. Since some infections by aerosolization after laboratory accidents are reported in humans, this route seems to be possible for TBEV [218, 219].

Contrary to that is the finding that those infections lead to a bi-phasic disease starting with a systemic phase followed by the CNS involvement later on [218]. Further, a recent study showed that the transmission of LGTV by aerosols, even for highly susceptible Ifnar$^{-/-}$ mice, was not possible [220]. In addition, although direct intranasal infection of Ifnar$^{-/-}$ mice led to a fatal outcome in most cases, the disease onset was delayed and the average survival increased [220]. Taken together, the collected information suggests that the OB is the brain part where the initial replication of LGTV is taking place. However, an entry via the olfactory route seems unlikely and a direct proof of the hypothesis is still missing. A further option for LGTV to enter the OB is a transport via the CSF. Flowing from the ventricles where it is produced, the CSF fills and circulates in the subarachnoid space [221] and engulfs a huge part of the OB's surface. For this reason, it is possible that the CSF transports infectious viral particles to the area of the OB. The CSF is constantly filtrated into the blood carrying dural sinuses of the meninges [222, 223] and is also drained by the meningeal lymphatic vessels. This work showed that the meninges actually were infected however; this was only found at the later time points of the LGTV infection (Figure 3C, Figure 11). This indicates that they are not the site of early viral replication and virus entry into the CNS. Going one step further, the meningeal lymphatic vessels are drained by the deep cervical lymph nodes [174]. Indeed, in Ifnar$^{-/-}$ mice, those deep cervical lymph nodes were infected with a significantly higher amount of LGTV in the early stage of infection compared to the adjacent superficial cervical lymph nodes, which do not drain the CSF [136]. This in turn indicated that the CSF and its producer, the CP, could be involved in the brain entry of LGTV. Interestingly, no correspondingly high viral titers were found in the CSF that could have led to extensive viral spreading across the brain (Figure 4). However, only very low amounts of CSF could be isolated from the mice, which could have resulted in concentrations of viral particles that lied under the detection level of the used assay. Although replicable LGTV particles were not detected in the CSF, the CP as its producer and location of the BCSFB was infected and was examined further, to elucidate the role of the tissue complex during a LGTV infection.

4.2 CP is significantly affected by LGTV infection in the absence of Ifnar

Although the CP has already been found to be infected in Ifnar$^{-/-}$ deficient mice after LGTV infection by histology [60], it has not been addressed if this structure plays a role in the early stages and might contribute to the initial entry of LGTV into the brain. In general, it has been shown that the CP has multiple immunomodulatory functions in an inflammatory environment and is involved in immune cell trafficking [224–227]. The disruption of the BCSFB allows an enhanced infiltration of immune cells and is a driver of neuroinflammation [228, 229]. Additionally, the CP is involved in many crucial transport processes supporting the brain homeostasis and with them provides several possible exploits a virus could use to enter the brain [230–232]. One main purpose of the CP is the uptake of substances from the blood to produce the CSF. As it has not been done before, in this work the CP was compared by qRT-PCR to other brain regions regarding the onset of LGTV detection in the brain. It has been shown that the OB is the brain region in which the RNA of LGTV was detectable earliest, when compared to the FC, the Cbel and the CP of Ifnar$^{-/-}$ and WT mice (Figure 2B-E). Interestingly, the CP of WT mice did not show any signs of infection during all measured time points while the CP of Ifnar$^{-/-}$ mice showed itself heavily infected. A preprint from Chotivan et al. [233] showed a similar difference in virus distribution for WT and Ifnar$^{-/-}$ mice after intracranial injection of LGTV. This supports the finding of this work that the impairment of type I IFN dependent immune response not only contributes to the disease severity but also influences the tropism of LGTV in the CNS. Additionally, the amount of LGTV in the CP of Ifnar$^{-/-}$ mice at 72 hpi was roughly ten times higher as in the OB at the same time point (Figure 2F). This indicates that the ability of the CP to control LGTV replication is strongly dependent on type I IFN and even increases in importance, regarding the later time points of the infection. Additionally, Baruch et al. showed that the CP is highly susceptible to aging induced changes of the type I IFN signaling and as a result influences brain function and CNS-specific immunity [234, 224]. This further supports the hypothesis, that the CPs ability to react properly to type I IFNs is a major factor for the control of the LGTV infection in the brain. In many other cases it has been shown or suggested, that the inflammatory response that is triggered by the virus can be as detrimental or worse as the underlying viral infection [5]. It has been shown elsewhere that even an ineffectively replicating, non-neuroinvasive virus can cause neurological disorders [235]. This further indicates that the strong viral replication in the CP in Ifnar$^{-/-}$ mice might be one factor that leads to the manifestation and lethal outcome of LGTV infections in highly susceptible mice.

4.3 LGTV infects barrier associated macrophages and pericytes in the CP of Ifnar$^{-/-}$ mice

Beyond the general infection setting, the identification of the cells that are infected in the CP might contribute to a better understanding of the infection. The epithelial cells of the CP are connected by tight junctions and hence are protecting the CSF and the brain against harmful agents. The infection of CP epithelial cells has already been shown as a possible entry into the CNS for other viruses like chikungunya virus [236] and JC polyomavirus [237]. In this work it has been shown, that the CP epithelial cells are no target of LGTV after SC injection (Figure 9). Interestingly, the preprint of Chotivan et al. [233] shows the infection of CP epithelial cells in Ifnar$^{-/-}$ mice after intracranial infection. This highlights, that LGTV shows a different tropism in the CNS depending on the entry route. Although being connected by tight junctions, the CP relies on the substances transported by the fenestrated CP endothelial cells [238], expected to provide enough space for viral particle to reach the epithelium. The results of this work had shown no signs of infection in the endothelial cells of the CP (Figure 10). For other viruses like HSV in newborn mice [239], the CP has already been shown as a suitable target and gateway. Also for parasites like *toxoplasma gondii* the CP has been shown as a passage into the CNS [201]. Additionally, entry strategies like para- or transcellular transport and a trojan horse mechanism have been shown or suggested for neuropathologic pathogens [209, 240]. In terms of brain entry via the CP, an interesting finding has been made for Zika virus. Pericytes were identified with a high possibility as the key cell population by which the Zika virus gains entry to the CNS [206]. Pericytes are described as a cell population with the ability to differentiate into different distinct forms [241, 242] and show a certain level of plasticity [243, 244]. Further, they are known to be important for the function of the BBB [245, 246] and they are in direct contact with the blood vessels and by this representing a feasible target for viral particles in the circulation [206]. Interestingly, in the present work it was shown that some CD140b^{+} pericytes were infected by LGTV in the CP of Ifnar$^{-/-}$ mice (Figure 10). This indicates that pericytes might play a role for the brain infiltration of LGTV into the CNS. However, the histological analyses in this work showed very clearly that a major population of the infected cells in the CP of Ifnar$^{-/-}$ mice was Iba-1^{+} (Figure 7). In the brain parenchyma, the most Iba-1^{+} cells are brain resident microglia. In the CP, the brain resident macrophages are called barrier associated macrophages (BAMs) or CNS-associated macrophages (CAMs). Macrophages in general are the largest class of immune cells in the CP [247].

Among those BAMs, two distinct subsets are distinguished. The stromal macrophages and the epiplexus macrophages [248, 247, 249]. Initially, the resident microglia in the brain are seeded from the yolk sac of the embryo in early development [247, 248]. However, it is known that peripheral monocytes are constantly replenishing the BAMs [250] and that the CP in an inflammatory environment is recruiting monocyte derived macrophages into the CNS [251, 225]. It has been published that TBEV infects monocytes/macrophages, dendritic cells, neutrophils and keratinocytes in C57Bl/6 mice after a tick bite [78]. For LGTV, macrophages, dendritic cells and B-cells have been identified as viral targets in Ifnar$^{-/-}$ mice in the periphery [60]. Taken together, migrating macrophages might play a role in the distribution of LGTV, even into the CNS. To assess if infiltrating cells play a role in the infection of the CP, a CD45 antibody was used in histology. The results revealed that CD45^{high} cells showed no signs of an LGTV infection in the CP. Further, the CD45^{high} cells did not show morphological traits of macrophages and were not positive for Iba-1 (Figure 7). As a result, it can be assumed that CD45^{high} infiltrating immune cells might not be a key factor for the entry of LGTV into the CNS.

4.4 Type I IFN response in Iba-1^{+} cells as possible key factor for protection against LGTV neurovirulence

Not only in the CP but also in the OB at 96 hpi it was shown in this work, that Iba-1^{+} cells were the major targets of LGTV in Ifnar$^{-/-}$ mice (Figure 6C+D). However, it could not be conclusively ascertained to which extend infiltrating macrophages are involved in the course of infection. The combination of the Iba-1 and the TMEM119 antibody for the clear identification of brain resident microglia in the OB was only partially successful. While the results were convincing for uninfected samples, the TMEM119 staining was rather unsteady for infected samples. Recently, Young et al. [252] showed, that microglia that are in proximity to inflammation have a decreased TMEM119 expression. In line with the observations in this work, this could explain the difficulty to explicitly distinguish between infiltrating and resident Iba-1^{+} cells in the OB.
Further, in the literature Iba-1^{+} cells were already described as targets for LGTV *in vivo* [60, 61] and also astrocytes could be infected by TBEV *in vitro* [179]. Nonetheless, neurons are considered the main targets for LGTV and TBEV in the brain [60, 61, 178] and are also affected by apoptosis upon infection [253, 254]. In this work, no LGTV infected neurons were identified (Figure 6A+B). One possible explanation for this discrepancy could be the used antibody against NeuN to stain the neurons.

While it is a reliable marker for postmitotic neurons, the levels of NeuN expression was found to be varying during stimulation [255]. Further, Lee and Pixley [256] showed that not all neurons in the glomerular layer of the OB are completely mature and therefore are lacking the expression of NeuN. Other studies indicate that the loss of NeuN immunoreactivity may be caused by the death of neurons [257] or the intermittent disturbed synthesis of the protein due to damage [258]. Summarized, this opens the possibility that infected neurons were not identified due to the lack of NeuN in the OB for different reasons. Another factor could be the nature of the used LGTV antibody's sensitivity. The results of this work already showed that the detection of viral RNA by qRT-PCR was more sensitive than the detection of viral NS3 by immunofluorescence microscopy. As immunohistology showed strong signals for LGTV in Iba-1^+ cells but no signal for LGTV in $NeuN^+$ cells in the OB, this could indicate that for $Ifnar^{-/-}$ mice the viral replication in Iba-1^+ cells is many times over the viral replication in $NeuN^+$ cells. Additionally, Iba-1^+ and $CD45^{low}$ cells were also identified as the major infected cell population in the CP and in the meninges (Figure 7, Figure 11). Taken together, this can lead to the assumption that the regular type I IFN response in brain resident Iba-1^+ cells is a key factor for the protection against LGTV neurovirulence.

4.5 BBB and BCSFB during LGTV infection

The BBB and the BCSFB are potential gateways for LGTV into the brain. The permeability of those barriers as well as their tight junctions are regulated differently in distinct brain regions [259]. This can be dependent on the distinct reactions on specific physiological circumstances [260] or on the cellular compositions and their specific protein expression profiles [261, 262]. Altogether, still very much is unknown about the heterogeneity of the BBB and the BCSFB [259]. For other flaviviruses, it has been shown that they can enter the brain while influencing the barriers but without them needed to be disrupted. For West Nile virus it has been reported, that overcoming the BBB *in vitro* does alter only specific tight junction proteins especially at later time points while cell-free WNV can reach the brain without altering the permeability of the BBB [24]. For Zika virus, a brain entry via the BCSFB *in vivo* has been shown to alter the barriers integrity making it leakier [206], but the virus is able to reach the brain without any disruption of the BBB [135].

For LGTV it had been shown that it reaches the CNS without a preceding disruption of the BBB [60] and also for TBEV the breakdown of the BBB was not necessary for the virus to reach the brain [133]. TBEV was also able to infect brain microvascular endothelial cells *in vitro* [132]. For LGTV this was also shown in this work, although this was only the case for later time points, while the virus already had reached the brain (Figure 3D). The possibility for some very early subliminal infection of the endothelial cells followed by basolateral virus release, transcytosis or paracytosis like suggested or shown for other viruses [135] is a further on option. As the literature and the results of this work showed, the OB is the brain region with the earliest LGTV replication independent of type I IFN (Figure 1). This makes it the number one candidate for the location of the initial LGTV entry into the brain. It has been shown for Zika virus that CLDN-7 is needed for an optimal replication of the virus inside the endothelial cells [263]. In other publications, the unique cellular response and cytokine expression for certain brain regions after immunological challenge were shown [264–266]. It needs to be further examined which unique conditions are present in the OB that facilitate an earlier entry for LGTV compared to all other sites of LGTV infection. As LGTV leads to a heterogeneous infection pattern in different brain regions, in this work tight junction proteins were examined regarding their expression levels in the different regions in response to a LGTV infection in WT and Ifnar$^{-/-}$ mice.

4.5.1 CLDN-5 expression does not correlate with early LGTV infection

The transmembrane CLDN-5 is the most abundant tight junction protein in the BBB and is considered substantial for the restriction of permeability [267, 268]. Belonging to the same family, CLDN-2 is more abundant in the BCSFB [162]. It is highly sensitive to inflammation and with its function as selective ion channel is discussed to be responsible for the restriction of permeability as well as a leaky barrier [164, 269, 165, 163]. The earliest detectable onset of LGTV infection was in the OB 24 hpi followed by the FC 48 hpi and was completely absent in the Cbel of WT mice (Figure 2B-D). However, the expression levels of CLDN-5 showed no differences across those brain regions (Figure 13A). The knockout of Ifnar led to an earlier detection of LGTV in the brain regions (Figure 2B-D) and further to different regulations of CLDN-5 levels across the respective regions (Figure 13B). The region with the significantly lowest CLDN-5 levels in Ifnar$^{-/-}$ mice was the Cbel. However, this did not correlate with the earliest or strongest LGTV infection.

The CLDN-5 levels in the BMVs collected from the whole brain of WT mice showed a significant increase until 48 hpi followed by a strong drop towards 72 hpi (Figure 16E). A similar expression pattern was observed for CLDN-2 in the CP. This suggests that the significant drops of CLDN-5 and CLDN-2 expression indicates towards a substantial increase of the BBB and BCSFB permeability at 72 hpi. The CLDN-5 and CLDN-2 expression levels in the BMVs and CP in Ifnar$^{-/-}$ mice were rather steady during the LGTV infection and even significantly higher at 72 hpi compared to WT mice for CLDN-5 (Figure 16E). Taken together, this indicates that the CLDN-5 and CLDN-2 levels and the changed barrier permeability are no defining factors for the initial LGTV brain entry and are instead rather facilitating the later LGTV infection.

4.5.2 ZO-1 expression reduced by LGTV in infection site independent manner

ZO-1 is a tight junction protein, which is located at the plasma membrane only in the cytosol. It is known as a scaffold protein able to connect a transmembrane tight junction protein like occludin to the actin cytoskeleton and by this enabling the stable linkage between cells via tight junctions [210–212]. While CLDN-5 was increasing during the early time points in all analyzed brain regions for WT mice, ZO-1 was slightly more stable and showed a rather decreasing behavior. Interestingly the Cbel and the CP were the brain regions that had the lowest levels of ZO-1 during all analyzed time points in the WT (Figure 15A, Figure 16A). However, in the Cbel and CP of WT mice no LGTV was detectable (Figure 2D+E). Only analyzing the WT mice could therefore lead to the assumption that higher ZO-1 levels correlated with earlier and stronger LGTV infection. Contrary to this assumption was the data from the Ifnar$^{-/-}$ mice. The Cbel in Ifnar$^{-/-}$ mice had the highest ZO-1 expression levels of all compared brain regions. Together with the CP (Figure 16A) the OB showed the lowest ZO-1 expression while the FC had only slightly lower levels than the Cbel (Figure 15B). Following the data from the Ifnar$^{-/-}$ mice could therefore lead to the assumption that the low expression of ZO-1 correlates with an early and heavy LGTV infection. Taken together this information can lead to the hypothesis that ZO-1, unlike CLDN-5, is regulated differently in distinct brain regions of WT mice.
Furthermore, type I IFN is important for the regulation of ZO-1 expression in steady state and a respective knockout leads to a significant change in the ZO-1 expression patterns of distinct brain regions during an LGTV infection. Another analyzed essential tight junction protein was Occludin. It occurs in the BBB and BCSFB as transmembrane protein and is involved in function, regulation and formation of the barriers [171, 270].

In its function it is dependent to a certain degree on the scaffolding feature of ZO-1, which connects it to the actin cytoskeleton [210–212]. As shown in Figure 16A+C, the expression of occludin in the CP was downregulated over the course of infection in WT mice as well as in Ifnar$^{-/-}$ mice. This resembled the data observed for ZO-1 in the CP. However, this comparison did not work for the BMVs, where occludin did not show any clear regulation while ZO-1 was significantly decreasing over time in Ifnar$^{-/-}$ mice. As a result, a direct connection between the regulation of ZO-1 or occludin expression and the entry site of LGTV into the CNS could not be shown. Additionally, although the Cbel and the CP showed no LGTV RNA in WT mice, the ZO-1 expression there did decrease in succession to the LGTV infection.

5. Material and methods

5.1 Materials

5.1.1 Consumables

The consumables used during the work process for this thesis are listed below (Table 2).

Table 2: List of consumables

Material	Detail	Manufacturer
Cell culture flask	25 cm^2, 75 cm^2, 175 cm^2,	Sarstedt AG
Cell culture plate	6 Well, 96 Well	Greiner bio-one, Sarstedt AG
Cell strainer	40 µm, Nylon	Corning
ceramic sphere	1/4''	MP-Biomedical
Costar® Stripette® serological pipette	10 ml, 25 ml	Corning
Discardit™ II syringe	20 ml	Becton Dickinson GmbH
Disposable base mold	37 mm x 24 mm x 10 mm	Ted Pella, Inc.
FALCON® Tube	Conical, 15 ml, 50 ml,	Corning
Fuzz free cellulose tissue	ZetBox®	ZVG
LightCycler multiwell plate	96 well, white	Roche Diagnostics GmbH
Micro-Fine™ + Demi Insulin syringe	U-100, 0,3 ml, 0,3 mm x 8 mm	Becton Dickinson GmbH
Microlance™ 3 cannula	0,8 mm x 40 mm	Becton Dickinson GmbH
Microscope cover slips	24 x 50 mm	Gerhard Menzel GmbH
Microscope slides SuperFrost® Plus	76 x 26 mm, cut edges, frosted	Gerhard Menzel GmbH
Omnican®-F Tuberculin syringe	1 ml, 0,3 mm x 12 mm	B|Braun
Pap pen	Liquid blocker	Science services
Petri dish		Sarstedt AG
Safe Seal Micro Tube	1,5 ml, 2 ml	Sarstedt AG
Scalpel	Feather disposable	Pfm medical AG

Material	Detail	Manufacturer
Screw-capped sample tube	2 ml	Biozym scientific GmbH
TipOne® Filter Tips	10/20 µl, 200 µl, 1000 µl	STARLAB
Vacutainer® Safety-Lok™ Blood collection Set	0,8 mm x 19 mm x 178 mm	Becton Dickinson GmbH

5.1.2 Chemicals and reagents

The different chemicals and reagents used for this work are listed below (Table 3).

Table 3: Chemicals and reagents

Material	Manufacturer
Bovine serum Albumin (BSA) Fraction V, pH 7	Capricorn Scientific GmbH
Chloroform	Fluka Analytical
D (+) Sucrose	Carl Roth GmbH & Co. KG
DAPI	Thermo Fisher Scientific Inc.
DNAse	Sigma Aldrich
Ethanol	Otto Fischar GmbH & Co. KG
Ethanol Absolute (denatured)	Th. Geyer GmbH & Co. KG
Fetal bovine serum	Capricorn scientific GmbH
Formaldehyde	Carl Roth GmbH & Co. KG
Gibco® DMEM with high glucose	Thermo Fisher Scientific Inc.
Gibco® HBSS without phenol red	Thermo Fisher Scientific Inc.
Gibco® HEPES buffer solution	Thermo Fisher Scientific Inc.
Gibco® RPMI	Thermo Fisher Scientific Inc.
Gibco® 1x PBS without Ca & Mg	Thermo Fisher Scientific Inc.
Gibco® Glutamax®	Thermo Fisher Scientific Inc.
Gibco® MEM	Thermo Fisher Scientific Inc.
Gibco® Penicillin/Streptomycin	Thermo Fisher Scientific Inc.

Material	Manufacturer
Glycin	Carl Roth GmbH & Co. KG
Goat serum	Sigma Aldrich
Incidin™ Liquid	Ecolab Deutschland GmbH
ISOLATE II RNA Micro Kit	Bioline
Isopropanol	J.T. Baker
KAPA probe fast universal qPCR Kit	KAPA Biosystems
KAPA SYBR fast qPCR master mix universal	KAPA Biosystems
Ketamin (10%)	Bela-Pharm GmbH & Co. KG
$KHCO_3$	Sigma Aldrich
Methocel® A15C	Sigma Aldrich
M-MLV reverse transcriptase kit	Invitrogen
Na_2EDTA	Sigma Aldrich
$Na_3C_6H_5O_7$	Merck
$NaHCO_3$	Sigma Aldrich
NaN_3	Carl Roth GmbH & Co. KG
NH_4Cl	Sigma Aldrich
peqGOLD Trifast	Peqlab
RNase free water	Sigma Aldrich
Roti®-Histofix 4%	Carl Roth GmbH & Co. KG
Sodium Pyruvate	Sigma Aldrich
Tissue Tek® O.C.T. compound	Sakura
Tris	Roche Diagnostics GmbH
Triton X-100	Sigma Aldrich
TrueBlue™ peroxidase substrate	SeraCare Life Sciences Inc.
Tween®20	Sigma Aldrich
Tween®80	Sigma Aldrich
Vectashield® Vibrance® mounting medium	Vector Laboratories
Xylazin (2%)	Serumwerk Bernburg AG

5.1.3 Virus

For this work, the Langat virus strain TP21 (provided by Gerhard Dobler) was used. VeroB4 cells were used for virus production and the concentration was ascertained by a FFU assay.

5.1.4 Laboratory Equipment

The following laboratory equipment was used for experiments covered in this thesis (Table 4).

Table 4: Laboratory equipment

Device	Type	Manufacturer
Autoclave	5075 EL	biomedis®
Centrifuge	Heraeus™ Multifuge™ X3R	Thermo Fisher Scientific Inc.
Centrifuge	-80 °C HFU 586 Basic	Heraeus
Centrifuge	HSP12	Heraeus
CO_2 Incubators	Thermo Scientific™ Heracell™ 150i	Thermo Fisher Scientific Inc.
Double-ended spatula	13 cm	Fine science tools
Forceps	Curved, 11,5 cm	Fine science tools
Freezer	-20°C -80°C HFU 586 Basic	Liebherr Heraeus
Fridge	Comfort	Liebherr
Fume hood	MC6	Waldner Inc.
Homogenizer	FastPrep-24™	MP-Biomedical
Iris scissors extra fine straight/pointed	8,5 cm	Fine science tools
LightCycler® 480 Instrument II	Light Cycler 480 II	Roche Diagnostics GmbH
Magnetic stirrers hot plate	MR 3001	Heidolph
Microlitrecentrifuge	Biofuge® pico	Heraeus
Micropipettes	10 µl, 20 µl, 100 µl, 200 µl, 1000 µl	Eppendorf
Microscope	Confocal, LSM 710	Carl Zeiss

Device	Type	Manufacturer
NanoDrop	Nanodrop 1000 ND-1000	Thermo Fisher Scientific Inc.
Pipette controller	PIPETBOY acu 2	Integra
Ringed forceps	3 x 0,75 mm, 9 cm	Fine science tools
Scale	1419MP8-1	Sartorius
Scissors pointed/blunt	10 cm	Fine science tools
Shaker	MTS 4	IKA®-Werke GmbH & Co. KG
Stereomicroscope	SZX2-ILLT	Olympus corporation
Sterile work bench	Heraeus HS15 Heraeus HSP12	Thermo Fisher Scientific Inc.
Water bath	Mod.Nr. 1002	GFL®

5.1.5 Computer software

Data collection, calculation and processing was done with Microsoft (MS) Office Professional 2016 Word, Excel and Power Point. To obtain microscopic pictures ZEN imaging software (Zen Black ed. 2012 SP5) was used. Images were processed with (Fiji) ImageJ 1.53q [271] (National Institutes of Health, USA). Graphs and statistical analysis were generated by GraphPad Prism (version 8.4.3 for Windows, GraphPad Software, San Diego, California USA, www.graphpad.com.). Citavi (Version 6.14, Swiss Academic Software GmbH) was used as reference management software.

5.1.6 Statistical analyses

Statistical analysis was done with GraphPad Prism (version 8.4.3 for Windows, GraphPad Software, San Diego, California USA, www.graphpad.com.) and non-parametric t-test as pairwise, two-tailed Mann-Whitney test was performed.

5.2 Methods

5.2.1 Animal experiments

Ethics statement

The animal experiments were performed in accordance with the guidelines of the animal welfare law (EU-directive 2010/63/EU). All animal experiments were approved by the Landesverwaltungsamt Sachsen-Anhalt and documented for the reference number 42502-2-1606 UniMD. The animals were housed and handled according to the guidelines of the Federation of European Laboratory Animal Science Associations (FELASA). The experiments were performed either in the biosafety level 2 (BSL2) laboratory of the institute for medical microbiology and hospital hygiene, Magdeburg or in the BSL2 unit at the animal facility at the Otto-von-Guericke University, Magdeburg. All preparative work was done under semi-sterile conditions and all devices were thoroughly cleaned and disinfected with 70% ethanol (Th. Geyer GmbH & Co. KG) and Incidin (Ecolab Deutschland GmbH).

Animal housing

In this study, mice with C57Bl/6 background were used. The wild type (C57Bl/6JOlaHsd) and the interferon-α-receptor-1 deficient transgenic variant (according to [272]) were bred and maintained under specific-pathogen-free (SPF) conditions. The genotype of transgenic animals in a C57BL/6 background was verified by PCR. Mice were maintained in individually ventilated IVC Green Line cages (Techniplast Germany GmbH) separated according to their gender. Mice had free access to food and water and were kept under standardized conditions, such as a 12/12 hour light-dark cycle, a maximum of 250 lux luminance, at 55% humidity and 22 °C.

Anesthesia and infection

6-8 week old male and female mice were used for the experiments. Both genera were used to exclude sex-depended effects. Mice were anesthetized with 100 µl/ 10 g body weight of a 10% ketamine (Bela-Pharm GmbH & Co. KG), 5% Xylazin (Serumwerk Bernburg AG) mixture in 0.9% NaCl through intraperitoneal injections.

It took around 5 minutes for the mice to reach complete unconsciousness, in which they remained for about 45 minutes. The unconscious mice were injected subcutaneously at their left hind leg with 20 µl 1 x PBS (Thermo Fisher Scientific Inc.) containing $1x10^2$ FFUs of LGTV. The health condition of the animals was monitored once (or twice if the score reached a certain limit) per day, to prevent mice to reach a high degree of burden. Mice expected to reach a high degree of burden were killed immediately to prevent unnecessary suffering. A detailed score sheet is appended to this work.

5.2.2 Cerebrospinal fluid and serum collection

CSF was collected by puncturing the *cisterna magna*. The Method is already published and used (e.g. [273, 274, 201]) and was adapted from there. Mice were deeply narcotized and killed by an overdose of CO_2 inhalation. Directly afterwards a small transversal incision in the skin located over the occiput was made with a scalpel (Pfm medical AG). By pulling the skin sagittal to both sides with two forceps (fine science tools), an area from the back of the head to the scapulae was exposed. Then the mice were brought in an angulated position with the head forming a circa 110° angle to the body. A stereomicroscope (Olympus) was used during further, mostly transversal incisions into subcutaneous tissue and muscle to reach the atlanto-occipital membrane with the dura mater of the *cisterna magna,* preferably without damaging any blood vessels. Directly before reaching the dura mater, two fine forceps were used instead of a scalpel to carefully remove tissue and muscles around the *cisterna magna* and expose a suitable area of it for the collection of the CSF. Then the dura mater was punctured lateral to the arteria *dorsalis spinalis* with the thin end of a fine-pulled glass capillary. The thicker end of the capillary was connected to a 1 ml syringe (Braun) by a flexible tube (Becton Dickinson GmbH). Once inside the CSF, the syringe was filled very gently to support the capillary action. On average, around 2 µl of CSF were collected. The collected CSF was then transferred into a 1,5 ml tube (Sarstedt AG) that was centrifuged at 13.000 rpm for 10 seconds. Then it was examined if any contamination with blood is visible and contaminated samples were discarded. The collected CSF was then transferred into a 1,5 ml tube already containing 100 µl of ice-cold DMEM (Thermo Fisher Scientific Inc.) followed by resuspending. The samples were then transferred into liquid nitrogen and afterwards stored at -80 °C until further usage. Directly afterwards, scissors (fine science tools) were used to open the thorax of the mice to gain access to the heart.

With a cannula (Becton Dickinson GmbH) on a 1 ml syringe, the right auricle was punctured to collect around 300 µl of blood. The blood was then kept at room temperature (RT) for 30 minutes. Afterwards, the blood was centrifuged at 13.000 rpm for 10 minutes to separate the serum. The serum was collected and transferred into liquid nitrogen and afterwards stored at -80 °C until further usage.

5.2.3 Brain isolation

Brains were isolated after the transcardial perfusion of mice with 3 x 20 ml of 1 x PBS for BMV isolation and with 2 x 20 ml for other analyses. For histological samples, the PBS perfusion was done directly after collecting the CSF from the *cisterna magna* and blood from the heart and was subsequently followed by perfusion with 20 ml Roti-Histofix 4% (Carl Roth GmbH & Co. KG) for fixation. For samples used for RNA isolation, mice were killed by inhalation of an overdose of CO_2 and right afterwards perfused with PBS without subsequent fixation. Thereafter, the Skin was removed from the upper half of the skull and the eyes and further remaining tissue were removed from the orbital cavities. A transversal cut through the cranial bone was made, longing from the left to the right anterolateral corner with fine scissors (fine science tools). Starting at the right of that incision, the skull was further cut in the frontal plane until 360° were reached and the skullcap could be removed as a whole. The brains could then be removed from the skull base with a spatula and were transferred into a well of a 6-well plate (Sarstedt AG) filled with 10 ml HBSS (Thermo Fisher Scientific Inc.) stored on ice. For RNA isolation, the brain was further dissected with a scalpel and two forceps under a stereo microscope. The OB and the Cbel were located and detached with forceps. The FC was cut off with the scalpel. Each sample was then transferred into a 1,5 ml screw-capped tube (Biozym scientific GmbH), put into liquid nitrogen and stored at -80 °C.

5.2.4. Meninges isolation

The isolation of the meninges has already been published elsewhere [275] and has been adapted for the experiments. After removing the skullcaps for brain isolation, they were transferred into a well of a 6-well plate filled with 10 ml HBSS stored on ice. The 6-well plates with the isolated skullcaps were put under a stereo microscope for the removal of the meninges from the bone.

With two fine forceps the meninges were loosened at the occipital area from the bone and then carefully and gradually pulled towards the nasal end of the skullcap. Processed that way, it was possible to isolate the meninges in most cases as a whole and without major fissures. The meninges where kept in HBSS on ice until further usage.

5.2.5 Choroid plexus isolation

The 6-well plates filled with 10 ml HBSS containing the brains were put under a stereo microscope. The brains for histological analyses were bisected exactly along the median longitudinal fissure separating the brain into the two hemispheres. One half was further processed for histological sectioning. The other half was kept in the HBSS under the stereo microscope for the isolation of the remaining part of the CP at the fourth ventricle and the lateral ventricle with two fine forceps. The isolated CP was kept in HBSS on ice until further usage. The brains for RNA isolation were not halved and the CP was isolated from the complete brain. The CP were pooled per brain and the tissue was transferred into 1,5 ml screw-capped tubes, put into liquid nitrogen and stored at -80 °C.

5.2.6 Brain microvessel isolation

As previously described [276] the BMVs were isolated with some alterations.
Isolated brains were rolled on clean, fuzz free cellulose tissue (ZVG) to remove the remaining parts of the meninges. The complete brain was minced with a scalpel inside a petri dish (Sarstedt AG) very diligent and transferred into a 15 ml Tube (Corning) together with 2 ml PBS/HEPES buffer containing PBS dosed with 10mM HEPES (Thermo Fisher Scientific Inc.). 10 µl of DNAse (Sigma Aldrich) were added, and the suspension was homogenized with a 5 ml pipette until no bigger tissue pieces were visible. The suspension was incubated for 5 minutes at 37 °C. After adding 5 ml of PBS/HEPES buffer, the suspension was centrifuged at 1000 g for 5 minutes. The supernatant was discarded and the pellet resuspended in 3 ml of a sterile filtered BSA/DMEM solution containing 20% (w/v) BSA (Capricorn scientific GmbH) in DMEM with pH adjusted to 7,4. The tube was closed and shaken vigorously for 10 seconds. The suspension was centrifuged at 1000g for 20 minutes at RT. Maximum acceleration speed and minimal deceleration speed were used. After centrifugation, the myelin layer together with the BSA solution was carefully removed and transferred into a fresh tube. The pellet was kept on ice. The steps were repeated until three tubes with a pellet were obtained per brain.

The remaining supernatant was discarded. The pellets were pooled, resuspended in 1 ml of the BSA solution and centrifuged at 1000g for 20 minutes at RT. The supernatant was discarded and the pellet resuspended in 1 ml of the PBS/HEPES buffer. The suspension was then pipetted on a reverted 40 µm cell strainer (Corning) over a 50 ml tube (Corning) and subsequently washed with 5 ml 1xPBS. The cell strainer was then flipped over and washed backwards with 5 ml 1xPBS into 15 ml tube to recover the microvessels. The suspension was centrifuged at 1000g for 5 minutes. The supernatant was carefully removed and discarded. The pellet was resuspended in 2 ml PBS and transferred into a 2 ml tube. This was centrifuged at 13000 rpm for 10 minutes. The supernatant was discarded and the tube containing the pellet with the microvessels was put into liquid nitrogen and afterwards stored at -80 °C for further usage.

5.2.7 Histology and Immunofluorescence labeling

Isolated half brains were fixed in 4% Roti® Histofix for 24 h at 4 °C and then transferred into a sucrose solution containing 30% (w/v) sucrose (Carl Roth GmbH & Co. KG) in PBS for 48 h at 4 °C. The samples were removed from the solution, placed in tissue molds (Ted Pella Inc.), covered completely in TissueTek® (Sakura) and then frozen and stored at -20 °C. The frozen and embedded brains were cut with a cryo-microtome to gain 30 µm sections. Those were brought on SuperFrost® Plus microscope slides (Gerhard Menzel GmbH). The samples needed to undergo an antigen retrieval process. Therefore sodium citrate buffer containing 10mM $Na_3C_6H_5O_7$ (Merck) and 0,05% Tween20 (Sigma Aldrich) in distilled water adjusted to pH 6.0, was filled in glass recs. They were put into a water bath (GFL), which was heated up to 95 °C. Until the citrate buffer reached the temperature, the slides were transferred into the recs and they were incubated at 90-95 °C for 20 minutes. Afterwards, the recs were removed from the water bath and kept at RT to cool down for 20 minutes. The slides were then removed and washed once in 1xPBS. The samples were framed with a pap pen (Science services) to prevent spilling of the used solutions afterwards. The immunostaining of the samples was done on the slides. Whole tissue mounts from the CP and the meninges were transferred into plastic tissue molds containing 1 ml of 4% Roti® Histofix. They were fixed for 20 minutes at RT. The fixation agent was removed and the samples were washed 2 x 10 minutes at RT with 2 ml Tris buffered saline (TBS) containing 0,1M Tris (Roche Diagnostics GmbH) and 0,9% NaCl in distilled water adjusted to pH 7,4. The immunostaining of the samples was done free floating.

All samples were incubated for 1h at RT with blocking solution containing 0.2% Triton X-100 (Sigma Aldrich) and 5% goat serum (Sigma Aldrich) in TBS. The blocking solution was removed and primary antibody solution containing 0.2% Triton X-100 and 5% goat serum in TBS was added for an overnight incubation at 4 °C. The used primary antibodies and dilutions are listed in Table 5. Additionally, for some samples biotinylated *solanum tuberosum* lectin (STL) (Vector Laboratories, Art.No. B-1165, 1:300 whole tissue mount, 1:500 tissue section) was used. After washing the samples two times for 5 minutes with TBS, the secondary antibody solution containing 2% BSA and 0,001 mg/ ml DAPI (Thermo Fisher Scientific Inc.) in TBS was added for 1 h at RT. The used secondary antibodies and dilutions are listed in Table 6. Further, for some samples Streptavidin (Jackson IRL, Art.No. 016-540-084, conjugate Alexa Fluor® 488, 1:500) was used. After the incubation, the samples were washed two times for 5 minutes with TBS. The sections that were stained on slides were mounted with Vectashield® Vibrance® mounting medium (Vector Laboratories) quickly after the last washing step, to prevent them from drying out. For the whole tissue mounts, subsequently after the final washing step, the samples were transferred into a petri dish completely filled with TBS, containing a SuperFrost® Plus microscope slide on the bottom. Using a stereo microscope, the samples in the TBS filled petri dish were unfolded, arranged and brought onto the microscope slide with two fine forceps. The microscope slide was removed out of the TBS stepwise while simultaneously arranging the sample on the slide. Once on the slide, the whole tissue mounts were mounted with Vectashield® Vibrance® mounting medium quickly after taking them out of the petri dish, to prevent them from drying out.

The following antibodies and dilutions were used for this work (Table 5 & Table 6):

Table 5: Primary antibodies for histology

Antigen	Species	Sourced from	Dilution
LGTV NS3 Protein	Chicken	kind gift from Sonja Best, NIAID, USA	1:2000
CD45	Rat	Synaptic Systems Clone GHH45/97A2 Cat.No. HS-427 017	1:400
E-Cadherin	Rabbit	Invitrogen Polyclonal Cat.No. PA5-85088	1:500
TMEM119	Rabbit	Synaptic Systems Polyclonal Cat.No. 400 002	1:500
Iba-1	Guinea pig	Synaptic Systems Clone Gp311H9 Cat.No. 234 308	1:250
NeuN	Guinea pig	Synaptic Systems Polyclonal Cat.No. 266 004	1:400
CD140b	Rat	Invitrogen Clone APB5 Cat.No. 14-1402-82	1:100

Table 6: Secondary antibodies for histology

Target	Host	Conjugate	Sourced from	Dilution
Chicken IgY	Goat	Alexa Fluor® 488	Invitrogen Cat.No. A-11039	1:1000
Chicken IgY	Goat	Alexa Fluor® 546	Invitrogen Cat.No. A-11040	1:800
Rat IgG	Goat	Alexa Fluor® 546	Invitrogen Cat.No. A-11081	1:800
Rat IgG	Goat	Alexa Fluor® 647	Invitrogen Cat.No. A-21247	1:800
Rabbit IgG	Goat	Alexa Fluor® 546	Invitrogen Cat.No. A-11010	1:800
Guinea pig IgG	Goat	Alexa Fluor® 647	Jackson IRL Cat.No. 106-605-003	1:500

5.2.8 RNA isolation and qRT-PCR

For the extraction of the total RNA from CP and meninges, the samples were processed with the ISOLATE II RNA Micro Kit (Bioline) according to the manufacturers specifications. For the extraction of the total RNA from the OB, FC, Cbel and the BMVs, the samples were homogenized with a ceramic sphere (1/4'', MP-Biomedical) in a Fast-Prep-24-homogenizer (MP-Biomedical) in peqGOLD Trifast (Peqlab) (1 ml for FC and Cbel, 500 µl for OB and BMVs) for 2 x 20s at 4,5 m/s. Afterwards, samples were left resting for 5 minutes at RT. For the further extraction, firstly a maximum of 1 ml of the homogenate was transferred into a new tube already containing chloroform (Fluka Analytical) (200 µl for FC and Cbel, 100 µl for OB and BMVs) which was then shaken for 15 seconds by hand. The suspension was then incubated for 10 minutes at RT and afterwards centrifuged at 13.000 rpm for 15 minutes at 4 °C. After centrifugation, the clear phase was carefully isolated and transferred into a new tube already containing 500 µl isopropanol (J.T. Baker). This was then gently mixed and incubated for 5 minutes at RT. Subsequently this step was followed by a further centrifugation at 13.000 rpm for 10 minutes at 4 °C. The supernatant was discarded and the pellet washed in 1 ml of 75% ethanol (Otto Fischar GmbH & Co. KG). The suspension was then centrifuged at 13.000 rpm for 10 minutes at 4 °C.

This washing step was repeated once and the pellet was left to dry afterwards at RT for 5-10 minutes. Finally the pellet was resuspended in 20-200 µl of RNase free water (Sigma) (depending on the amount of sample material) and RNA concentration was measured at the NanoDrop (Thermo Fisher Scientific Inc.). For cDNA synthesis, the M-MLV reverse transcriptase kit (Invitrogen) was used according to the manufacturers specifications. 1 µg of the isolated RNA was used for cDNA synthesis. For the analyses of the LGTV RNA, the KAPA probe fast universal qPCR Kit (KAPA Biosystems) was used according to the manufacturers specifications together with the primers for LGTV NS3 (Table 7) and a probe for LGTV NS3 (FAM-AGAGA-CAGATCCCTGATGG-BHQ1). For the analyses of CLDN-2, CLDN-5, occludin and ZO-1 the KAPA SYBR fast qPCR master mix universal (KAPA Biosystems) was used together with the respective primers (Table 7) according to the manufacturers specifications. For comparison, the housekeeping gene β-actin was analyzed in the same way. For all analyses, the 1:10 diluted cDNA out of 1 µg RNA was used. The Samples were analyzed in LightCycler multiwell plates (96 well, white, Roche) with the LightCycler® 480 Instrument II (Roche). The ratio of LGTV or the tight junction proteins to β-actin was analyzed with the LightCycler® Software 480 II (Roche).

5.2.9 Focus forming unit assay

For the FFU assay, Vero cells (ATCC) were seeded with a density of $2x10^4$ cells per well in a 96-well plate (Sarstedt AG) in 100 µl of Vero cell culture medium containing RPMI (Thermo Fisher Scientific Inc.) with 25mM HEPES, 10% FBS (Capricorn scientific GmbH), 1% pyruvate (Sigma Aldrich) and 1% penicillin/streptomycin (Thermo Fisher Scientific Inc.). After 24 h, the cell layer reached about 80% confluence. At this time point, the samples from the serum and CSF isolations were thawed and eight serial dilutions by factor ten were made ranging from 10^{-1} to 10^{-8} in DMEM. The Vero cell culture medium was aspirated from the plates, the wells were washed once with 100 µl PBS and 50 µl of the respective dilutions were added per well. After incubating the plates 2 h at 37 °C and 5% CO_2 the dilutions were aspirated and 100 µl of overlay medium containing MEM (Thermo Fisher Scientific Inc.) with 1,5% methocel (Sigma Aldrich), 2% penicillin/streptomycin, 1% Glutamax® (Thermo Fisher Scientific Inc.), 4,2 g/ L BSA, 20mM HEPES, 2,4 g/ L $NaHCO_3$ (Sigma Aldrich) and 34% H_2O was added. The plates were then incubated for 48h at 37 °C and 5% CO_2. After the incubation, the overlay medium was aspirated and the wells were washed with 150 µl PBS three times. Subsequently, the Plates were put in a bath of 6% formaldehyde (Carl Roth GmbH & Co. KG) in 0,9% NaCl solution.

After 30 minutes of fixation, the cells were fixed and the virus inactivated. The plates were washed thoroughly in tap water, tapped dry on tissues and 60 µl of permeabilisation solution containing PBS with 0,5% Triton X-100, 0,05% Tween80 (Sigma Aldrich) and 20 mM Glycin (Carl Roth GmbH & Co. KG) was added per well. After 20 minutes, the solution was removed and the wells were washed once with 150 µl washing solution (PBS with 0,05% Tween80). The washing step was followed by adding 50 µl of primary antibody solution (PBS with 10% FBS, 0,05% Tween80, 0,1% NaN3 (Carl Roth GmbH & Co. KG), mouse anti-TBEV E-protein antibody 1:1000 [277]) to each well. After 1h, the primary antibody solution was removed and the wells were washed twice with 150 µl washing solution respectively. Then 50 µl of secondary antibody solution (PBS with 10% FBS, 0,05% Tween80, goat anti-mouse antibody conjugated with horseradish peroxidase 1:2000 (Jackson IRL, Cat.No. 115-035-003)) was added per well. Subsequently after an incubation time of 1h, the solution was removed and the wells were washed again twice with 150 µl washing solution. The assay was proceeded by adding 60 µl of TrueBlue peroxidase substrate (SeraCare life sciences Inc.) to each well and incubating the plates for 30 minutes. After incubation, the solution was discarded and the wells were examined with a stereomicroscope. The manifested purple foci were counted and the FFUs were calculated.

Table 7: Primers for qRT-PCR

Gene	GenBank Access Number	Forward	Reverse
CLDN-2 (mouse)	NM_016675.4	GACGGCTCCGTTTTCTAGATGC	TCGTTTGGCTGCTGCTCTTG
CLDN-5 (mouse)	NM_013805.4	TCTGCTGGTTCGCCAACAT	CGGCACCGTCGGATCA
Occludin (mouse)	NM_008756.2	TGGCAAGCGATCATACCCAGAG	CTGCCTGAAGTCATCCACACTC
ZO-1 (mouse)	NM_009386.2	GTTGGTACGGTGCCCTGAAAGA	GCTGACAGGTAGGACAGACGAT
LGTV NS3 (mouse)	NP_740299.1	AACGGAGCCATAGCCAGTGA	AACCCGTCCCGCCACTC
β-actin	BC138614.1	TGGAATCCTGTGGCATCCATGAAA	TAAAACGCAGCTCAGTAACAGTCCG

6. References

[1] **Süss J**; Klaus, Christine; Diller, Roland; Schrader, Christina; Wohanka, Nikolaus; Abel, Ulrich. 2006. TBE incidence versus virus prevalence and increased prevalence of the TBE virus in Ixodes ricinus removed from humans. Int J Med Microbiol 296 Suppl 40:63–68. doi:10.1016/j.ijmm.2005.12.005.

[2] **Dobler P**; Erber, W.; Bröker, M.; Schmit, P.D.H.J. 2019. The TBE Book: 2nd Edition. Global Health Press Pte Limited.

[3] **Mansfield KL**; Johnson, N.; Phipps, L. P.; Stephenson, J. R.; Fooks, A. R.; Solomon, T. 2009. Tick-borne encephalitis virus - a review of an emerging zoonosis. J Gen Virol 90:1781–1794. doi:10.1099/vir.0.011437-0.

[4] **Taba P**; Schmutzhard, E.; Forsberg, P.; Lutsar, I.; Ljøstad, U.; Mygland, Å.; Levchenko, I.; Strle, F.; Steiner, I. 2017. EAN consensus review on prevention, diagnosis and management of tick-borne encephalitis. Eur J Neurol 24:1214-e61. doi:10.1111/ene.13356.

[5] **Giraudon P**; Bernard, A. 2010. Inflammation in neuroviral diseases. J Neural Transm (Vienna) 117:899–906. doi:10.1007/s00702-010-0402-y.

[6] **Desforges M**; Le Coupanec, A.; Dubeau, P.; Bourgouin, A.; Lajoie, L.; Dube, M.; Talbot, P. J. 2019. Human Coronaviruses and Other Respiratory Viruses: Underestimated Opportunistic Pathogens of the Central Nervous System? Viruses 12. doi:10.3390/v12010014.

[7] **Caballero MT**; Polack, F. P. 2018. Respiratory syncytial virus is an "opportunistic" killer. Pediatr Pulmonol 53:664–667. doi:10.1002/ppul.23963.

[8] **Lafon M.** 2008. Immune evasion, a critical strategy for rabies virus. Dev Biol (Basel) 131:413–419.

[9] **Aurelian L.** 2005. HSV-induced apoptosis in herpes encephalitis. Curr Top Microbiol Immunol 289:79–111. doi:10.1007/3-540-27320-4_4.

[10] **Mackenzie JS**; Gubler, D. J.; Petersen, L. R. 2004. Emerging flaviviruses: the spread and resurgence of Japanese encephalitis, West Nile and dengue viruses. Nat Med 10:S98-109. doi:10.1038/nm1144.

[11] **Koyuncu OO**; Hogue, I. B.; Enquist, L. W. 2013. Virus infections in the nervous system. Cell Host Microbe 13:379–393. doi:10.1016/j.chom.2013.03.010.

[12] **Feige L**; Zaeck, L. M.; Sehl-Ewert, J.; Finke, S.; Bourhy, H. 2021. Innate Immune Signaling and Role of Glial Cells in Herpes Simplex Virus- and Rabies Virus-Induced Encephalitis. Viruses 13. doi:10.3390/v13122364.

[13] **Fooks AR**; Cliquet, F.; Finke, S.; Freuling, C.; Hemachudha, T.; Mani, R. S.; Muller, T.; Nadin-Davis, S.; Picard-Meyer, E.; Wilde, H.; Banyard, A. C. 2017. Rabies. Nat Rev Dis Primers 3:17091. doi:10.1038/nrdp.2017.91.

[14] **Ugolini G.** 2011. Rabies virus as a transneuronal tracer of neuronal connections. Adv Virus Res 79:165–202. doi:10.1016/B978-0-12-387040-7.00010-X.

[15] **Smith G.** 2012. Herpesvirus transport to the nervous system and back again. Annu Rev Microbiol 66:153–176. doi:10.1146/annurev-micro-092611-150051.

[16] **Plakhov IV**; Arlund, E. E.; Aoki, C.; Reiss, C. S. 1995. The earliest events in vesicular stomatitis virus infection of the murine olfactory neuroepithelium and entry of the central nervous system. Virology 209:257–262. doi:10.1006/viro.1995.1252.

[17] **Sauder C**; Staeheli, P. 2003. Rat model of borna disease virus transmission: epidemiological implications. J Virol 77:12886–12890. doi:10.1128/jvi.77.23.12886-12890.2003.

[18] **Lafay F**; Coulon, P.; Astic, L.; Saucier, D.; Riche, D.; Holley, A.; Flamand, A. 1991. Spread of the CVS strain of rabies virus and of the avirulent mutant AvO1 along the olfactory pathways of the mouse after intranasal inoculation. Virology 183:320–330. doi:10.1016/0042-6822(91)90145-2.

[19] **Astic L**; Saucier, D.; Coulon, P.; Lafay, F.; Flamand, A. 1993. The CVS strain of rabies virus as transneuronal tracer in the olfactory system of mice. Brain Res 619:146–156. doi:10.1016/0006-8993(93)91606-s.

[20] **Mori I**; Nishiyama, Y.; Yokochi, T.; Kimura, Y. 2005. Olfactory transmission of neurotropic viruses. J Neurovirol 11:129–137. doi:10.1080/13550280590922793.

[21] **Tabor-Godwin JM**; Ruller, C. M.; Bagalso, N.; An, N.; Pagarigan, R. R.; Harkins, S.; Gilbert, P. E.; Kiosses, W. B.; Gude, N. A.; Cornell, C. T.; Doran, K. S.; Sussman, M. A.; Whitton, J. L.; Feuer, R. 2010. A novel population of myeloid cells responding to coxsackievirus infection assists in the dissemination of virus within the neonatal CNS. J Neurosci 30:8676–8691. doi:10.1523/JNEUROSCI.1860-10.2010.

[22] **Falangola MF**; Hanly, A.; Galvao-Castro, B.; Petito, C. K. 1995. HIV infection of human choroid plexus: a possible mechanism of viral entry into the CNS. J Neuropathol Exp Neurol 54:497–503. doi:10.1097/00005072-199507000-00003.

[23] **Feuer R**; Mena, I.; Pagarigan, R. R.; Harkins, S.; Hassett, D. E.; Whitton, J. L. 2003. Coxsackievirus B3 and the neonatal CNS: the roles of stem cells, developing neurons, and apoptosis in infection, viral dissemination, and disease. Am J Pathol 163:1379–1393. doi:10.1016/S0002-9440(10)63496-7.

[24] **Verma S**; Lo, Y.; Chapagain, M.; Lum, S.; Kumar, M.; Gurjav, U.; Luo, H.; Nakatsuka, A.; Nerurkar, V. R. 2009. West Nile virus infection modulates human brain microvascular endothelial cells tight junction proteins and cell adhesion molecules: Transmigration across the in vitro blood-brain barrier. Virology 385:425–433. doi:10.1016/j.virol.2008.11.047.

[25] **Casiraghi C**; Dorovini-Zis, K.; Horwitz, M. S. 2011. Epstein-Barr virus infection of human brain microvessel endothelial cells: a novel role in multiple sclerosis. J Neuroimmunol 230:173–177. doi:10.1016/j.jneuroim.2010.08.003.

[26] **Fletcher NF**; Wilson, G. K.; Murray, J.; Hu, K.; Lewis, A.; Reynolds, G. M.; Stamataki, Z.; Meredith, L. W.; Rowe, I. A.; Luo, G.; Lopez-Ramirez, M. A.; Baumert, T. F.; Weksler, B.; Couraud, P. O.; Kim, K. S.; Romero, I. A.; Jopling, C.; Morgello, S.; Balfe, P.; McKeating, J. A. 2012. Hepatitis C virus infects the endothelial cells of the blood-brain barrier. Gastroenterology 142:634-643 e6. doi:10.1053/j.gastro.2011.11.028.

[27] **Altan-Bonnet N.** 2016. Extracellular vesicles are the Trojan horses of viral infection. Curr Opin Microbiol 32:77–81. doi:10.1016/j.mib.2016.05.004.

[28] **Reisen WK.** 2017. Epidemiology, p. 7–34. *In* Marcondes CB (ed), Arthropod Borne Diseases. Springer International Publishing, Cham.

[29] International Committee on Taxonomy of Viruses (ICTV). Accessed 10 October, 2022.

[30] **Thomas SJ**; Endy, T. P.; Rothman, A. L.; Barrett, A. D. 2019. Flaviviruses, p. 2013–2039. *In* Mandell, Douglas, and Bennett's Principles and Practice of Infectious Diseases E-Book, 9th ed., vol. 1. Elsevier Health Sciences.

[31] **Dobler G.** 2010. Zoonotic tick-borne flaviviruses. Vet Microbiol 140:221–228. doi:10.1016/j.vetmic.2009.08.024.

[32] **Weissenbock H**; Hubalek, Z.; Bakonyi, T.; Nowotny, N. 2010. Zoonotic mosquito-borne flaviviruses: worldwide presence of agents with proven pathogenicity and potential candidates of future emerging diseases. Vet Microbiol 140:271–280. doi:10.1016/j.vetmic.2009.08.025.

[33] **Gould EA**; Solomon, T. 2008. Pathogenic flaviviruses. Lancet 371:500–509. doi:10.1016/S0140-6736(08)60238-X.

[34] **Gritsun TS**; Gould, E. A. 2008. Tick-bourne encephalitis Viruses (Flaviviridae), p. 45–54. *In* Encyclopedia of Virology, vol. 3. Elsevier.

[35] **Wang X**; Li, S. H.; Zhu, L.; Nian, Q. G.; Yuan, S.; Gao, Q.; Hu, Z.; Ye, Q.; Li, X. F.; Xie, D. Y.; Shaw, N.; Wang, J.; Walter, T. S.; Huiskonen, J. T.; Fry, E. E.; Qin, C. F.; Stuart, D. I.; Rao, Z. 2017. Near-atomic structure of Japanese encephalitis virus reveals critical determinants of virulence and stability. Nat Commun 8:14. doi:10.1038/s41467-017-00024-6.

[36] **Sirohi D**; Chen, Z.; Sun, L.; Klose, T.; Pierson, T. C.; Rossmann, M. G.; Kuhn, R. J. 2016. The 3.8 A resolution cryo-EM structure of Zika virus. Science 352:467–470. doi:10.1126/science.aaf5316.

[37] **Kuhn RJ**; Zhang, W.; Rossmann, M. G.; Pletnev, S. V.; Corver, J.; Lenches, E.; Jones, C. T.; Mukhopadhyay, S.; Chipman, P. R.; Strauss, E. G.; Baker, T. S.; Strauss, J. H. 2002. Structure of dengue virus: implications for flavivirus organization, maturation, and fusion. Cell 108:717–725. doi:10.1016/s0092-8674(02)00660-8.

[38] **Zhang Y**; Corver, J.; Chipman, P. R.; Zhang, W.; Pletnev, S. V.; Sedlak, D.; Baker, T. S.; Strauss, J. H.; Kuhn, R. J.; Rossmann, M. G. 2003. Structures of immature flavivirus particles. EMBO J 22:2604–2613. doi:10.1093/emboj/cdg270.

[39] **Robertson SJ**; Mitzel, D. N.; Taylor, R. T.; Best, S. M.; Bloom, M. E. 2009. Tick-borne flaviviruses: dissecting host immune responses and virus countermeasures. Immunol Res 43:172–186. doi:10.1007/s12026-008-8065-6.

[40] **Murray CL**; Jones, C. T.; Rice, C. M. 2008. Architects of assembly: roles of Flaviviridae non-structural proteins in virion morphogenesis. Nat Rev Microbiol 6:699–708. doi:10.1038/nrmicro1928.

[41] **Lindenbach BD**; Rice, C. M. 2003. Molecular biology of flaviviruses. Adv Virus Res 59:23–61. doi:10.1016/s0065-3527(03)59002-9.

[42] **Mukhopadhyay S**; Kim, B. S.; Chipman, P. R.; Rossmann, M. G.; Kuhn, R. J. 2003. Structure of West Nile virus. Science 302:248. doi:10.1126/science.1089316.

[43] **Yu IM**; Zhang, W.; Holdaway, H. A.; Li, L.; Kostyuchenko, V. A.; Chipman, P. R.; Kuhn, R. J.; Rossmann, M. G.; Chen, J. 2008. Structure of the immature dengue virus at low pH primes proteolytic maturation. Science 319:1834–1837. doi:10.1126/science.1153264.

[44] **Smit JM**; Moesker, B.; Rodenhuis-Zybert, I.; Wilschut, J. 2011. Flavivirus cell entry and membrane fusion. Viruses 3:160–171. doi:10.3390/v3020160.

[45] **Kopecky J**; Grubhoffer, L.; Kovar, V.; Jindrak, L.; Vokurkova, D. 1999. A putative host cell receptor for tick-borne encephalitis virus identified by anti-idiotypic antibodies and virus affinoblotting. Intervirology 42:9–16. doi:10.1159/000024954.

[46] **Maldov DG**; Karganova, G. G.; Timofeev, A. V. 1992. Tick-borne encephalitis virus interaction with the target cells. Arch Virol 127:321–325. doi:10.1007/BF01309594.

[47] **Rodrigues R**; Danskog, Katarina; Överby, Anna K.; Arnberg, Niklas. 2019. Characterizing the cellular attachment receptor for Langat virus. PLoS One 14:e0217359. doi:10.1371/journal.pone.0217359.

[48] **Hackett BA**; Cherry, S. 2018. Flavivirus internalization is regulated by a size-dependent endocytic pathway. Proc Natl Acad Sci U S A 115:4246–4251. doi:10.1073/pnas.1720032115.

[49] **Kroschewski H**; Allison, S. L.; Heinz, F. X.; Mandl, C. W. 2003. Role of heparan sulfate for attachment and entry of tick-borne encephalitis virus. Virology 308:92–100. doi:10.1016/s0042-6822(02)00097-1.

[50] **Zhang Y**; Kaufmann, B.; Chipman, P. R.; Kuhn, R. J.; Rossmann, M. G. 2007. Structure of immature West Nile virus. J Virol 81:6141–6145. doi:10.1128/JVI.00037-07.

[51] **Apte-Sengupta S**; Sirohi, D.; Kuhn, R. J. 2014. Coupling of replication and assembly in flaviviruses. Curr Opin Virol 9:134–142. doi:10.1016/j.coviro.2014.09.020.

[52] **Knyazhanskaya E**; Morais, Marc C.; Choi, Kyung H. 2021. Flavivirus enzymes and their inhibitors. Enzymes 49:265–303. doi:10.1016/bs.enz.2021.07.006.

[53] **Pierson TC**; Diamond, M. S. 2012. Degrees of maturity: the complex structure and biology of flaviviruses. Curr Opin Virol 2:168–175. doi:10.1016/j.coviro.2012.02.011.

[54] **Sips GJ**; Wilschut, J.; Smit, J. M. 2012. Neuroinvasive flavivirus infections. Rev Med Virol 22:69–87. doi:10.1002/rmv.712.

[55] **Gritsun TS**; Frolova, T. V.; Pogodina, V. V.; Lashkevich, V. A.; Venugopal, K.; Gould, E. A. 1993. Nucleotide and deduced amino acid sequence of the envelope gene of the Vasilchenko strain of TBE virus; comparison with other flaviviruses. Virus Res 27:201–209. doi:10.1016/0168-1702(93)90082-x.

[56] **Agudelo M**; Palus, Martin; Keeffe, Jennifer R.; Bianchini, Filippo; Svoboda, Pavel; Salát, Jiří; Peace, Avery; Gazumyan, Anna; Cipolla, Melissa; Kapoor, Tania; Guidetti, Francesca; Yao, Kai-Hui; Elsterová, Jana; Teislerová, Dana; Chrdle, Aleš; Hönig, Václav; Oliveira, Thiago; West, Anthony P.; Lee, Yu E.; Rice, Charles M.; MacDonald, Margaret R.; Bjorkman, Pamela J.; Růžek, Daniel; Robbiani, Davide F.; Nussenzweig, Michel C.

2021. Broad and potent neutralizing human antibodies to tick-borne flaviviruses protect mice from disease. J Exp Med 218. doi:10.1084/jem.20210236.

[57] **VanBlargan LA**; Errico, John M.; Kafai, Natasha M.; Burgomaster, Katherine E.; Jethva, Prashant N.; Broeckel, Rebecca M.; Meade-White, Kimberly; Nelson, Christopher A.; Himansu, Sunny; Wang, David; Handley, Scott A.; Gross, Michael L.; Best, Sonja M.; Pierson, Theodore C.; Fremont, Daved H.; Diamond, Michael S. 2021. Broadly neutralizing monoclonal antibodies protect against multiple tick-borne flaviviruses. J Exp Med 218. doi:10.1084/jem.20210174.

[58] **Gritsun TS**; Lashkevich, V. A.; Gould, E. A. 2003. Tick-borne encephalitis. Antiviral Research 57:129–146. doi:10.1016/s0166-3542(02)00206-1.

[59] **Cornelius ADA**; Hosseini, S.; Schreier, S.; Fritzsch, D.; Weichert, L.; Michaelsen-Preusse, K.; Fendt, M.; Kroger, A. 2020. Langat virus infection affects hippocampal neuron morphology and function in mice without disease signs. J Neuroinflammation 17:278. doi:10.1186/s12974-020-01951-w.

[60] **Weber E**; Finsterbusch, K.; Lindquist, R.; Nair, S.; Lienenklaus, S.; Gekara, N. O.; Janik, D.; Weiss, S.; Kalinke, U.; Overby, A. K.; Kroger, A. 2014. Type I interferon protects mice from fatal neurotropic infection with Langat virus by systemic and local antiviral responses. J Virol 88:12202–12212. doi:10.1128/JVI.01215-14.

[61] **Kurhade C**; Zegenhagen, L.; Weber, E.; Nair, S.; Michaelsen-Preusse, K.; Spanier, J.; Gekara, N. O.; Kroger, A.; Overby, A. K. 2016. Type I Interferon response in olfactory bulb, the site of tick-borne flavivirus accumulation, is primarily regulated by IPS-1. J Neuroinflammation 13:22. doi:10.1186/s12974-016-0487-9.

[62] **Süss J.** 2011. Tick-borne encephalitis 2010: epidemiology, risk areas, and virus strains in Europe and Asia-an overview. Ticks Tick Borne Dis 2:2–15. doi:10.1016/j.ttbdis.2010.10.007.

[63] **Smith CEG.** 1956. A virus resembling Russian spring-summer encephalitis virus from an ixodid tick in Malaya. Nature 178:581–582. doi:10.1038/178581a0.

[64] **Ličková M**; Fumačová Havlíková, Sabína; Sláviková, Monika; Klempa, Boris. 2021. Alimentary Infections by Tick-Borne Encephalitis Virus. Viruses 14. doi:10.3390/v14010056.

[65] **Bakhvalova VN**; Potapova, O. F.; Panov, V. V.; Morozova, O. V. 2009. Vertical transmission of tick-borne encephalitis virus between generations of adapted reservoir small rodents. Virus Res 140:172–178. doi:10.1016/j.virusres.2008.12.001.

[66] **Bakhvalova VN**; Dobrotvorsky, Andrey K.; Panov, Viktor V.; Matveeva, Vera A.; Tkachev, Sergey E.; Morozova, Olga V. 2006. Natural tick-borne encephalitis virus infection among wild small mammals in the southeastern part of western Siberia, Russia. Vector Borne Zoonotic Dis 6:32–41. doi:10.1089/vbz.2006.6.32.

[67] **Labuda M**; Jones, L. D.; Williams, T.; Danielova, V.; Nuttall, P. A. 1993. Efficient transmission of tick-borne encephalitis virus between cofeeding ticks. J Med Entomol 30:295–299. doi:10.1093/jmedent/30.1.295.

[68] **Slovák M**; Kazimírová, Mária; Siebenstichová, Marta; Ustaníková, Katarína; Klempa, Boris; Gritsun, Tamara; Gould, Ernest A.; Nuttall, Patricia A. 2014. Survival dynamics of

tick-borne encephalitis virus in Ixodes ricinus ticks. Ticks Tick Borne Dis 5:962–969. doi:10.1016/j.ttbdis.2014.07.019.

[69] **Duniewicz M.** 1976. Klinisches Bild der Zentraleuropäischen Zeckenenzephalitis. MMW Munch Med Wochenschr 118:1609–1612.

[70] **Kaiser R.** 1999. The clinical and epidemiological profile of tick-borne encephalitis in southern Germany 1994-98: a prospective study of 656 patients. Brain 122 (Pt 11):2067–2078. doi:10.1093/brain/122.11.2067.

[71] **Kaiser R.** 2012. Tick-borne encephalitis: Clinical findings and prognosis in adults. Wien Med Wochenschr 162:239–243. doi:10.1007/s10354-012-0105-0.

[72] **Ziebart-Schroth A.** 1972. Frühsommermeningoenzephalitis (FSME). Klinik und besondere Verlaufsformen. Wien Klin Wochenschr 84:778–781.

[73] **Ackermann R**; Rehse-Küpper, B. 1979. Die Zentraleuropäische Enzephalitis in der Bundesrepublik Deutschland. Fortschr Neurol Psychiatr Grenzgeb 47:103–122.

[74] **Bogovic P**; Kastrin, A.; Lotric-Furlan, S.; Ogrinc, K.; Zupanc, T. A.; Korva, M.; Knap, N.; Strle, F. 2022. Clinical and Laboratory Characteristics and Outcome of Illness Caused by Tick-Borne Encephalitis Virus without Central Nervous System Involvement. Emerg Infect Dis 28:291–301. doi:10.3201/eid2802.211661.

[75] **Kunz C.** 1992. Tick-borne encephalitis in Europe. Acta Leiden 60:1–14.

[76] **Dumpis U**; Crook, D.; Oksi, J. 1999. Tick-borne encephalitis. Clin Infect Dis 28:882–890. doi:10.1086/515195.

[77] **Lotric-Furlan S**; Avsic-Zupanc, T.; Strle, F. 2000. Is an isolated initial phase of a tick-borne encephalitis a common event? Clin Infect Dis 30:987–988. doi:10.1086/313838.

[78] **Labuda M**; Austyn, J. M.; Zuffova, E.; Kozuch, O.; Fuchsberger, N.; Lysy, J.; Nuttall, P. A. 1996. Importance of localized skin infection in tick-borne encephalitis virus transmission. Virology 219:357–366. doi:10.1006/viro.1996.0261.

[79] **Yu C**; Achazi, Katharina; Möller, Lars; Schulzke, Joerg D.; Niedrig, Matthias; Bücker, Roland. 2014. Tick-borne encephalitis virus replication, intracellular trafficking, and pathogenicity in human intestinal Caco-2 cell monolayers. PLoS One 9:e96957. doi:10.1371/journal.pone.0096957.

[80] **Dörrbecker B**; Dobler, Gerhard; Spiegel, Martin; Hufert, Frank T. 2010. Tick-borne encephalitis virus and the immune response of the mammalian host. Travel Med Infect Dis 8:213–222. doi:10.1016/j.tmaid.2010.05.010.

[81] **Lindqvist R**; Upadhyay, Arunkumar; Överby, Anna K. 2018. Tick-Borne Flaviviruses and the Type I Interferon Response. Viruses 10. doi:10.3390/v10070340.

[82] **Levy DE**; Marie, I. J.; Durbin, J. E. 2011. Induction and function of type I and III interferon in response to viral infection. Curr Opin Virol 1:476–486. doi:10.1016/j.coviro.2011.11.001.

[83] **Schroder K**; Tschopp, Jurg. 2010. The inflammasomes. Cell 140:821–832. doi:10.1016/j.cell.2010.01.040.

[84] **Takeuchi O**; Akira, S. 2010. Pattern recognition receptors and inflammation. Cell 140:805–820. doi:10.1016/j.cell.2010.01.022.

[85] **Alexopoulou L**; Holt, A. C.; Medzhitov, R.; Flavell, R. A. 2001. Recognition of double-stranded RNA and activation of NF-kappaB by Toll-like receptor 3. Nature 413:732–738. doi:10.1038/35099560.

[86] **Chen Y**; Lin, Junhong; Zhao, Yao; Ma, Xianping; Yi, Huashan. 2021. Toll-like receptor 3 (TLR3) regulation mechanisms and roles in antiviral innate immune responses. J Zhejiang Univ Sci B 22:609–632. doi:10.1631/jzus.B2000808.

[87] **Kawai T**; Akira, Shizuo. 2008. Toll-like receptor and RIG-I-like receptor signaling. Ann N Y Acad Sci 1143:1–20. doi:10.1196/annals.1443.020.

[88] **Akira S**; Uematsu, S.; Takeuchi, O. 2006. Pathogen recognition and innate immunity. Cell 124:783–801. doi:10.1016/j.cell.2006.02.015.

[89] **Heil F**; Hemmi, Hiroaki; Hochrein, Hubertus; Ampenberger, Franziska; Kirschning, Carsten; Akira, Shizuo; Lipford, Grayson; Wagner, Hermann; Bauer, Stefan. 2004. Species-specific recognition of single-stranded RNA via toll-like receptor 7 and 8. Science 303:1526–1529. doi:10.1126/science.1093620.

[90] **Lund JM**; Alexopoulou, Lena; Sato, Ayuko; Karow, Margaret; Adams, Niels C.; Gale, Nicholas W.; Iwasaki, Akiko; Flavell, Richard A. 2004. Recognition of single-stranded RNA viruses by Toll-like receptor 7. Proc Natl Acad Sci U S A 101:5598–5603. doi:10.1073/pnas.0400937101.

[91] **Wang JP**; Liu, Ping; Latz, Eicke; Golenbock, Douglas T.; Finberg, Robert W.; Libraty, Daniel H. 2006. Flavivirus activation of plasmacytoid dendritic cells delineates key elements of TLR7 signaling beyond endosomal recognition. J Immunol 177:7114–7121. doi:10.4049/jimmunol.177.10.7114.

[92] **Yoneyama M**; Kikuchi, Mika; Natsukawa, Takashi; Shinobu, Noriaki; Imaizumi, Tadaatsu; Miyagishi, Makoto; Taira, Kazunari; Akira, Shizuo; Fujita, Takashi. 2004. The RNA helicase RIG-I has an essential function in double-stranded RNA-induced innate antiviral responses. Nat Immunol 5:730–737. doi:10.1038/ni1087.

[93] **Hornung V**; Ellegast, Jana; Kim, Sarah; Brzózka, Krzysztof; Jung, Andreas; Kato, Hiroki; Poeck, Hendrik; Akira, Shizuo; Conzelmann, Karl-Klaus; Schlee, Martin; Endres, Stefan; Hartmann, Gunther. 2006. 5'-Triphosphate RNA is the ligand for RIG-I. Science 314:994–997. doi:10.1126/science.1132505.

[94] **Saito T**; Gale, Michael. 2008. Differential recognition of double-stranded RNA by RIG-I-like receptors in antiviral immunity. J Exp Med 205:1523–1527. doi:10.1084/jem.20081210.

[95] **Yamamoto M**; Sato, Shintaro; Hemmi, Hiroaki; Hoshino, Katsuaki; Kaisho, Tsuneyasu; Sanjo, Hideki; Takeuchi, Osamu; Sugiyama, Masanaka; Okabe, Masaru; Takeda, Kiyoshi; Akira, Shizuo. 2003. Role of adaptor TRIF in the MyD88-independent toll-like receptor signaling pathway. Science 301:640–643. doi:10.1126/science.1087262.

[96] **Kawai T**; Sato, Shintaro; Ishii, Ken J.; Coban, Cevayir; Hemmi, Hiroaki; Yamamoto, Masahiro; Terai, Kenta; Matsuda, Michiyuki; Inoue, Jun-ichiro; Uematsu, Satoshi;

Takeuchi, Osamu; Akira, Shizuo. 2004. Interferon-alpha induction through Toll-like receptors involves a direct interaction of IRF7 with MyD88 and TRAF6. Nat Immunol 5:1061–1068. doi:10.1038/ni1118.

[97] **Meylan E**; Curran, Joseph; Hofmann, Kay; Moradpour, Darius; Binder, Marco; Bartenschlager, Ralf; Tschopp, Jürg. 2005. Cardif is an adaptor protein in the RIG-I antiviral pathway and is targeted by hepatitis C virus. Nature 437:1167–1172. doi:10.1038/nature04193.

[98] **Seth RB**; Sun, Lijun; Ea, Chee-Kwee; Chen, Zhijian J. 2005. Identification and characterization of MAVS, a mitochondrial antiviral signaling protein that activates NF-kappaB and IRF 3. Cell 122:669–682. doi:10.1016/j.cell.2005.08.012.

[99] **Kawai T**; Takahashi, Ken; Sato, Shintaro; Coban, Cevayir; Kumar, Himanshu; Kato, Hiroki; Ishii, Ken J.; Takeuchi, Osamu; Akira, Shizuo. 2005. IPS-1, an adaptor triggering RIG-I- and Mda5-mediated type I interferon induction. Nat Immunol 6:981–988. doi:10.1038/ni1243.

[100] **Xu L-G**; Wang, Yan-Yi; Han, Ke-Jun; Li, Lian-Yun; Zhai, Zhonghe; Shu, Hong-Bing. 2005. VISA is an adapter protein required for virus-triggered IFN-beta signaling. Mol Cell 19:727–740. doi:10.1016/j.molcel.2005.08.014.

[101] **Ghita L**; Breitkopf, Veronika; Mulenge, Felix; Pavlou, Andreas; Gern, Olivia Luise; Durán, Verónica; Prajeeth, Chittappen Kandiyil; Kohls, Moritz; Jung, Klaus; Stangel, Martin; Steffen, Imke; Kalinke, Ulrich. 2021. Sequential MAVS and MyD88/TRIF signaling triggers anti-viral responses of tick-borne encephalitis virus-infected murine astrocytes. J Neurosci Res 99:2478–2492. doi:10.1002/jnr.24923.

[102] **Honda K**; Taniguchi, Tadatsugu. 2006. IRFs: master regulators of signalling by Toll-like receptors and cytosolic pattern-recognition receptors. Nat Rev Immunol 6:644–658. doi:10.1038/nri1900.

[103] **Platanias LC.** 2005. Mechanisms of type-I- and type-II-interferon-mediated signalling. Nat Rev Immunol 5:375–386. doi:10.1038/nri1604.

[104] **Stark GR**; Kerr, I. M.; Williams, B. R.; Silverman, R. H.; Schreiber, R. D. 1998. How cells respond to interferons. Annu Rev Biochem 67:227–264. doi:10.1146/annurev.biochem.67.1.227.

[105] **Schoggins JW.** 2014. Interferon-stimulated genes: roles in viral pathogenesis. Curr Opin Virol 6:40–46. doi:10.1016/j.coviro.2014.03.006.

[106] **Schoggins JW**; Wilson, Sam J.; Panis, Maryline; Murphy, Mary Y.; Jones, Christopher T.; Bieniasz, Paul; Rice, Charles M. 2011. A diverse range of gene products are effectors of the type I interferon antiviral response. Nature 472:481–485. doi:10.1038/nature09907.

[107] **Stetson DB**; Medzhitov, Ruslan. 2006. Type I interferons in host defense. Immunity 25:373–381. doi:10.1016/j.immuni.2006.08.007.

[108] **Chmielewska AM**; Gómez-Herranz, Maria; Gach, Paulina; Nekulova, Marta; Bagnucka, Małgorzata A.; Lipińska, Andrea D.; Rychłowski, Michał; Hoffmann, Weronika; Król, Ewelina; Vojtesek, Borivoj; Sloan, Richard D.; Bieńkowska-Szewczyk, Krystyna; Hupp,

Ted; Ball, Kathryn. 2022. The Role of IFITM Proteins in Tick-Borne Encephalitis Virus Infection. J Virol 96:e0113021. doi:10.1128/JVI.01130-21.

[109] **Lindqvist R**; Kurhade, C.; Gilthorpe, J. D.; Overby, A. K. 2018. Cell-type- and region-specific restriction of neurotropic flavivirus infection by viperin. J Neuroinflammation 15:80. doi:10.1186/s12974-018-1119-3.

[110] **Panayiotou C**; Lindqvist, Richard; Kurhade, Chaitanya; Vonderstein, Kirstin; Pasto, Jenny; Edlund, Karin; Upadhyay, Arunkumar S.; Överby, Anna K. 2018. Viperin Restricts Zika Virus and Tick-Borne Encephalitis Virus Replication by Targeting NS3 for Proteasomal Degradation. J Virol 92. doi:10.1128/JVI.02054-17.

[111] **Taylor RT**; Lubick, Kirk J.; Robertson, Shelly J.; Broughton, James P.; Bloom, Marshall E.; Bresnahan, Wade A.; Best, Sonja M. 2011. TRIM79α, an interferon-stimulated gene product, restricts tick-borne encephalitis virus replication by degrading the viral RNA polymerase. Cell Host Microbe 10:185–196. doi:10.1016/j.chom.2011.08.004.

[112] **Barkhash AV**; Perelygin, Andrey A.; Babenko, Vladimir N.; Myasnikova, Natalia G.; Pilipenko, Pavel I.; Romaschenko, Aida G.; Voevoda, Mikhail I.; Brinton, Margo A. 2010. Variability in the 2'-5'-oligoadenylate synthetase gene cluster is associated with human predisposition to tick-borne encephalitis virus-induced disease. J Infect Dis 202:1813–1818. doi:10.1086/657418.

[113] **Miorin L**; Albornoz, Amelina; Baba, Marycelin M.; D'Agaro, Pierlanfranco; Marcello, Alessandro. 2012. Formation of membrane-defined compartments by tick-borne encephalitis virus contributes to the early delay in interferon signaling. Virus Res 163:660–666. doi:10.1016/j.virusres.2011.11.020.

[114] **Överby AK**; Popov, Vsevolod L.; Niedrig, Matthias; Weber, Friedemann. 2010. Tick-Borne Encephalitis Virus Delays Interferon Induction and Hides Its Double-Stranded RNA in Intracellular Membrane Vesicles. J Virol 84:8470–8483. doi:10.1128/JVI.00176-10.

[115] **Overby AK**; Weber, Friedemann. 2011. Hiding from intracellular pattern recognition receptors, a passive strategy of flavivirus immune evasion. Virulence 2:238–240. doi:10.4161/viru.2.3.16162.

[116] **Robertson SJ**; Lubick, K. J.; Freedman, B. A.; Carmody, A. B.; Best, S. M. 2014. Tick-borne flaviviruses antagonize both IRF-1 and type I IFN signaling to inhibit dendritic cell function. J Immunol 192:2744–2755. doi:10.4049/jimmunol.1302110.

[117] **Selinger M**; Tykalová, Hana; Štěrba, Ján; Věchtová, Pavlína; Vavrušková, Zuzana; Lieskovská, Jaroslava; Kohl, Alain; Schnettler, Esther; Grubhoffer, Libor. 2019. Tick-borne encephalitis virus inhibits rRNA synthesis and host protein production in human cells of neural origin. PLoS Negl Trop Dis 13:e0007745. doi:10.1371/journal.pntd.0007745.

[118] **Cervantes-Salazar M**; Angel-Ambrocio, A. H.; Soto-Acosta, R.; Bautista-Carbajal, P.; Hurtado-Monzon, A. M.; Alcaraz-Estrada, S. L.; Ludert, J. E.; Del Angel, R. M. 2015. Dengue virus NS1 protein interacts with the ribosomal protein RPL18: this interaction is required for viral translation and replication in Huh-7 cells. Virology 484:113–126. doi:10.1016/j.virol.2015.05.017.

[119] **Avirutnan P**; Hauhart, R. E.; Somnuke, P.; Blom, A. M.; Diamond, M. S.; Atkinson, J. P. 2011. Binding of flavivirus nonstructural protein NS1 to C4b binding protein modulates complement activation. J Immunol 187:424–433. doi:10.4049/jimmunol.1100750.

[120] **Chen J**; Ng, M. M.; Chu, J. J. 2015. Activation of TLR2 and TLR6 by Dengue NS1 Protein and Its Implications in the Immunopathogenesis of Dengue Virus Infection. PLoS Pathog 11:e1005053. doi:10.1371/journal.ppat.1005053.

[121] **Rastogi M**; Sharma, N.; Singh, S. K. 2016. Flavivirus NS1: a multifaceted enigmatic viral protein. Virol J 13:131. doi:10.1186/s12985-016-0590-7.

[122] **Kuzmenko YV**; Starodubova, E. S.; Karganova, G. G.; Timofeev, A. V.; Karpov, V. L. 2016. Nonstructural protein 1 of tick-borne encephalitis virus activates the expression of immunoproteasome subunits. Mol Biol (Mosk) 50:353–359. doi:10.7868/S0026898416020129.

[123] **Uchil PD**; Satchidanandam, V. 2003. Architecture of the flaviviral replication complex. Protease, nuclease, and detergents reveal encasement within double-layered membrane compartments. J Biol Chem 278:24388–24398. doi:10.1074/jbc.M301717200.

[124] **Munoz-Jordan JL**; Laurent-Rolle, M.; Ashour, J.; Martinez-Sobrido, L.; Ashok, M.; Lipkin, W. I.; Garcia-Sastre, A. 2005. Inhibition of alpha/beta interferon signaling by the NS4B protein of flaviviruses. J Virol 79:8004–8013. doi:10.1128/JVI.79.13.8004-8013.2005.

[125] **Silva PA**; Pereira, C. F.; Dalebout, T. J.; Spaan, W. J.; Bredenbeek, P. J. 2010. An RNA pseudoknot is required for production of yellow fever virus subgenomic RNA by the host nuclease XRN1. J Virol 84:11395–11406. doi:10.1128/JVI.01047-10.

[126] **Munoz-Jordan JL**; Sanchez-Burgos, G. G.; Laurent-Rolle, M.; Garcia-Sastre, A. 2003. Inhibition of interferon signaling by dengue virus. Proc Natl Acad Sci U S A 100:14333–14338. doi:10.1073/pnas.2335168100.

[127] **Best SM**; Morris, K. L.; Shannon, J. G.; Robertson, S. J.; Mitzel, D. N.; Park, G. S.; Boer, E.; Wolfinbarger, J. B.; Bloom, M. E. 2005. Inhibition of interferon-stimulated JAK-STAT signaling by a tick-borne flavivirus and identification of NS5 as an interferon antagonist. J Virol 79:12828–12839. doi:10.1128/JVI.79.20.12828-12839.2005.

[128] **Best SM.** 2017. The Many Faces of the Flavivirus NS5 Protein in Antagonism of Type I Interferon Signaling. J Virol 91. doi:10.1128/JVI.01970-16.

[129] **Lubick KJ**; Robertson, Shelly J.; McNally, Kristin L.; Freedman, Brett A.; Rasmussen, Angela L.; Taylor, R. Travis; Walts, Avram D.; Tsuruda, Seitaro; Sakai, Mizuki; Ishizuka, Mariko; Boer, Elena F.; Foster, Erin C.; Chiramel, Abhilash I.; Addison, Conrad B.; Green, Richard; Kastner, Daniel L.; Katze, Michael G.; Holland, Steven M.; Forlino, Antonella; Freeman, Alexandra F.; Boehm, Manfred; Yoshii, Kentaro; Best, Sonja M. 2015. Flavivirus Antagonism of Type I Interferon Signaling Reveals Prolidase as a Regulator of IFNAR1 Surface Expression. Cell Host Microbe 18:61–74. doi:10.1016/j.chom.2015.06.007.

[130] **Javorsky A**; Humbert, Patrick O.; Kvansakul, Marc. 2022. Molecular basis of Tick Born encephalitis virus NS5 mediated subversion of apico-basal cell polarity signalling. Biochem J 479:1303–1315. doi:10.1042/BCJ20220037.

[131] **Ellencrona K**; Syed, Asim; Johansson, Magnus. 2009. Flavivirus NS5 associates with host-cell proteins zonula occludens-1 (ZO-1) and regulating synaptic membrane exocytosis-2 (RIMS2) via an internal PDZ binding mechanism. Biol Chem 390:319–323. doi:10.1515/BC.2009.041.

[132] **Palus M**; Vancova, M.; Sirmarova, J.; Elsterova, J.; Perner, J.; Ruzek, D. 2017. Tick-borne encephalitis virus infects human brain microvascular endothelial cells without compromising blood-brain barrier integrity. Virology 507:110–122. doi:10.1016/j.virol.2017.04.012.

[133] **Růžek D**; Salát, Jiří; Singh, Sunit K.; Kopecký, Jan. 2011. Breakdown of the blood-brain barrier during tick-borne encephalitis in mice is not dependent on CD8+ T-cells. PLoS One 6:e20472. doi:10.1371/journal.pone.0020472.

[134] **Zhou W**; Woodson, M.; Neupane, B.; Bai, F.; Sherman, M. B.; Choi, K. H.; Neelakanta, G.; Sultana, H. 2018. Exosomes serve as novel modes of tick-borne flavivirus transmission from arthropod to human cells and facilitates dissemination of viral RNA and proteins to the vertebrate neuronal cells. PLoS Pathog 14:e1006764. doi:10.1371/journal.ppat.1006764.

[135] **Papa MP**; Meuren, Lana M.; Coelho, Sharton V. A.; Lucas, Carolina G. de Oliveira; Mustafá, Yasmin M.; Lemos Matassoli, Flavio; Silveira, Paola P.; Frost, Paula S.; Pezzuto, Paula; Ribeiro, Milene R.; Tanuri, Amilcar; Nogueira, Mauricio L.; Campanati, Loraine; Bozza, Marcelo T.; Paula Neto, Heitor A.; Pimentel-Coelho, Pedro M.; Figueiredo, Claudia P.; Aguiar, Renato S. de; Arruda, Luciana B. de. 2017. Zika Virus Infects, Activates, and Crosses Brain Microvascular Endothelial Cells, without Barrier Disruption. Front Microbiol 8:2557. doi:10.3389/fmicb.2017.02557.

[136] **Schreier S.** 2021. Untersuchung zur Transmission, Virusverbreitung und Pathogenität der Zecken-übertragenen Flaviviren Tick-borne encephalitis Vrius und Langat Virus in Mäusen.

[137] **Cipolla MJ.** 2009. *In* The Cerebral Circulation, San Rafael (CA).

[138] **Muoio V**; Persson, P. B.; Sendeski, M. M. 2014. The neurovascular unit - concept review. Acta Physiol (Oxf) 210:790–798. doi:10.1111/apha.12250.

[139] **Harder DR**; Zhang, C.; Gebremedhin, D. 2002. Astrocytes function in matching blood flow to metabolic activity. News Physiol Sci 17:27–31. doi:10.1152/physiologyonline.2002.17.1.27.

[140] **Armstead WM**; Raghupathi, R. 2011. Endothelin and the neurovascular unit in pediatric traumatic brain injury. Neurol Res 33:127–132. doi:10.1179/016164111X12881719352138.

[141] **Abbott NJ**; Friedman, A. 2012. Overview and introduction: the blood-brain barrier in health and disease. Epilepsia 53 Suppl 6:1–6. doi:10.1111/j.1528-1167.2012.03696.x.

[142] **Takeshita Y**; Ransohoff, R. M. 2012. Inflammatory cell trafficking across the blood-brain barrier: chemokine regulation and in vitro models. Immunol Rev 248:228–239. doi:10.1111/j.1600-065X.2012.01127.x.

[143] **Vorbrodt AW**; Dobrogowska, D. H. 2003. Molecular anatomy of intercellular junctions in brain endothelial and epithelial barriers: electron microscopist's view. Brain Res Brain Res Rev 42:221–242. doi:10.1016/s0165-0173(03)00177-2.

[144] **Boado RJ**; Pardridge, W. M. 1993. Glucose deprivation causes posttranscriptional enhancement of brain capillary endothelial glucose transporter gene expression via GLUT1 mRNA stabilization. J Neurochem 60:2290–2296. doi:10.1111/j.1471-4159.1993.tb03516.x.

[145] **Lyck R**; Ruderisch, N.; Moll, A. G.; Steiner, O.; Cohen, C. D.; Engelhardt, B.; Makrides, V.; Verrey, F. 2009. Culture-induced changes in blood-brain barrier transcriptome: implications for amino-acid transporters in vivo. J Cereb Blood Flow Metab 29:1491–1502. doi:10.1038/jcbfm.2009.72.

[146] **Engelhardt B**; Sorokin, L. 2009. The blood-brain and the blood-cerebrospinal fluid barriers: function and dysfunction. Semin Immunopathol 31:497–511. doi:10.1007/s00281-009-0177-0.

[147] **Zlokovic BV.** 2008. The blood-brain barrier in health and chronic neurodegenerative disorders. Neuron 57:178–201. doi:10.1016/j.neuron.2008.01.003.

[148] **Laterra J**; Keep, R.; Betz, A. L.; Goldstein, G. W. 1999. Blood—Cerebrospinal Fluid Barrier. *In* Siegel GJ, Agranoff BW, Albers RW, et al. (ed), Basic Neurochemistry: Molecular, Cellular and Medical Aspects, 6th ed. Lippincott-Raven, Philadelphia.

[149] **Solar P**; Zamani, A.; Kubickova, L.; Dubovy, P.; Joukal, M. 2020. Choroid plexus and the blood-cerebrospinal fluid barrier in disease. Fluids Barriers CNS 17:35. doi:10.1186/s12987-020-00196-2.

[150] **Schielke GP**; Betz, A. L. 1992. Electrolyte Transport, p. 221–243. *In* Bradbury MWB (ed), Physiology and Pharmacology of the Blood-Brain Barrier. Springer Berlin Heidelberg, Berlin, Heidelberg.

[151] **Buckley MW**; McGavern, D. B. 2022. Immune dynamics in the CNS and its barriers during homeostasis and disease. Immunol Rev 306:58–75. doi:10.1111/imr.13066.

[152] **Iliff JJ**; Wang, M.; Liao, Y.; Plogg, B. A.; Peng, W.; Gundersen, G. A.; Benveniste, H.; Vates, G. E.; Deane, R.; Goldman, S. A.; Nagelhus, E. A.; Nedergaard, M. 2012. A paravascular pathway facilitates CSF flow through the brain parenchyma and the clearance of interstitial solutes, including amyloid beta. Sci Transl Med 4:147ra111. doi:10.1126/scitranslmed.3003748.

[153] **Rua R**; McGavern, D. B. 2018. Advances in Meningeal Immunity. Trends Mol Med 24:542–559. doi:10.1016/j.molmed.2018.04.003.

[154] **Alves de Lima K**; Rustenhoven, J.; Kipnis, J. 2020. Meningeal Immunity and Its Function in Maintenance of the Central Nervous System in Health and Disease. Annu Rev Immunol 38:597–620. doi:10.1146/annurev-immunol-102319-103410.

[155] **Mastorakos P**; McGavern, D. 2019. The anatomy and immunology of vasculature in the central nervous system. Sci Immunol 4. doi:10.1126/sciimmunol.aav0492.

[156] **Zihni C**; Mills, C.; Matter, K.; Balda, M. S. 2016. Tight junctions: from simple barriers to multifunctional molecular gates. Nat Rev Mol Cell Biol 17:564–580. doi:10.1038/nrm.2016.80.

[157] **Castro Dias M**; Mapunda, J. A.; Vladymyrov, M.; Engelhardt, B. 2019. Structure and Junctional Complexes of Endothelial, Epithelial and Glial Brain Barriers. Int J Mol Sci 20. doi:10.3390/ijms20215372.

[158] **Otani T**; Nguyen, T. P.; Tokuda, S.; Sugihara, K.; Sugawara, T.; Furuse, K.; Miura, T.; Ebnet, K.; Furuse, M. 2019. Claudins and JAM-A coordinately regulate tight junction formation and epithelial polarity. J Cell Biol 218:3372–3396. doi:10.1083/jcb.201812157.

[159] **Diamond JM.** 1977. Twenty-first Bowditch lecture. The epithelial junction: bridge, gate, and fence. Physiologist 20:10–18.

[160] **van Meer G**; Simons, K. 1986. The function of tight junctions in maintaining differences in lipid composition between the apical and the basolateral cell surface domains of MDCK cells. EMBO J 5:1455–1464. doi:10.1002/j.1460-2075.1986.tb04382.x.

[161] **Ikenouchi J**; Suzuki, M.; Umeda, K.; Ikeda, K.; Taguchi, R.; Kobayashi, T.; Sato, S. B.; Stolz, D. B.; Umeda, M. 2012. Lipid polarity is maintained in absence of tight junctions. J Biol Chem 287:9525–9533. doi:10.1074/jbc.M111.327064.

[162] **Kratzer I**; Vasiljevic, A.; Rey, C.; Fevre-Montange, M.; Saunders, N.; Strazielle, N.; Ghersi-Egea, J. F. 2012. Complexity and developmental changes in the expression pattern of claudins at the blood-CSF barrier. Histochem Cell Biol 138:861–879. doi:10.1007/s00418-012-1001-9.

[163] **Meoli L**; Gunzel, D. 2020. Channel functions of claudins in the organization of biological systems. Biochim Biophys Acta Biomembr 1862:183344. doi:10.1016/j.bbamem.2020.183344.

[164] **Amasheh S**; Meiri, N.; Gitter, A. H.; Schoneberg, T.; Mankertz, J.; Schulzke, J. D.; Fromm, M. 2002. Claudin-2 expression induces cation-selective channels in tight junctions of epithelial cells. J Cell Sci 115:4969–4976. doi:10.1242/jcs.00165.

[165] **Furuse M**; Furuse, K.; Sasaki, H.; Tsukita, S. 2001. Conversion of zonulae occludentes from tight to leaky strand type by introducing claudin-2 into Madin-Darby canine kidney I cells. J Cell Biol 153:263–272. doi:10.1083/jcb.153.2.263.

[166] **Kostrewa D**; Brockhaus, M.; D'Arcy, A.; Dale, G. E.; Nelboeck, P.; Schmid, G.; Mueller, F.; Bazzoni, G.; Dejana, E.; Bartfai, T.; Winkler, F. K.; Hennig, M. 2001. X-ray structure of junctional adhesion molecule: structural basis for homophilic adhesion via a novel dimerization motif. EMBO J 20:4391–4398. doi:10.1093/emboj/20.16.4391.

[167] **Bazzoni G.** 2006. Endothelial tight junctions: permeable barriers of the vessel wall. Thromb Haemost 95:36–42.

[168] **Jia W**; Martin, T. A.; Zhang, G.; Jiang, W. G. 2013. Junctional adhesion molecules in cerebral endothelial tight junction and brain metastasis. Anticancer Res 33:2353–2359.

[169] **Martinez-Estrada OM**; Villa, A.; Breviario, F.; Orsenigo, F.; Dejana, E.; Bazzoni, G. 2001. Association of junctional adhesion molecule with calcium/calmodulin-dependent serine protein kinase (CASK/LIN-2) in human epithelial caco-2 cells. J Biol Chem 276:9291–9296. doi:10.1074/jbc.M006991200.

[170] **Fanning AS**; Ma, T. Y.; Anderson, J. M. 2002. Isolation and functional characterization of the actin binding region in the tight junction protein ZO-1. FASEB J 16:1835–1837. doi:10.1096/fj.02-0121fje.

[171] **Feldman GJ**; Mullin, J. M.; Ryan, M. P. 2005. Occludin: structure, function and regulation. Adv Drug Deliv Rev 57:883–917. doi:10.1016/j.addr.2005.01.009.

[172] **van Itallie CM**; Anderson, J. M. 1997. Occludin confers adhesiveness when expressed in fibroblasts. J Cell Sci 110 (Pt 9):1113–1121. doi:10.1242/jcs.110.9.1113.

[173] **Kuwabara H**; Kokai, Y.; Kojima, T.; Takakuwa, R.; Mori, M.; Sawada, N. 2001. Occludin regulates actin cytoskeleton in endothelial cells. Cell Struct Funct 26:109–116. doi:10.1247/csf.26.109.

[174] **Louveau A**; Smirnov, I.; Keyes, T. J.; Eccles, J. D.; Rouhani, S. J.; Peske, J. D.; Derecki, N. C.; Castle, D.; Mandell, J. W.; Lee, K. S.; Harris, T. H.; Kipnis, J. 2015. Structural and functional features of central nervous system lymphatic vessels. Nature 523:337–341. doi:10.1038/nature14432.

[175] **Saksida A**; Duh, D.; Lotric-Furlan, S.; Strle, F.; Petrovec, M.; Avsic-Zupanc, T. 2005. The importance of tick-borne encephalitis virus RNA detection for early differential diagnosis of tick-borne encephalitis. J Clin Virol 33:331–335. doi:10.1016/j.jcv.2004.07.014.

[176] **Saksida A**; Jakopin, N.; Jelovsek, M.; Knap, N.; Fajs, L.; Lusa, L.; Lotric-Furlan, S.; Bogovic, P.; Arnez, M.; Strle, F.; Avsic-Zupanc, T. 2018. Virus RNA Load in Patients with Tick-Borne Encephalitis, Slovenia. Emerg Infect Dis 24:1315–1323. doi:10.3201/eid2407.180059.

[177] **Holzmann H.** 2003. Diagnosis of tick-borne encephalitis. Vaccine 21 Suppl 1:S36-40. doi:10.1016/s0264-410x(02)00819-8.

[178] **Gelpi E**; Preusser, M.; Garzuly, F.; Holzmann, H.; Heinz, F. X.; Budka, H. 2005. Visualization of Central European tick-borne encephalitis infection in fatal human cases. J Neuropathol Exp Neurol 64:506–512. doi:10.1093/jnen/64.6.506.

[179] **Palus M**; Bily, T.; Elsterova, J.; Langhansova, H.; Salat, J.; Vancova, M.; Ruzek, D. 2014. Infection and injury of human astrocytes by tick-borne encephalitis virus. J Gen Virol 95:2411–2426. doi:10.1099/vir.0.068411-0.

[180] **Mullen RJ**; Buck, C. R.; Smith, A. M. 1992. NeuN, a neuronal specific nuclear protein in vertebrates. Development 116:201–211. doi:10.1242/dev.116.1.201.

[181] **Young K**; Morrison, Helena. 2018. Quantifying Microglia Morphology from Photomicrographs of Immunohistochemistry Prepared Tissue Using ImageJ. J Vis Exp. doi:10.3791/57648.

[182] **Davalos D**; Grutzendler, Jaime; Yang, Guang; Kim, Jiyun V.; Zuo, Yi; Jung, Steffen; Littman, Dan R.; Dustin, Michael L.; Gan, Wen-Biao. 2005. ATP mediates rapid microglial response to local brain injury in vivo. Nat Neurosci 8:752–758. doi:10.1038/nn1472.

[183] **Boche D**; Perry, V. H.; Nicoll, J. A. R. 2013. Review: activation patterns of microglia and their identification in the human brain. Neuropathol Appl Neurobiol 39:3–18. doi:10.1111/nan.12011.

[184] **Yamasaki R**; Lu, H.; Butovsky, O.; Ohno, N.; Rietsch, A. M.; Cialic, R.; Wu, P. M.; Doykan, C. E.; Lin, J.; Cotleur, A. C.; Kidd, G.; Zorlu, M. M.; Sun, N.; Hu, W.; Liu, L.; Lee, J. C.; Taylor, S. E.; Uehlein, L.; Dixon, D.; Gu, J.; Floruta, C. M.; Zhu, M.; Charo, I. F.; Weiner, H. L.; Ransohoff, R. M. 2014. Differential roles of microglia and monocytes in the inflamed central nervous system. J Exp Med 211:1533–1549. doi:10.1084/jem.20132477.

[185] **Wohleb ES**; Fenn, A. M.; Pacenta, A. M.; Powell, N. D.; Sheridan, J. F.; Godbout, J. P. 2012. Peripheral innate immune challenge exaggerated microglia activation, increased the number of inflammatory CNS macrophages, and prolonged social withdrawal in socially defeated mice. Psychoneuroendocrinology 37:1491–1505. doi:10.1016/j.psyneuen.2012.02.003.

[186] **Shemer A**; Grozovski, J.; Tay, T. L.; Tao, J.; Volaski, A.; Suss, P.; Ardura-Fabregat, A.; Gross-Vered, M.; Kim, J. S.; David, E.; Chappell-Maor, L.; Thielecke, L.; Glass, C. K.; Cornils, K.; Prinz, M.; Jung, S. 2018. Engrafted parenchymal brain macrophages differ from microglia in transcriptome, chromatin landscape and response to challenge. Nat Commun 9:5206. doi:10.1038/s41467-018-07548-5.

[187] **Geissmann F**; Manz, M. G.; Jung, S.; Sieweke, M. H.; Merad, M.; Ley, K. 2010. Development of monocytes, macrophages, and dendritic cells. Science 327:656–661. doi:10.1126/science.1178331.

[188] **Ohsawa K**; Imai, Y.; Kanazawa, H.; Sasaki, Y.; Kohsaka, S. 2000. Involvement of Iba1 in membrane ruffling and phagocytosis of macrophages/microglia. J Cell Sci 113 (Pt 17):3073–3084. doi:10.1242/jcs.113.17.3073.

[189] **Bennett ML**; Bennett, F. C.; Liddelow, S. A.; Ajami, B.; Zamanian, J. L.; Fernhoff, N. B.; Mulinyawe, S. B.; Bohlen, C. J.; Adil, A.; Tucker, A.; Weissman, I. L.; Chang, E. F.; Li, G.; Grant, G. A.; Hayden Gephart, M. G.; Barres, B. A. 2016. New tools for studying microglia in the mouse and human CNS. Proc Natl Acad Sci U S A 113:E1738-46. doi:10.1073/pnas.1525528113.

[190] **Satoh J**; Kino, Y.; Asahina, N.; Takitani, M.; Miyoshi, J.; Ishida, T.; Saito, Y. 2016. TMEM119 marks a subset of microglia in the human brain. Neuropathology 36:39–49. doi:10.1111/neup.12235.

[191] **Gonzalez Ibanez F**; Picard, K.; Bordeleau, M.; Sharma, K.; Bisht, K.; Tremblay, M. E. 2019. Immunofluorescence Staining Using IBA1 and TMEM119 for Microglial Density, Morphology and Peripheral Myeloid Cell Infiltration Analysis in Mouse Brain. J Vis Exp. doi:10.3791/60510.

[192] **Hermiston ML**; Xu, Z.; Weiss, A. 2003. CD45: a critical regulator of signaling thresholds in immune cells. Annu Rev Immunol 21:107–137. doi:10.1146/annurev.immunol.21.120601.140946.

[193] **Martin E**; El-Behi, Mohamed; Fontaine, Bertrand; Delarasse, Cecile. 2017. Analysis of Microglia and Monocyte-derived Macrophages from the Central Nervous System by Flow Cytometry. J Vis Exp. doi:10.3791/55781.

[194] **Martin E**; Boucher, Céline; Fontaine, Bertrand; Delarasse, Cécile. 2017. Distinct inflammatory phenotypes of microglia and monocyte-derived macrophages in Alzheimer's disease models: effects of aging and amyloid pathology. Aging Cell 16:27–38. doi:10.1111/acel.12522.

[195] **Sedgwick JD**; Schwender, S.; Imrich, H.; Dorries, R.; Butcher, G. W.; Meulen, V. ter. 1991. Isolation and direct characterization of resident microglial cells from the normal and inflamed central nervous system. Proc Natl Acad Sci U S A 88:7438–7442. doi:10.1073/pnas.88.16.7438.

[196] **Ford AL**; Goodsall, A. L.; Hickey, W. F.; Sedgwick, J. D. 1995. Normal adult ramified microglia separated from other central nervous system macrophages by flow cytometric sorting. Phenotypic differences defined and direct ex vivo antigen presentation to myelin basic protein-reactive CD4+ T cells compared. J Immunol 154:4309–4321.

[197] **Hartig W**; Reichenbach, A.; Voigt, C.; Boltze, J.; Bulavina, L.; Schuhmann, M. U.; Seeger, J.; Schusser, G. F.; Freytag, C.; Grosche, J. 2009. Triple fluorescence labelling of neuronal, glial and vascular markers revealing pathological alterations in various animal models. J Chem Neuroanat 37:128–138. doi:10.1016/j.jchemneu.2008.10.003.

[198] **Michalski D**; Pitsch, R.; Pillai, D. R.; Mages, B.; Aleithe, S.; Grosche, J.; Martens, H.; Schlachetzki, F.; Hartig, W. 2017. Delayed histochemical alterations within the neurovascular unit due to transient focal cerebral ischemia and experimental treatment with neurotrophic factors. PLoS One 12:e0174996. doi:10.1371/journal.pone.0174996.

[199] **van Roy F**; Berx, G. 2008. The cell-cell adhesion molecule E-cadherin. Cell Mol Life Sci 65:3756–3788. doi:10.1007/s00018-008-8281-1.

[200] **Nollet F**; Kools, P.; van Roy, F. 2000. Phylogenetic analysis of the cadherin superfamily allows identification of six major subfamilies besides several solitary members. J Mol Biol 299:551–572. doi:10.1006/jmbi.2000.3777.

[201] **Figueiredo CA**; Steffen, J.; Morton, L.; Arumugam, S.; Liesenfeld, O.; Deli, M. A.; Kroger, A.; Schuler, T.; Dunay, I. R. 2022. Immune response and pathogen invasion at the choroid plexus in the onset of cerebral toxoplasmosis. J Neuroinflammation 19:17. doi:10.1186/s12974-021-02370-1.

[202] **Madarame H**; Seuberlich, T.; Abril, C.; Zurbriggen, A.; Vandevelde, M.; Oevermann, A. 2011. The distribution of E-cadherin expression in listeric rhombencephalitis of ruminants indicates its involvement in Listeria monocytogenes neuroinvasion. Neuropathol Appl Neurobiol 37:753–767. doi:10.1111/j.1365-2990.2011.01183.x.

[203] **Hellstrom M**; Kalen, M.; Lindahl, P.; Abramsson, A.; Betsholtz, C. 1999. Role of PDGF-B and PDGFR-beta in recruitment of vascular smooth muscle cells and pericytes during

embryonic blood vessel formation in the mouse. Development 126:3047–3055. doi:10.1242/dev.126.14.3047.

[204] **Song S**; Ewald, A. J.; Stallcup, W.; Werb, Z.; Bergers, G. 2005. PDGFRbeta+ perivascular progenitor cells in tumours regulate pericyte differentiation and vascular survival. Nat Cell Biol 7:870–879. doi:10.1038/ncb1288.

[205] **Winkler EA**; Bell, R. D.; Zlokovic, B. V. 2010. Pericyte-specific expression of PDGF beta receptor in mouse models with normal and deficient PDGF beta receptor signaling. Mol Neurodegener 5:32. doi:10.1186/1750-1326-5-32.

[206] **Kim J**; Alejandro, B.; Hetman, M.; Hattab, E. M.; Joiner, J.; Schroten, H.; Ishikawa, H.; Chung, D. H. 2020. Zika virus infects pericytes in the choroid plexus and enters the central nervous system through the blood-cerebrospinal fluid barrier. PLoS Pathog 16:e1008204. doi:10.1371/journal.ppat.1008204.

[207] **Wolburg H**; Lippoldt, A. 2002. Tight junctions of the blood-brain barrier: development, composition and regulation. Vascul Pharmacol 38:323–337. doi:10.1016/s1537-1891(02)00200-8.

[208] **Barichello T**; Generoso, J. S.; Collodel, A.; Petronilho, F.; Dal-Pizzol, F. 2021. The blood-brain barrier dysfunction in sepsis. Tissue Barriers 9:1840912. doi:10.1080/21688370.2020.1840912.

[209] **Lauer AN**; Tenenbaum, T.; Schroten, H.; Schwerk, C. 2018. The diverse cellular responses of the choroid plexus during infection of the central nervous system. Am J Physiol Cell Physiol 314:C152-C165. doi:10.1152/ajpcell.00137.2017.

[210] **Rao RK**; Basuroy, S.; Rao, V. U.; Karnaky, K. J., Jr.; Gupta, A. 2002. Tyrosine phosphorylation and dissociation of occludin-ZO-1 and E-cadherin-beta-catenin complexes from the cytoskeleton by oxidative stress. Biochem J 368:471–481. doi:10.1042/BJ20011804.

[211] **Itoh M**; Nagafuchi, A.; Moroi, S.; Tsukita, S. 1997. Involvement of ZO-1 in cadherin-based cell adhesion through its direct binding to alpha catenin and actin filaments. J Cell Biol 138:181–192. doi:10.1083/jcb.138.1.181.

[212] **Fanning AS**; Jameson, B. J.; Jesaitis, L. A.; Anderson, J. M. 1998. The tight junction protein ZO-1 establishes a link between the transmembrane protein occludin and the actin cytoskeleton. J Biol Chem 273:29745–29753. doi:10.1074/jbc.273.45.29745.

[213] **Cho H**; Proll, Sean C.; Szretter, Kristy J.; Katze, Michael G.; Gale, Michael; Diamond, Michael S. 2013. Differential innate immune response programs in neuronal subtypes determine susceptibility to infection in the brain by positive-stranded RNA viruses. Nat Med 19:458–464. doi:10.1038/nm.3108.

[214] **Omalu BI**; Shakir, Abdulrazek A.; Wang, Guoji; Lipkin, W. Ian; Wiley, Clayton A. 2003. Fatal fulminant pan-meningo-polioencephalitis due to West Nile virus. Brain Pathol 13:465–472. doi:10.1111/j.1750-3639.2003.tb00477.x.

[215] **Gordon B**; Selnes, O. A.; Hart, J.; Hanley, D. F.; Whitley, R. J. 1990. Long-term cognitive sequelae of acyclovir-treated herpes simplex encephalitis. Arch Neurol 47:646–647. doi:10.1001/archneur.1990.00530060054017.

[216] **Boyles DA**; Schwarz, Madeline M.; Albe, Joseph R.; McMillen, Cynthia M.; O'Malley, Katherine J.; Reed, Douglas S.; Hartman, Amy L. 2021. Development of Rift valley fever encephalitis in rats is mediated by early infection of olfactory epithelium and neuroinvasion across the cribriform plate. J Gen Virol 102. doi:10.1099/jgv.0.001522.

[217] **Kumari P**; Rothan, Hussin A.; Natekar, Janhavi P.; Stone, Shannon; Pathak, Heather; Strate, Philip G.; Arora, Komal; Brinton, Margo A.; Kumar, Mukesh. 2021. Neuroinvasion and Encephalitis Following Intranasal Inoculation of SARS-CoV-2 in K18-hACE2 Mice. Viruses 13. doi:10.3390/v13010132.

[218] **Avšič-Županc T**; Poljak, M.; Matičič, M.; Radšel-Medvešček, A.; LeDuc, J.W; Stiasny, K.; Kunz, C.; Heinz, F.X. 1995. Laboratory acquired tick-borne meningoencephalitis: characterisation of virus strains. Clin Diagn Virol 4:51–59. doi:10.1016/0928-0197(94)00062-y.

[219] **Haymaker W**; Sather, G. E.; Hammon, W. M. 1955. Accidental Russian spring-summer viral encephalitis cases occurring in two laboratory workers, one fatal, with postmortem study. AMA Arch Neurol Psychiatry 73:609–630.

[220] **Schreier S**; Cebulski, Kristin; Kröger, Andrea. 2021. Contact-dependent transmission of Langat and tick-borne encephalitis virus in type I interferon receptor-1 deficient mice. J Virol. doi:10.1128/JVI.02039-20.

[221] **Yang L**; Kress, B. T.; Weber, H. J.; Thiyagarajan, M.; Wang, B.; Deane, R.; Benveniste, H.; Iliff, J. J.; Nedergaard, M. 2013. Evaluating glymphatic pathway function utilizing clinically relevant intrathecal infusion of CSF tracer. J Transl Med 11:107. doi:10.1186/1479-5876-11-107.

[222] **Johanson CE**; Duncan, John A.; Klinge, Petra M.; Brinker, Thomas; Stopa, Edward G.; Silverberg, Gerald D. 2008. Multiplicity of cerebrospinal fluid functions: New challenges in health and disease. Cerebrospinal Fluid Res 5:10. doi:10.1186/1743-8454-5-10.

[223] **Weller RO**; Djuanda, Effie; Yow, Hong-Yeen; Carare, Roxana O. 2009. Lymphatic drainage of the brain and the pathophysiology of neurological disease. Acta Neuropathol 117:1–14. doi:10.1007/s00401-008-0457-0.

[224] **Baruch K**; Ron-Harel, Noga; Gal, Hilah; Deczkowska, Aleksandra; Shifrut, Eric; Ndifon, Wilfred; Mirlas-Neisberg, Nataly; Cardon, Michal; Vaknin, Ilan; Cahalon, Liora; Berkutzki, Tamara; Mattson, Mark P.; Gomez-Pinilla, Fernando; Friedman, Nir; Schwartz, Michal. 2013. CNS-specific immunity at the choroid plexus shifts toward destructive Th2 inflammation in brain aging. Proc Natl Acad Sci U S A 110:2264–2269. doi:10.1073/pnas.1211270110.

[225] **Shechter R**; Miller, Omer; Yovel, Gili; Rosenzweig, Neta; London, Anat; Ruckh, Julia; Kim, Ki-Wook; Klein, Eugenia; Kalchenko, Vyacheslav; Bendel, Peter; Lira, Sergio A.; Jung, Steffen; Schwartz, Michal. 2013. Recruitment of beneficial M2 macrophages to injured spinal cord is orchestrated by remote brain choroid plexus. Immunity 38:555–569. doi:10.1016/j.immuni.2013.02.012.

[226] **Schwartz M**; Baruch, Kuti. 2014. The resolution of neuroinflammation in neurodegeneration: leukocyte recruitment via the choroid plexus. EMBO J 33:7–22. doi:10.1002/embj.201386609.

[227] **Kunis G**; Baruch, Kuti; Miller, Omer; Schwartz, Michal. 2015. Immunization with a Myelin-Derived Antigen Activates the Brain's Choroid Plexus for Recruitment of Immunoregulatory Cells to the CNS and Attenuates Disease Progression in a Mouse Model of ALS. J Neurosci 35:6381–6393. doi:10.1523/JNEUROSCI.3644-14.2015.

[228] **Fleischer V**; Gonzalez-Escamilla, Gabriel; Ciolac, Dumitru; Albrecht, Philipp; Küry, Patrick; Gruchot, Joel; Dietrich, Michael; Hecker, Christina; Müntefering, Thomas; Bock, Stefanie; Oshaghi, Mohammadsaleh; Radetz, Angela; Cerina, Manuela; Krämer, Julia; Wachsmuth, Lydia; Faber, Cornelius; Lassmann, Hans; Ruck, Tobias; Meuth, Sven G.; Muthuraman, Muthuraman; Groppa, Sergiu. 2021. Translational value of choroid plexus imaging for tracking neuroinflammation in mice and humans. Proc Natl Acad Sci U S A 118. doi:10.1073/pnas.2025000118.

[229] **Wilson EH**; Weninger, Wolfgang; Hunter, Christopher A. 2010. Trafficking of immune cells in the central nervous system. J Clin Invest 120:1368–1379. doi:10.1172/JCI41911.

[230] **Praetorius J**; Damkier, Helle Hasager. 2017. Transport across the choroid plexus epithelium. Am J Physiol Cell Physiol 312:C673-C686. doi:10.1152/ajpcell.00041.2017.

[231] **Liddelow SA**; Dzięgielewska, Katarzyna M.; Møllgård, Kjeld; Whish, Sophie C.; Noor, Natassya M.; Wheaton, Benjamin J.; Gehwolf, Renate; Wagner, Andrea; Traweger, Andreas; Bauer, Hannelore; Bauer, Hans-Christian; Saunders, Norman R. 2014. Cellular specificity of the blood-CSF barrier for albumin transfer across the choroid plexus epithelium. PLoS One 9:e106592. doi:10.1371/journal.pone.0106592.

[232] **Grapp M**; Wrede, Arne; Schweizer, Michaela; Hüwel, Sabine; Galla, Hans-Joachim; Snaidero, Nicolas; Simons, Mikael; Bückers, Johanna; Low, Philip S.; Urlaub, Henning; Gärtner, Jutta; Steinfeld, Robert. 2013. Choroid plexus transcytosis and exosome shuttling deliver folate into brain parenchyma. Nat Commun 4:2123. doi:10.1038/ncomms3123.

[233] **Chotiwan N**; Rosendal, Ebba; Willekens, Stefanie M. A.; Schexnaydre, Erin; Nilsson, Emma; Lindqvist, Richard; Hahn, Max; Mihai, Ionut Sebastian; Morini, Federico; Zhang, Jianguo; Ebel, Gregory D.; Carlson, Lars-Anders; Henriksson, Johan; Ahlgren, Ulf; Marcellino, Daniel; Överby, Anna K. 2021. Type I interferon shapes the distribution and tropism of tick-borne flavivirus.

[234] **Baruch K**; Deczkowska, A.; David, E.; Castellano, J. M.; Miller, O.; Kertser, A.; Berkutzki, T.; Barnett-Itzhaki, Z.; Bezalel, D.; Wyss-Coray, T.; Amit, I.; Schwartz, M. 2014. Aging. Aging-induced type I interferon response at the choroid plexus negatively affects brain function. Science 346:89–93. doi:10.1126/science.1252945.

[235] **Hosseini S**; Wilk, E.; Michaelsen-Preusse, K.; Gerhauser, I.; Baumgartner, W.; Geffers, R.; Schughart, K.; Korte, M. 2018. Long-Term Neuroinflammation Induced by Influenza A Virus Infection and the Impact on Hippocampal Neuron Morphology and Function. J Neurosci 38:3060–3080. doi:10.1523/JNEUROSCI.1740-17.2018.

[236] **Couderc T**; Chrétien, Fabrice; Schilte, Clémentine; Disson, Olivier; Brigitte, Madly; Guivel-Benhassine, Florence; Touret, Yasmina; Barau, Georges; Cayet, Nadège; Schuffenecker, Isabelle; Desprès, Philippe; Arenzana-Seisdedos, Fernando; Michault, Alain; Albert, Matthew L.; Lecuit, Marc. 2008. A mouse model for Chikungunya: young

age and inefficient type-I interferon signaling are risk factors for severe disease. PLoS Pathog 4:e29. doi:10.1371/journal.ppat.0040029.

[237] **O'Hara BA**; Gee, Gretchen V.; Atwood, Walter J.; Haley, Sheila A. 2018. Susceptibility of Primary Human Choroid Plexus Epithelial Cells and Meningeal Cells to Infection by JC Virus. J Virol 92. doi:10.1128/JVI.00105-18.

[238] **Bearer EL**; Orci, L. 1985. Endothelial fenestral diaphragms: a quick-freeze, deep-etch study. J Cell Biol 100:418–428. doi:10.1083/jcb.100.2.418.

[239] **Wilcox DR**; Folmsbee, Stephen S.; Muller, William J.; Longnecker, Richard. 2016. The Type I Interferon Response Determines Differences in Choroid Plexus Susceptibility between Newborns and Adults in Herpes Simplex Virus Encephalitis. mBio 7:e00437-16. doi:10.1128/mBio.00437-16.

[240] **Dando SJ**; Mackay-Sim, Alan; Norton, Robert; Currie, Bart J.; St John, James A.; Ekberg, Jenny A. K.; Batzloff, Michael; Ulett, Glen C.; Beacham, Ifor R. 2014. Pathogens penetrating the central nervous system: infection pathways and the cellular and molecular mechanisms of invasion. Clin Microbiol Rev 27:691–726. doi:10.1128/CMR.00118-13.

[241] **Johnson MB**; Wang, Peter P.; Atabay, Kutay D.; Murphy, Elisabeth A.; Doan, Ryan N.; Hecht, Jonathan L.; Walsh, Christopher A. 2015. Single-cell analysis reveals transcriptional heterogeneity of neural progenitors in human cortex. Nat Neurosci 18:637–646. doi:10.1038/nn.3980.

[242] **He L**; Vanlandewijck, Michael; Mäe, Maarja Andaloussi; Andrae, Johanna; Ando, Koji; Del Gaudio, Francesca; Nahar, Khayrun; Lebouvier, Thibaud; Laviña, Bàrbara; Gouveia, Leonor; Sun, Ying; Raschperger, Elisabeth; Segerstolpe, Åsa; Liu, Jianping; Gustafsson, Sonja; Räsänen, Markus; Zarb, Yvette; Mochizuki, Naoki; Keller, Annika; Lendahl, Urban; Betsholtz, Christer. 2018. Single-cell RNA sequencing of mouse brain and lung vascular and vessel-associated cell types. Sci Data 5:180160. doi:10.1038/sdata.2018.160.

[243] **Dore-Duffy P.** 2008. Pericytes: pluripotent cells of the blood brain barrier. Curr Pharm Des 14:1581–1593. doi:10.2174/138161208784705469.

[244] **Göritz C**; Dias, David O.; Tomilin, Nikolay; Barbacid, Mariano; Shupliakov, Oleg; Frisén, Jonas. 2011. A pericyte origin of spinal cord scar tissue. Science 333:238–242. doi:10.1126/science.1203165.

[245] **Daneman R**; Zhou, Lu; Kebede, Amanuel A.; Barres, Ben A. 2010. Pericytes are required for blood-brain barrier integrity during embryogenesis. Nature 468:562–566. doi:10.1038/nature09513.

[246] **Armulik A**; Genové, Guillem; Mäe, Maarja; Nisancioglu, Maya H.; Wallgard, Elisabet; Niaudet, Colin; He, Liqun; Norlin, Jenny; Lindblom, Per; Strittmatter, Karin; Johansson, Bengt R.; Betsholtz, Christer. 2010. Pericytes regulate the blood-brain barrier. Nature 468:557–561. doi:10.1038/nature09522.

[247] **Dani N**; Herbst, Rebecca H.; McCabe, Cristin; Green, Gilad S.; Kaiser, Karol; Head, Joshua P.; Cui, Jin; Shipley, Frederick B.; Jang, Ahram; Dionne, Danielle; Nguyen, Lan; Rodman, Christopher; Riesenfeld, Samantha J.; Prochazka, Jan; Prochazkova, Michaela; Sedlacek, Radislav; Zhang, Feng; Bryja, Vitezslav; Rozenblatt-Rosen, Orit;

Habib, Naomi; Regev, Aviv; Lehtinen, Maria K. 2021. A cellular and spatial map of the choroid plexus across brain ventricles and ages. Cell 184:3056-3074.e21. doi:10.1016/j.cell.2021.04.003.

[248] **Cui J**; Xu, Huixin; Lehtinen, Maria K. 2021. Macrophages on the margin: choroid plexus immune responses. Trends Neurosci 44:864–875. doi:10.1016/j.tins.2021.07.002.

[249] **Jordão MJC**; Sankowski, Roman; Brendecke, Stefanie M.; Sagar; Locatelli, Giuseppe; Tai, Yi-Heng; Tay, Tuan Leng; Schramm, Eva; Armbruster, Stephan; Hagemeyer, Nora; Groß, Olaf; Mai, Dominic; Çiçek, Özgün; Falk, Thorsten; Kerschensteiner, Martin; Grün, Dominic; Prinz, Marco. 2019. Single-cell profiling identifies myeloid cell subsets with distinct fates during neuroinflammation. Science 363. doi:10.1126/science.aat7554.

[250] **Goldmann T**; Wieghofer, P.; Jordao, M. J.; Prutek, F.; Hagemeyer, N.; Frenzel, K.; Amann, L.; Staszewski, O.; Kierdorf, K.; Krueger, M.; Locatelli, G.; Hochgerner, H.; Zeiser, R.; Epelman, S.; Geissmann, F.; Priller, J.; Rossi, F. M.; Bechmann, I.; Kerschensteiner, M.; Linnarsson, S.; Jung, S.; Prinz, M. 2016. Origin, fate and dynamics of macrophages at central nervous system interfaces. Nat Immunol 17:797–805. doi:10.1038/ni.3423.

[251] **Ge R**; Tornero, Daniel; Hirota, Masao; Monni, Emanuela; Laterza, Cecilia; Lindvall, Olle; Kokaia, Zaal. 2017. Choroid plexus-cerebrospinal fluid route for monocyte-derived macrophages after stroke. J Neuroinflammation 14:153. doi:10.1186/s12974-017-0909-3.

[252] **Young KF**; Gardner, Rebeca; Sariana, Victoria; Whitman, Susan A.; Bartlett, Mitchell J.; Falk, Torsten; Morrison, Helena W. 2021. Can quantifying morphology and TMEM119 expression distinguish between microglia and infiltrating macrophages after ischemic stroke and reperfusion in male and female mice? J Neuroinflammation 18:58. doi:10.1186/s12974-021-02105-2.

[253] **Růžek D**; Vancová, Marie; Tesařová, Martina; Ahantarig, Arunee; Kopecký, Jan; Grubhoffer, Libor. 2009. Morphological changes in human neural cells following tick-borne encephalitis virus infection. J Gen Virol 90:1649–1658. doi:10.1099/vir.0.010058-0.

[254] **Prikhod'ko GG**; Prikhod'ko, E. A.; Cohen, J. I.; Pletnev, A. G. 2001. Infection with Langat Flavivirus or expression of the envelope protein induces apoptotic cell death. Virology 286:328–335. doi:10.1006/viro.2001.0980.

[255] **Weyer A**; Schilling, Karl. 2003. Developmental and cell type-specific expression of the neuronal marker NeuN in the murine cerebellum. J Neurosci Res 73:400–409. doi:10.1002/jnr.10655.

[256] **Lee VM**; Pixley, S. K. 1994. Age and differentiation-related differences in neuron-specific tubulin immunostaining of olfactory sensory neurons. Brain Res Dev Brain Res 83:209–215. doi:10.1016/0165-3806(94)00139-1.

[257] **Davoli MA**; Fourtounis, J.; Tam, J.; Xanthoudakis, S.; Nicholson, D.; Robertson, G. S.; Ng, G. Y.; Xu, D. 2002. Immunohistochemical and biochemical assessment of caspase-3 activation and DNA fragmentation following transient focal ischemia in the rat. Neuroscience 115:125–136. doi:10.1016/s0306-4522(02)00376-7.

[258] **Unal-Cevik I**; Kilinc, M.; Gursoy-Ozdemir, Y.; Gurer, G.; Dalkara, T. 2004. Loss of NeuN immunoreactivity after cerebral ischemia does not indicate neuronal cell loss: a cautionary note. Brain Res 1015:169–174. doi:10.1016/j.brainres.2004.04.032.

[259] **Wilhelm I**; Nyúl-Tóth, Ádám; Suciu, Maria; Hermenean, Anca; Krizbai, István A. 2016. Heterogeneity of the blood-brain barrier. Tissue Barriers 4:e1143544. doi:10.1080/21688370.2016.1143544.

[260] **Villalba N**; Baby, Sheon; Cha, Byeong J.; Yuan, Sarah Y. 2020. Site-specific opening of the blood-brain barrier by extracellular histones. J Neuroinflammation 17:281. doi:10.1186/s12974-020-01950-x.

[261] **Villaseñor R**; Kuennecke, Basil; Ozmen, Laurence; Ammann, Michelle; Kugler, Christof; Grüninger, Fiona; Loetscher, Hansruedi; Freskgård, Per-Ola; Collin, Ludovic. 2017. Region-specific permeability of the blood–brain barrier upon pericyte loss. J Cereb Blood Flow Metab 37:3683–3694. doi:10.1177/0271678X17697340.

[262] **Nyúl-Tóth Á**; Suciu, Maria; Molnár, Judit; Fazakas, Csilla; Haskó, János; Herman, Hildegard; Farkas, Attila E.; Kaszaki, József; Hermenean, Anca; Wilhelm, Imola; Krizbai, István A. 2016. Differences in the molecular structure of the blood-brain barrier in the cerebral cortex and white matter: an in silico, in vitro, and ex vivo study. Am J Physiol Heart Circ Physiol 310:H1702-14. doi:10.1152/ajpheart.00774.2015.

[263] **Zoladek J**; Legros, Vincent; Jeannin, Patricia; Chazal, Maxime; Pardigon, Nathalie; Ceccaldi, Pierre-Emmanuel; Gessain, Antoine; Jouvenet, Nolwenn; Afonso, Philippe V. 2021. Zika Virus Requires the Expression of Claudin-7 for Optimal Replication in Human Endothelial Cells. Front Microbiol 12:746589. doi:10.3389/fmicb.2021.746589.

[264] **Silverman HA**; Dancho, Meghan; Regnier-Golanov, Angelique; Nasim, Mansoor; Ochani, Mahendar; Olofsson, Peder S.; Ahmed, Mohamed; Miller, Edmund J.; Chavan, Sangeeta S.; Golanov, Eugene; Metz, Christine N.; Tracey, Kevin J.; Pavlov, Valentin A. 2014. Brain Region-Specific Alterations in the Gene Expression of Cytokines, Immune Cell Markers and Cholinergic System Components during Peripheral Endotoxin-Induced Inflammation. Mol Med 20:601–611. doi:10.2119/molmed.2014.00147.

[265] **Kipp M**; Norkute, Akvile; Johann, Sonja; Lorenz, Leila; Braun, Alena; Hieble, Andrea; Gingele, Stefan; Pott, Friederike; Richter, Janek; Beyer, Cordian. 2008. Brain-region-specific astroglial responses in vitro after LPS exposure. J Mol Neurosci 35:235–243. doi:10.1007/s12031-008-9057-7.

[266] **Brandi E**; Torres-Garcia, Laura; Svanbergsson, Alexander; Haikal, Caroline; Di Liu; Li, Wen; Li, Jia-Yi. 2022. Brain region-specific microglial and astrocytic activation in response to systemic lipopolysaccharides exposure. Front Aging Neurosci 14:910988. doi:10.3389/fnagi.2022.910988.

[267] **Ohtsuki S**; Yamaguchi, H.; Katsukura, Y.; Asashima, T.; Terasaki, T. 2008. mRNA expression levels of tight junction protein genes in mouse brain capillary endothelial cells highly purified by magnetic cell sorting. J Neurochem 104:147–154. doi:10.1111/j.1471-4159.2007.05008.x.

[268] **Daneman R**; Zhou, L.; Agalliu, D.; Cahoy, J. D.; Kaushal, A.; Barres, B. A. 2010. The mouse blood-brain barrier transcriptome: a new resource for understanding the development and function of brain endothelial cells. PLoS One 5:e13741. doi:10.1371/journal.pone.0013741.

[269] **Luettig J**; Rosenthal, R.; Barmeyer, C.; Schulzke, J. D. 2015. Claudin-2 as a mediator of leaky gut barrier during intestinal inflammation. Tissue Barriers 3:e977176. doi:10.4161/21688370.2014.977176.

[270] **Castro V**; Bertrand, L.; Luethen, M.; Dabrowski, S.; Lombardi, J.; Morgan, L.; Sharova, N.; Stevenson, M.; Blasig, I. E.; Toborek, M. 2016. Occludin controls HIV transcription in brain pericytes via regulation of SIRT-1 activation. FASEB J 30:1234–1246. doi:10.1096/fj.15-277673.

[271] **Schindelin J**; Arganda-Carreras, I.; Frise, E.; Kaynig, V.; Longair, M.; Pietzsch, T.; Preibisch, S.; Rueden, C.; Saalfeld, S.; Schmid, B.; Tinevez, J. Y.; White, D. J.; Hartenstein, V.; Eliceiri, K.; Tomancak, P.; Cardona, A. 2012. Fiji: an open-source platform for biological-image analysis. Nat Methods 9:676–682. doi:10.1038/nmeth.2019.

[272] **Müller U**; Steinhoff, U.; Reis, L. F.; Hemmi, S.; Pavlovic, J.; Zinkernagel, R. M.; Aguet, M. 1994. Functional role of type I and type II interferons in antiviral defense. Science 264:1918–1921.

[273] **Liu L**; Herukka, S. K.; Minkeviciene, R.; van Groen, T.; Tanila, H. 2004. Longitudinal observation on CSF Abeta42 levels in young to middle-aged amyloid precursor protein/presenilin-1 doubly transgenic mice. Neurobiol Dis 17:516–523. doi:10.1016/j.nbd.2004.08.005.

[274] **Liu L**; Duff, K. 2008. A technique for serial collection of cerebrospinal fluid from the cisterna magna in mouse. J Vis Exp. doi:10.3791/960.

[275] **Louveau A**; Filiano, A. J.; Kipnis, J. 2018. Meningeal whole mount preparation and characterization of neural cells by flow cytometry. Curr Protoc Immunol 121:e50. doi:10.1002/cpim.50.

[276] **Nakagawa S**; Deli, Mária A.; Kawaguchi, Hiroko; Shimizudani, Takeshi; Shimono, Takanori; Kittel, Agnes; Tanaka, Kunihiko; Niwa, Masami. 2009. A new blood-brain barrier model using primary rat brain endothelial cells, pericytes and astrocytes. Neurochem Int 54:253–263. doi:10.1016/j.neuint.2008.12.002.

[277] **Niedrig M**; Klockmann, U.; Lang, W.; Roeder, J.; Burk, S.; Modrow, S.; Pauli, G. 1994. Monoclonal antibodies directed against tick-borne encephalitis virus with neutralizing activity in vivo. Acta Virol 38:141–149.

7. Attachment

Glossary

(+)ssRNA	Positive sense single stranded ribonucleic acid
µg	Microgram
µm	Micrometer
ABC	ATP-binding cassette
ATP	Adenosine triphosphate
BAMs	Barrier associated macrophages
BBB	Blood-brain-barrier
BCSFB	Blood-cerebrospinal fluid-barrier
BHS	Blut-Hirn-Schranke
BLS	Blut-Liquor-Schranke
BMECs	Brain microvascular endothelial cells
BMVs	Brain microvessels
BSA	Bovine serum albumin
C	Capsid
C°	Grad Celsius
CAMs	CNS-associated macrophages
Cbel	Cerebellum
CD	Cluster of differentiation
cDNA	Complementary DNA
CLDN	Claudin
CNS	Central nervous system
CP	Choroid plexus
DAPI	4’,6-diamidino-2-phenylindole
DENV	Dengue virus
DMEM	Dulbecco’s modified eagle’s medium
DNA	Deoxyribonucleic acid
DNAse	Deoxyribonuklease
ds	Double stranded

E	Envelope
ER	Endoplasmic reticulum
FBS	Fetal bovine serum
FC	Frontal cortex
FFUs	Focus forming units
GFAP	Glial fibrillary acidic protein
h	Hours
HEPES	(4-(2-hydroxyethyl)-1-piperazineethanesulfonic acid)
hpi	Hours post infection
Iba-1	Ionized calcium-binding adapter molecule 1
IFITMs	Interferon-induced transmembrane proteins
IFN	Interferon
Ifnar	Interferon-α receptor
$Ifnar^{-/-}$	Interferon-α receptor deficient
Ig	Immunoglobulin
IRF	Interferon regulatory factor
ISGs	Interferon stimulated genes
ISRE	Interferon-stimulated response element
JAK	Janus kinase
JAMs	Junction adhesion molecules
JEV	Japanese encephalitis virus
l	Liter
LGTV	Langat virus
M	Membrane
$MAVS^{-/-}$	Mitochondrial antiviral-signaling protein deficient
MDA-5	Melanoma differentiation-associated protein-5
mg	Milligram
ml	Milliliter
MyD88	Myeloid differentiation primary response 88
n	Number
NaCl	Sodium chloride
NeuN	Neuronal nuclei

NF-κB	Nuclear factor - κB
ns	Not significant
NS	Nonstructural protein
NVU	Neurovascular unit
OB	Olfactory bulb
PAMPs	Pathogen associated molecular patterns
PBS	Phosphate buffered saline
PDGFRβ	Platelet-derived growth factor receptor β
PNS	Peripheral nervous system
prM	Precursor-membrane
PRRs	Pattern recognition receptors
qRT-PCR	Quantitative real-time, reverse transcriptase polymerase chain reaction
RIG-I	Retinoic acid-inducible gene I
rpm	Rounds per minute
RT	Room temperature
RVFV	Rift valley fever virus
SARS-CoV-2	Severe acute respiratory syndrome coronavirus-2
SC	Subcutaneous
SEM	Standard error of the mean
STAT	Signal transducer and activator of transcription
TBEV	Tick-borne encephalitis virus
TBS	Tris-buffered saline
TIR	Toll-interleukin-1 receptor
TLR	Toll-like receptor
TMEM119	Transmembrane protein 119
TRIF	TIR-domain-containing adapter-inducing interferon-β
TRIM	Tripartite motif
Tris	Tris(hydroxymethyl)aminomethane
TYK	Tyrosine-protein kinase
VSV	Vesicular stomatitis virus
WNV	West Nile virus

WT	Wild-type C57BL/6
YFV	Yellow fever virus
ZO-1	Zonula occludens-1 protein

List of figures

Figure 1: Simplified depiction of the type I interferon signaling pathways

Figure 2: Detection of LGTV in different brain regions via qRT-PCR

Figure 3: Detection of LGTV in relevant tissue for the BBB and the BCSFB

Figure 4: The CSF shows no LGTV RNA after infection with LGTV

Figure 5: Immunohistological detection of LGTV in OB, CP and meninges of Ifnar-/- mice 96 hpi.

Figure 6: LGTV infects Iba-1+ cells in the OB of Ifnar-/- mice 96 hpi.

Figure 7: LGTV infects CD45low Iba-1+ cells in the CP of Ifnar-/- mice 72 hpi.

Figure 8: LGTV infected cells are located near blood vessels in the OB of Ifnar-/- mice 96 hpi.

Figure 9: Epithelial cells in the CP are no target of LGTV in Ifnar-/- mice 72 hpi

Figure 10: Sparse LGTV infection of pericytes near blood vessels in the CP of Ifnar-/- mice 72 hpi.

Figure 11: CD45+ cells and Iba-1+ cells in the meninges are infected by LGTV in Ifnar-/- mice 72 hpi.

Figure 12: CLDN-5 expression is dependent on type I IFN in different brain regions

Figure 13: CLDN-5 is differentially regulated across brain regions in Ifnar-/- mice

Figure 14: ZO-1 regulation is dependent on type I IFN in different brain regions

Figure 15: ZO-1 5 is differentially regulated across brain regions in WT and Ifnar-/- mice

Figure 16: ZO-1 is tightly regulated in the CP during LGTV infection

List of tables

Table 1: Summary of significant up- and downregulations for CLDN-5 and ZO-1

Table 2: List of consumables

Table 3: Chemicals and reagents

Table 4: Laboratory equipment

Table 5: Primary antibodies for histology

Table 6: Secondary antibodies for histology

Table 7: Primers for qRT-PCR

Score Sheet: Ableitung von kumulativen Abbruchkriterien

Beobachtung *zu erwartende Belastungsanzeichen, deren Gewichtung und zu ergreifende Maßnahmen*	**Punktewertung**
I Körpergewicht	
- unbeeinflusst oder Anstieg	**0**
- Gewichtsreduktion <5%	**1**
- Gewichtsreduktion 5-14%	**5**
- Gewichtsreduktion 15-17%	**10**
- Gewichtsreduktion 18-20%	**15**
- Gewichtsreduktion >20%, **alleiniges Abbruchkriterium**	20
II Allgemeinzustand	
- Fell glatt, glänzend; Körperöffnungen sauber; Augen klar, glänzend	0
- Felldefekte (verminderte oder übersteigerte Körperpflege)	1
- Fell stumpf, ungeordnet, ungepflegte Körperöffnungen, Augen trüb; erhöhter Muskeltonus	5
- schmutziges Fell, verklebte oder feuchte Körperöffnungen, unnormale Haltung, Augen trüb; hoher Muskeltonus	10
- Verkrampfungen, Lähmungen (Rumpfmuskulatur, Extremitäten); „Katzenbuckel"; Atemgeräusche; Tier fühlt sich kalt an,	20
III Spontanverhalten	
- normales Verhalten (Lokomotion, Neugier, Sozialkontakte)	0
- geringe Abweichungen vom Normalverhalten	1
- ungewöhnliches Verhalten, eingeschränkte Motorik oder Hyperkinetik	5
- Selbstisolation, Lethargie; ausgeprägte Hyperkinetik bzw. Verhaltensstereotypien; Koordinationsstörungen; Schmerzreaktion beim Berühren	20
IV Klinischer Befund	
- Atmung normal, Schleimhäute gut durchblutet, feucht, glatt, glänzend	0
- geringe Abweichungen von der Normalsituation	1
- schnelle oder flache Atmung	15
Bewertung, Maßnahmen	**Punktsumme**
Belastungsgrad 0 = keine Belastung	0
Belastungsgrad 1 = geringe Belastung, sorgfältig weiter beobachten	1-9
Belastungsgrad 2 = mittelgradige Belastung; Beobachtungsintervall erhöhen (mindestens 2 x täglich)	10-19
Belastungsgrad 3 = schwere Belastung; sofort Versuch am betroffenen Tier abbrechen und Tier einschläfern	20 oder höher

angelehnt an Morton and Griffiths (Vet Rec. 1985 Apr 20; 116(16): 431-6)

Kontrolle der Tiere:

Zur Beurteilung des Gesundheitszustandes eines Tieres wird dieses Score Sheet herangezogen. Die Kontrolle der Tiere erfolgt wie im Antrag für die einzelnen Versuche angegeben. Alle Tiere werden zu Versuchsbeginn und im Verlauf gewogen. Die Tiere werden zusätzlich regelmäßig auf die in der Tabelle aufgeführten Parameter hin beobachtet. Bei Erreichen einer Gesamtpunktezahl von > 10 werden die Tiere 2x täglich morgens und abends beurteilt. Sollte eine Punktezahl von 20 erreicht werden, wird das Tier unverzüglich schmerzfrei getötet.

Eine Gewichtsabnahme > 20% ist **für alle Versuche** als alleiniges Abbruchkriterium festgelegt. Zeigt ein Tier einen Gewichtsverlust von > 20% berechnet auf sein Ausgangsgewicht, wird es unverzüglich aus dem Versuch genommen und schmerzfrei getötet.